National Library of Canada

Acquisitions and Bibliographic Services Branch

395 Wellington Street
Ottawa, Ontario
K1A 0N4

Bibliothèque nationale du Canada

Direction des acquisitions et des services bibliographiques

395, rue Wellington
Ottawa (Ontario)
K1A 0N4

Your file Votre référence

Our file Notre référence

NOTICE

The quality of this microform is heavily dependent upon the quality of the original thesis submitted for microfilming. Every effort has been made to ensure the highest quality of reproduction possible.

If pages are missing, contact the university which granted the degree.

Some pages may have indistinct print especially if the original pages were typed with a poor typewriter ribbon or if the university sent us an inferior photocopy.

Reproduction in full or in part of this microform is governed by the Canadian Copyright Act, R.S.C. 1970, c. C-30, and subsequent amendments.

AVIS

La qualité de cette microforme dépend grandement de la qualité de la thèse soumise au microfilmage. Nous avons tout fait pour assurer une qualité supérieure de reproduction.

S'il manque des pages, veuillez communiquer avec l'université qui a conféré le grade.

La qualité d'impression de certaines pages peut laisser à désirer, surtout si les pages originales ont été dactylographiées à l'aide d'un ruban usé ou si l'université nous a fait parvenir une photocopie de qualité inférieure.

La reproduction, même partielle, de cette microforme est soumise à la Loi canadienne sur le droit d'auteur, SRC 1970, c. C-30, et ses amendements subséquents.

Canada

UNIVERSITY OF ALBERTA

A STUDY OF SOME OPERATING VARIABLES IN THE COLUMN FLOTATION OF FINE COAL

BY

DENISE K. GARAND

(C)

A thesis submitted to the Faculty of Graduate Studies and Research in partial fullfillment of the requirements for the degree of **MASTER OF SCIENCE**

IN

MINERAL ENGINEERING

DEPARTMENT OF MINING, METALLURGICAL AND PETROLEUM ENGINEERING

EDMONTON, ALBERTA

FALL 1993

National Library of Canada

Acquisitions and Bibliographic Services Branch

395 Wellington Street
Ottawa, Ontario
K1A 0N4

Bibliothèque nationale du Canada

Direction des acquisitions et des services bibliographiques

395, rue Wellington
Ottawa (Ontario)
K1A 0N4

Your file Votre référence

Our file Notre référence

The author has granted an irrevocable non-exclusive licence allowing the National Library of Canada to reproduce, loan, distribute or sell copies of his/her thesis by any means and in any form or format, making this thesis available to interested persons.

L'auteur a accordé une licence irrévocable et non exclusive permettant à la Bibliothèque nationale du Canada de reproduire, prêter, distribuer ou vendre des copies de sa thèse de quelque manière et sous quelque forme que ce soit pour mettre des exemplaires de cette thèse à la disposition des personnes intéressées.

The author retains ownership of the copyright in his/her thesis. Neither the thesis nor substantial extracts from it may be printed or otherwise reproduced without his/her permission.

L'auteur conserve la propriété du droit d'auteur qui protège sa thèse. Ni la thèse ni des extraits substantiels de celle-ci ne doivent être imprimés ou autrement reproduits sans son autorisation.

ISBN 0-315-88189-5

Canada

UNIVERSITY OF ALBERTA

RELEASE FORM

NAME OF AUTHOR: **DENISE K. GARAND**

TITLE OF THESIS: **A STUDY OF SOME OPERATING VARIABLES IN THE COLUMN FLOTATION OF FINE COAL**

DEGREE: **MASTERS OF SCIENCE**

YEAR THIS DEGREE GRANTED: **AUGUST, 1993**

Permission is hearby granted to the University of Alberta Library to reproduce single copies of this thesis and to lend of sell such copies for private, scholarly or scientific research purposes only.

The author reserves all other publication and other rights in association with the copyright in the thesis, and except as hereinbefore provided neither the thesis nor any substantial portion thereof may be printed or otherwise reproduced in any material form whatever without the author's prior written permission.

Denise Garand

Denise Garand
13519 - 129 Street
Edmonton, Alberta
T5L 1K4, Canada

August 30, 1993

UNIVERSITY OF ALBERTA

FACULTY OF GRADUATE STUDIES AND RESEARCH

The undersigned certify that they have read, and recommend to the Faculty of Graduate Studies and Research for acceptance, a thesis entitled **A STUDY OF SOME OPERATING VARIABLES IN THE COLUMN FLOTATION OF FINE COAL** submitted by **DENISE GARAND** in partial fulfilment of the requirements for the degree of **MASTER OF SCIENCE** in **MINERAL ENGINEERING**.

Dr. N.O Egiebor

Prof. L.R. Plitt

Dr. W.S.Tortike

Dr. A. Pierre

Dr. J.H. Masliyah

August 26, 1993

DEDICATION

This thesis is for my husband Doug,
and my children Leanne and Mark.

ABSTRACT

The processing of fine coal of less than 75 microns in size is known to present several problems, including high mineral content, particle oxidation and the generation of slimes. For these reasons, fine coal is usually discarded before reaching the flotation circuit regardless of its potential value. Column flotation has been identified as a possible method for treating fine coal particles. However, the effect of the coal particle size and other operating variables on column flotation system efficiency for fine coal washing have not been clearly defined. This has important implications in the development of a feasible, fine particle, flotation system for coal.

An experimental design using latin squares and multivariate analysis was implemented to study the effects of wash water flow rate, gas flow rate, and frother dosage on the efficiency of column flotation for a fine sized coal sample.

The results show that the yield and grade of the fine coal concentrate is dependent on the operating conditions, particularly with respect to the gas flow rate and the wash water flow rate. These results suggest that the column flotation of fine coal requires much more rigorous control of the operating conditions to achieve a good performance, as compared to the flotation of coarse coal samples which provide a very stable operating system, for which a wide range of operating conditions can result in acceptable performance.

ACKNOWLEDGEMENTS

I would like to acknowledge and thank all the people who contributed to this thesis project. In particular, I would like to extend my thanks to the following people and organizations:

To Dr. N.O. Egiebor and Prof. L.R. Plitt for their support and supervision throughout the project.

To Mr. J. Zalischuk, and Mr. D. Scrimger for their help in completing the experimental runs and sample analyses.

To Mr. Edgar Horner, Plant Superintendent, and Mr. John Hinds, Plant Supervisor, Smokey River Coal Limited for supplying the coal sample used for this project.

To the Mineral Engineering department academic and administrative staff, in particular Mr. B. Mohamedbhai, Mr. D. Booth, and Mrs. K. Whiting, and my friends and cohabitants in Room 178 for all their help and advise.

CANMET's Western Research Laboratory for financially funding this project and for providing technical support.

To my family and friends for their support and encouragement when I needed it most. And most especially to my husband Doug for his patience and understanding.

Thank you to all of you!

TABLE OF CONTENTS

1.0 INTRODUCTION 1
1.1 CANADIAN FLOTATION COLUMN DESIGN 2
1.1.1 OPERATING PRINCIPLES 3
1.1.2 MECHANISMS 4
1.2 FLOTATION REAGENTS 5
1.2.1 COLLECTORS 5
1.2.2 FROTHERS 6
1.3 PROJECT SCOPE AND OBJECTIVES 7

2.0 LITERATURE REVIEW 9
2.1 COLLECTION ZONE 9
2.1.1 KINETICS 9
2.1.1.1 GAS HOLDUP AND BUBBLE DIAMETER 10
2.1.1.2 PARTICLE COLLECTION 16
2.1.2 MIXING CHARACTERISTICS 21
2.1.3 CARRYING RATE 25
2.2 FROTH ZONE 26
2.2.1 FROTH STRUCTURE 27
2.2.1.1 ENTRAINMENT AND CLEANING MECHANISMS . 27
2.2.1.2 BUBBLE COALESCENCE AND FROTH COLLAPSE 30
2.2.2 FROTH CARRYING CAPACITY 32
2.3 CONTROL, MODELLING AND SIMULATION 34
2.3.1 ZONE INTERACTION 34
2.3.2 CONTROL STRATEGIES 37
2.3.3 COLUMN FLOTATION SCALE-UP 40

3.0 EXPERIMENTAL 46
3.1 EQUIPMENT SETUP 46
3.1.1 MATERIAL BALANCES 48
3.1.2 GAS HOLDUP AND INTERFACE LEVEL 50
3.2 SAMPLE ANALYSES 50
3.2.1 FEED SAMPLE PREPARATION 50
3.2.2 SIZE AND ASH DISTRIBUTION 52

3.2.3 YIELD AND GRADE 55
3.3 EXPERIMENTAL DESIGN 56
3.3.1 DESIGN VARIABLES 57
3.3.2 LATIN SQUARES 59
3.3.3 DATA ANALYSIS 61

4.0 RESULTS AND DISCUSSION 65
4.1 FINE RESULTS 65
4.1.1 LATIN SQUARE ANALYSIS OF FINE RESULTS . . . 66
4.1.1.1 ANOVA ANALYSIS 67
4.1.1.2 GAS ANALYSIS 69
4.1.1.3 WASH WATER ANALYSIS 74
4.1.1.4 FROTHER ANALYSIS 78
4.1.2 ANALYSIS OF INDIVIDUAL FINE RESULTS 81
4.2 COARSE RESULTS 85
4.2.1 LATIN SQUARE ANALYSIS OF COARSE RESULTS . . 85
4.2.1.1 ANOVA ANALYSIS 86
4.2.1.2 GAS ANALYSIS 89
4.2.1.3 WASH WATER ANALYSIS 93
4.2.1.4 FROTHER ANALYSIS 95
4.3 COMPARISON 98

5.0 CONCLUSIONS 100
5.1 SUMMARY OF RESULTS 100
5.2 COMPARISON OF COLUMN AND CELL FLOTATION . . . 102
5.3 AREAS FOR FUTURE WORK 102

REFERENCES 104

APPENDIX A 109
Procedure for wet screen analysis 110
Procedure for ash analysis 111
Procedure for Denver Cell Flotation 111

APPENDIX B 112
Column Flotation Verification Experiments 114

Batch Denver Cell Flotation Results 119

APPENDIX C 121
Sample Bubble Size Calculations 122
Bubble Size Program 127
Sample Results from Bubble Size Program 131

APPENDIX D 132
Bias Flow Rate Calculations 132

APPENDIX E 138
Screen Analysis of Concentrate Samples 138

LIST OF TABLES

Table 3.1 Latin Square Design 60

Table 3.2 Experimental Plan. 61

Table 3.3 Latin Square F Table. 63

Table 4.1 Experimental results for the fine experiments. 66

Table 4.2 ANOVA analysis of concentrate ash for fine experiments. 68

Table 4.3 ANOVA analysis of $yield_1$ for fine experiments. 69

Table 4.4 Gas analysis for fine experiments. 70

Table 4.5 Wash water analysis for fine experiments. . . 74

Table 4.6 Frother analysis for fine experiments. . . . 78

Table 4.7 Experimental results for coarse experiments. 86

Table 4.8 ANOVA analysis of concentrate ash for coarse experiments. 87

Table 4.9 ANOVA analysis of $yield_1$ for coarse experiments. 88

Table 4.10 Gas analysis of coarse experiments. 90

Table 4.11 Wash water analysis of coarse experiments. . 93

Table 4.12 Frother analysis of coarse experiments. . . 95

Table B.1 Results for the fine verification experiments. 114

Table B.2 Results for coarse verification experiments. 114

Table B.3 Denver cell flotation dosage test for the fine coal sample. 119

Table B.4 Denver cell flotation rate test for the fine coal sample. 120

Table C.1 Mean bubble size as a function of gas flow rate for fine experiments. 124

Table C.2 Mean bubble size as a function of frother dosage for fine experiments. 125

Table C.3 Mean bubble size as a function of gas flow rate for coarse experiments. 126

Table C.4 Mean bubble size as a function of frother dosage for coarse experiments. 126

Table D.1 Bias flow rate as a function of gas flow rate for fine experiments, with a wash water flow rate of 0.75ℓ/min. 135

Table D.2 Bias flow rate as a function of wash water rate for fine experiments. 136

Table D.3 Bias flow rate as a function of gas flow rate for coarse experiments, with a wash water flow rate of 0.75ℓ/min. 137

Table D.4 Bias flow rate as a function of wash water rate for coarse experiments. 137

LIST OF FIGURES

Figure 1.1 Schematic diagram of a flotation column (adapted from Finch and Dobby, 1990). 2

Figure 1.2 Contact angle between a bubble and particle in an aqueous medium (adapted from Wills, 1985). . . . 6

Figure 1.3 Collector adsorption on a mineral surface (adapted from Wills, 1985). 6

Figure 1.4 Frother Action (adapted from Wills, 1985). . 7

Figure 2.1 Bubble diameter versus gas flow rate per unit area of sparger (adapted from Xu and Finch, 1988). . 17

Figure 2.2 Calculated contact time with respect to particle and bubble size, for particle specific gravity of 2.6 (adapted from Ye and Miller, 1989). 18

Figure 2.3 Schematic diagram of particle bubble collisions (adapted from Schulze et al., 1989). 19

Figure 2.4 Flow regimes as a function of gas holdup and superficial gas rate (adapted from Finch and Dobby, 1990). 21

Figure 2.5 Schematic diagram of a N_d mixed zones model (adapted from Mavros et al., 1989). 25

Figure 2.6 Froth structure (adapted from Yianatos et al., 1986). 28

Figure 2.7 Height of a transfer unit modelling of the froth zone (adapted from Yianatos et al. 1987). 30

Figure 2.8 Graphical determination of transfer units and cleaning factor (adapted from Yianatos et al., 1987). 31

Figure 2.9 Process control matrix (adapted from Finch and Dobby, 1990). 35

Figure 2.10 Stabilizing control schemes currently in use: a) level control and b) level and bias control (adapted from Finch and Dobby, 1990). 39

Figure 2.11 Effect of H:D and collection zone height on the recovery, vessel dispersion number, and mean particle residence time (adapted from Yianatos et al.,1988). 44

Figure 2.12 Grade-recovery relationship with H:D ratio and feed rate (adapted from Yianatos et al., 1988). . . 45

Figure 3.1 Flotation column set-up. 47

Figure 3.2 Material Balances around the column. 49

Figure 3.3 Fine particle size distribution. 53

Figure 3.4 Coarse particle size distribution. 54

Figure 4.1 Effect of gas flow rate on $yield_1$ for fine experiments. 72

Figure 4.2 Effect of gas flow rate on $yield_2$ for fine experiments. 73

Figure 4.3 Effect of gas flow rate on concentrate ash for fine experiments. 73

Figure 4.4 Gas holdup as a function of gas flow rate for fine experiments. 74

Figure 4.5 Effect of wash water flow rate on $yield_1$ for fine experiments. 76

Figure 4.6 Effect of wash water flow rate on $yield_2$ for fine experiments. 77

Figure 4.7 Effect of wash water flow rate on concentrate ash for fine experiments. 77

Figure 4.8 Effect of frother dosage on $yield_1$ for fine experiments. 79

Figure 4.9 Effect of frother dosage on $yield_2$ for fine experiments. 80

Figure 4.10 Effect of frother dosage on concentrate ash for fine experiments. 80

Figure 4.11 Effects of gas and wash water on $yield_1$ for fine experiments. 82

Figure 4.12 Effect of gas and wash water on $yield_2$ for fine experiments. 83

Figure 4.13 Effect of gas and wash water on concentrate ash for fine experiments. 84

Figure 4.14 Effect of gas flow rate on $yield_1$ for coarse experiments. 91

Figure 4.15 Effect of gas flow rate on $yield_2$ for coarse experiments. 91

Figure 4.16 Effect of gas on concentrate ash for coarse experiments. 92

Figure 4.17 Gas holdup as a function of gas flow rate. 92

Figure 4.18 Effect of wash water flow rate on $yield_1$ for coarse experiments. 94

Figure 4.19 Effect of wash water flow rate on $yield_2$ for coarse experiments. 94

Figure 4.20 Effect of wash water flow rate on concentrate ash for coarse experiments. 95

Figure 4.21 Effect of frother dosage on $yield_1$ for coarse experiments. 96

Figure 4.22 Effect of frother dosage on $yield_2$ for coarse experiments. 97

Figure 4.23 Effect of frother dosage on concentrate ash for coarse experiments. 97

Figure B.1 Effect of wash water on $yield_1$ for fine verification experiments, with a gas flow rate of 1.5 ℓ/min and a frother dosage of 21 ppm. 116

Figure B.2 Effect of wash water on $yield_2$ for fine verification experiments, with a gas flow rate of 1.5 ℓ/min and a frother dosage of 21 ppm. 116

Figure B.3 Effect of wash water on concentrate ash for fine verification experiments, with a constant gas flow rate (1.5 ℓ/min) and a constant frother dosage (21 ppm). 117

Figure B.4 Effect of frother on $yield_1$ for fine verification experiments, with constant flow rates for gas (1.5 ℓ/min) and wash water (1.0 ℓ/min). . . . 117

Figure B.5 Effect of frother on $yield_2$ for fine verification experiments, with constant flow rates for gas (1.5 ℓ/min) and wash water (1.0 ℓ/min). . . . 118

Figure B.6 Effect of frother on concentrate ash for fine verification experiments, with constant flow rates for gas (1.5 ℓ/min) and wash water (1.0 ℓ/min). . . . 118

Figure E.1 Effect of wash water flow rate on the weight size fractions in the concentrate for fine experiments. 139

Figure E.2 Effect of wash water on ash content in each size fraction in the concentrate for fine experiments. 139

Figure E.3 Effect of wash water flow rate on the weight size fractions in the concentrate for coarse experiments. 140

Figure E.4 Effect of wash water on ash content in each size fraction in the concentrate for coarse experiments. 140

LIST OF SYMBOLS

A	- surface or cross-sectional area (cm^2)
a	- ash content (%)
A,B,C,D	- Experimental design variables
BR	- bias ratio
C	- tracer concentration
CF	- average cleaning factor
C_a	- carrying capacity of the froth zone (g/cm^2 s)
C_p	- heat capacity of water (J/g °C)
C_r	- carrying rate of the collection zone (g/cm^2 s)
C,n	- empirical constants relating d_b to V_g (Eqn 14)
C_1,n	- empirical constants relating d_b to V_g (Eqn 16)
d_c	- column diameter (cm)
d_b	- bubble diameter (mm)
d_p	- particle size diameter (μm)
df	- degrees of freedom
E_a	- attachment efficiency
E_c	- collision efficiency
E_d	- axial dispersion coefficient (J/s cm °C)
E_k	- collection efficiency
g	- acceleration due to gravity (cm/s^2)
F	- calculated F-ratio
H	- height (m)
I	- number of set levels
i,j,k	- set levels of design variables A, B, and C
K	- tracer conductivity (S)
K_1	- fraction of the bubble surface area covered by a monolayer of particles
K_o, C_o	- distribution coefficients for small columns
k	- flotation rate constant (s^{-1})
MS	- mean sum of squares
m	- subscript for universal mean
m	- function of Reynolds number
N	- total number of experiments

N_d - vessel dispersion number

$N_{(\mu,\sigma 2)}$ - normal distribution function

p - calculated tolerance level

Q - volumetric flow rate (ℓ/min)

q - empirical constant relating d_{b0} to V_g (Eqn 31)

R - recovery (%)

Re - Reynolds number

RS - raw sum of squares

R_s - ratio of sparger surface area to column cross-section area

rem - subscript for remainder

SS - sum of squares

T - raw total of all test results

T - temperature (°C)

t - time (s)

t_c - contact time (ms)

t_i - induction time (ms)

t_i, t_j, t_k - totals of populations A, B, and C respectively

V - superficial velocity (cm/s)

V_{gl} - drift flux (cm/s)

V_∞ - terminal bubble velocity (cm/s)

$V_{p,\infty}$ - particle settling velocity (cm/s)

W_{tr} - weight of tracer (g)

X_f - entrainment factor

X_{ijkl} - experimental result at variable levels i, j, and k with experimental error ε_{ijkl}

x - axial distance from tracer injection point (cm)

Y - percent yield (%)

z - distance from the interface level (z_0) in the froth (cm)

α_i - the effect of variable A at the i^{th} level

α, β - empirical constants relating ε_g to V_g (Eqn 15)

β_j - the effect of variable B at the j^{th} level

γ_k - the effect of variable C at the k^{th} level

ΔL - distance between two manometers (cm)

Δh - height difference between two manometers (cm)

ε_g - gas holdup
λ - ratio of backflow to net flow
μ - viscosity (g/cm s)
μ - universal mean
ρ - density (g/cm^3)
Φ_l - liquid volume fraction
σ_e^2 - error distribution about the universal mean
τ - mean residence time (s)
χ - mass fraction of solids

SUBSCRIPTS

B - bias
b - bubble
c - column
col - collection zone
conc - concentrate
f - feed
fr - froth zone
g - gas
l - liquid
p - particle, or solids
s - sparger
sl - slurry
t - tailings
ww - wash water

1.0 INTRODUCTION

The flotation column is an innovative new approach to coal and mineral dressing operations aimed at providing higher quality products from lower quality feed materials. There are several variations of flotation columns presently operating or being developed. These designs include: the Canadian column, the WEMCO/Leeds column (Degner and Sabey, 1988), the Packed column (Yang, 1988), the pneumatic flotation cell (Bahr et al., 1985), the Diester column (Parekh et al., 1986), the Flotaire column (Zipperian and Svensson, 1988), the Hydrochem column (Schneider and Van Weert, 1988), the Jameson cell (Jameson, 1988), and several other designs. The one thing that all these designs have in common is that they all use a column to allow for longer bubble-particle contact times. The design variations range from co-current flow (gas/feed) to counter--current flow, and from mechanical mixers to no mixers (Parekh et al., 1986). The most well known and commonly used is the Canadian column (Finch and Dobby, 1990), and it is the focus of this thesis work. From this point forward, the use of the words "column flotation" will refer to the Canadian column. The Canadian flotation column was developed and patented in the early 1960's, by Boutin and Tremblay (Canadian patents 680,576 and 694,547).

The basic principles of flotation remain the same for both column and cell flotation. Separation is affected by exploiting the differences in the surface characteristics of the minerals. The hydrophylic materials are removed in the tailings stream, and the hydrophobic materials will attach to air bubbles and float to the concentrate stream. In addition, reagents are added to enhance the process, to allow for the maximum efficiency from the system. The design of the flotation column has three main differences from conventional

cell flotation: the geometrical design, no mechanical parts are involved (bubble generation through an air sparger), and the use of wash water to clean the froth zone.

1.1 CANADIAN FLOTATION COLUMN DESIGN

A schematic diagram of a flotation column is presented in figure 1.1. Industrial flotation columns are typically 9-15 m high and 50 to 300 cm in diameter. The cross-section may be either square (design of the Column Flotation Company of Canada) or circular (design of most homemade units). The size of a flotation column is designated by either the side of the square column or the diameter for a circular column.

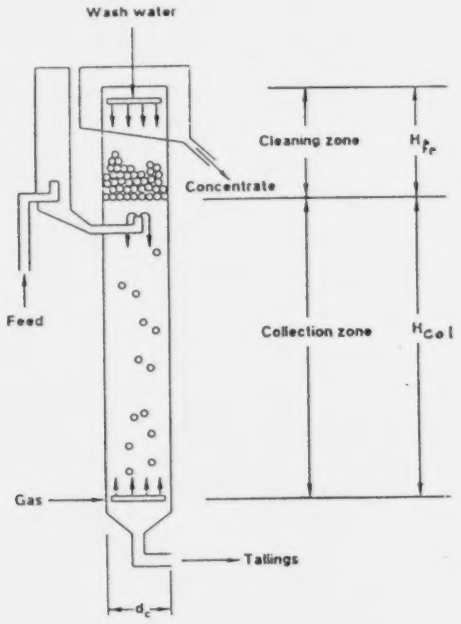

Figure 1.1 Schematic diagram of a flotation column (adapted from Finch and Dobby, 1990).

The main control parameters for the column are the material flow rates. The different material streams include:

feed, tailings, concentrate, wash water, gas, and bias. The material flow rate is reported as either superficial velocity (flux), J_i, or as volumetric flow rate, Q_i, where i denotes the different material streams. Superficial velocity is defined as the volumetric flow rate divided by the column cross-sectional area. All superficial velocities are designated as positive in the upwards direction, except the bias rate. Note that the gas rates are measured at atmospheric pressure: either at the top of the column or using a calibrated measuring device. This convention allows the pressure differential (due to the weight of the water), and the subsequent bubble expansion to be discounted, and therefore gas rates can be compared for different heights of columns.

There are three distinct zones over the column height: the collection zone, the froth washing zone, and the conventional froth zone. Each zone has a specific purpose: recovery occurs in the collection zone; the washing zone controls the grade; and the conventional froth zone transports the concentrate to the launder (Dobby and Finch, 1986-b). For the sake of simplicity in modelling, only two zones are represented: the froth zone and the collection zone. The transition between the two zones is called the interface level. The interface level is defined by the sharp difference in the fractional gas holdup, defined as the volume fraction of gas in the column.

1.1.1 OPERATING PRINCIPLES

The flotation column is designed to have counter-current flow between feed and gas streams, to allow for better bubble-particle contact times. The feed slurry is introduced into the column just below the interface level, and it descends against a rising swarm of gas bubbles generated at the bottom of the column, by a sparger.

Wash water is added just below the lip, through a system of perforated pipes or sprinklers. Wash water has two functions: to wash the entrained particles from the froth, and to stabilize the bubble bed by preventing coalescence (Dobby and Finch, 1986-b). The wash water stream will be split between the tailings and the concentrate streams, determined by the water balance across the interface. The net flow of water across the interface level is defined as the operating bias, with positive bias defined as downward flow. A direct method of measuring the actual operating bias is currently unavailable, therefore it is estimated by the difference in the feed and tailings flow rates (Moys and Finch, 1988). By maintaining the tailings flow rate at a higher flow rate than the feed, a positive bias can be obtained (net downward flow of water), thus washing the froth.

1.1.2 MECHANISMS

There are two main performance indicators for a separation process: recovery and grade. The relationship between the two parameters is inversely proportional (dependant on the fraction of middlings particles). In addition, these two parameters are determined separately in opposing zones. Recovery is determined in the collection zone, while the grade is primarily controlled in the froth zone.

The recovery of minerals is dependant on the collection process in the collection zone. Collection of a mineral particle follows two steps: a particle-bubble collision, followed by attachment if the particle is sufficiently hydrophobic. The collection process is dependant on many factors, including: feed grade, gas rate, particle rate, the ratio of particle to bubble diameter, and reagent dosages.

The product grade is determined by: the feed grade and

the cleaning of entrained particles from the froth. The mechanism of entrainment occurs when very fine particles become carried into the froth in the thin film of water surrounding the bubble. The cleaning mechanism is accomplished by the drainage of wash water through the froth, along the water film boundary. This allows the continuous replacement of the film, thereby washing as well as stabilizing the froth (Groppo, 1986). The main cleaning action occurs near the interface level, for moderate gas rates (Yianatos et al., 1986). With deep froth beds (greater than 1 m), upgrading may occur due to selective washing of middlings as bubbles coalesce (Yianatos et al., 1988).

1.2 FLOTATION REAGENTS

The two main types of flotation reagents are collectors and frothers (Wills, 1985). Reagents play an important role in the flotation process. They are added to enhance the efficiency, and control the process. This section will provide a brief summary of both types.

1.2.1 COLLECTORS

Collectors are used to enhance the hydrophobic characteristics of the mineral surface. The degree of hydrophobicity is determined from the contact angle of the mineral surface and air bubble in the presence of water, as shown in figure 1.2. Naturally hydrophobic minerals, such as graphite, sulphur, molybdenite, diamond, coal, and talc consist of non-polar molecules held together by Van der Waals forces. They have high contact angles in the range of 60° to 90°. Hydrocarbon collectors may be added to increase the contact angle of these minerals, by creating a thin hydrophobic film on the mineral surface.

For polar minerals (ionic or strong covalent bonding), the surface must be given a hydrophobic character, and therefore the collectors have a different structure. They are asymmetric molecules, consisting of a polar head which dissociates in solution (anionic or cationic depending on the surface chemistry) and an organic tail. The polar head adsorbs onto the mineral's surface, leaving an organic tail sticking out (figure 1.3), thus creating a new highly hydrophobic surface area.

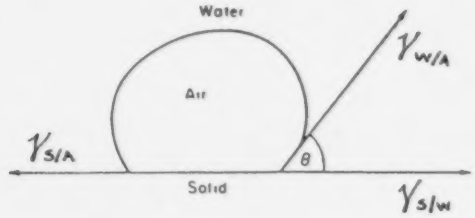

Figure 1.2 Contact angle between a bubble and particle in an aqueous medium (adapted from Wills, 1985).

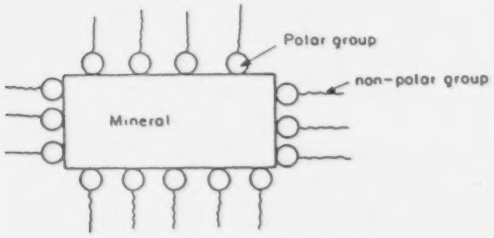

Figure 1.3 Collector adsorption on a mineral surface (adapted from Wills, 1985).

1.2.2 FROTHERS

Frothers have two purposes: to create a stable dispersion

of fine bubbles in the pulp zone and a stable froth, as well as decreasing the mean bubble diameter. The chemical composition of a frother is similar to that of an ionic collector, also consisting of a polar head and an organic tail. The organic tail adsorbs onto the air-water interface of the bubble, leaving the polar head on the surface of the bubble. The polar head of the frother will react with the water, thereby hydrating the surface of the bubble. This action will strengthen the surface tension of the bubble, therefore creating a more stable bubble. Figure 1.4 shows a schematic view of the frother action.

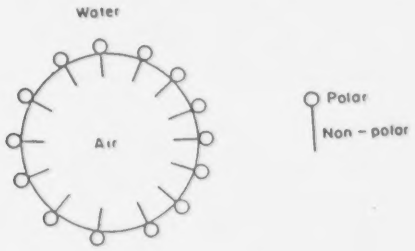

Figure 1.4 Frother Action (adapted from Wills, 1985).

1.3 PROJECT SCOPE AND OBJECTIVES

The overall objective of this project is to study the effect of three major column operating variables, viz; gas flow rates, wash water flow rate, and frother concentration, on the washing efficiency of fine sized coal (d_{50} = 35μm) in terms of product yield, and concentrate grade (ash content) as performance parameters. The results obtained from the fine coal study will be compared with those from a relatively coarse sample (d_{50}= 250μm) in terms of the performance parameters under similar experimental conditions. The experimental data will be evaluated using a multivariate

analysis technique employing the Latin Square experimental design and analysis of variance (ANOVA). Consequently, this objective is divided into three parts.

1. The determination of the effects of varying the operating conditions on the washability of fine coal in terms of yield, and concentrate grade using a statistical experimental design.

2. An investigation of the differences in the flotation response between the fine sized coal sample and a relatively coarse sample in terms of the performance parameters outlined above.

3. The evaluation of the experimental data using a multivariate analysis approach from which the optimal operating conditions can be determined for each particle size distribution.

2.0 LITERATURE REVIEW

2.1 COLLECTION ZONE

There has been extensive effort placed on modelling the behaviour of the collection zone in a flotation column. Studies on the collection zone have generally been divided into kinetics, mixing characteristics, and carrying rate. Product recovery is determined in the collection zone.

2.1.1 KINETICS

Column flotation kinetics is dependant on the particle collection process. The two most important factors in the collection process is bubble diameter d_b, and flotation rate constant k.

In column flotation, the commonly used bubble generation systems produce a wide distribution of bubble sizes, which have caused a variety of design problems, and operating difficulties. Therefore, the estimation of the mean bubble diameter, and the size distribution become an integral part of any column flotation model (Dobby et al., 1988).

The particle collection process is generally believed to be the rate determining step in a flotation process. A probability model was developed to describe the collection process in two stages: particle-bubble collision followed by attachment (Dobby and Finch, 1986-a). The development of a procedure to determine flotation rate constants for column flotation has also become an essential component to a complete description of the collection zone behaviour.

2.1.1.1 GAS HOLDUP AND BUBBLE DIAMETER

Gas holdup is used to estimate the mean bubble diameter. Gas holdup is determined from pressure measurements at two pre-determined levels. Gas holdup can be calculated from the following formula if two water manometers are used to measure the pressure differential.

$$\varepsilon_g = 1 - \frac{\rho_l}{\rho_{sl}}\left(1 - \frac{\Delta h}{\Delta L}\right) \qquad (1)$$

where: ΔL is the distance between the two manometers, and Δh is the difference between the manometer readings, ρ_l and ρ_{sl} are the densities of the liquid (water) and slurry respectively.

Bubble size distribution depends on a number factors, including gas flow rate, frother type and dosage, and the type of sparger (Zhou, 1992). For simplicity, the size distribution is estimated by the sauter mean diameter, and a statistical distribution function. The bubble size distribution in the collection zone corresponds closely to a normal distribution. There are several methods for estimating the bubble diameter. One of these methods is a theoretically derived model based on the drift flux analysis (Dobby, Yianatos, and Finch, 1988) and there are several empirically derived models based on column operating conditions.

The theoretically derived model based on the drift flux analysis has been described by a number of authors. A detailed description of this method was given in the paper by Dobby, Yianatos, and Finch, 1988. The calculation of a mean sauter bubble size, can be approximated using the drift flux model.

The drift-flux analysis is used to relate phase flow rates, holdup, and physical properties. Using drift-flux analysis, the terminal bubble rise velocity, V_∞ can be estimated, and can be used to calculate the bubble diameter (Dobby et al., 1988). The drift flux model was developed using a single bubble-water system, and then expanded to fit a bubble swarm-water system, and then finally to a gas-slurry system. For a two-phase (gas-water) system, the drift-flux, V_{gl}, is calculated with the following formula:

$$V_{gl} = \frac{V_g}{\varepsilon_g} - \frac{V_l}{(1-\varepsilon_g)} \qquad (2)$$

where: V_g and V_l are the superficial velocities (flow rate divided by the column cross-section) of the gas and liquid respectively, and ε_g is the fractional gas holdup. The drift-flux can be related to the terminal bubble velocity by:

$$V_{gl} = V_\infty(1-\varepsilon_g)^{1-m} \qquad (3)$$

where: m is a function of the bubble Reynolds number, Re_b. The estimation of m can be determined from one of the following:

$$m=\left(4.45+18\frac{d_b}{d_c}\right)Re_b^{-0.1} \qquad 1 \le Re_b \le 200$$
$$m=4.45Re_b^{-0.1} \qquad 200 \le Re_b \le 500 \qquad (4)$$

where,

$$Re_b = \frac{d_b V_\infty \rho_l}{\mu_l} \qquad (5)$$

By combining equations (3) and (4), the terminal bubble velocity can be expressed as:

$$V_\infty = \frac{V_g}{\varepsilon_g (1-\varepsilon_g)^m} - \frac{(V_g+V_l)}{(1-\varepsilon_g)^m} \qquad (6)$$

The correlation between bubble diameter and terminal rise velocity, for a bubble swarm is expressed by:

$$d_b = \sqrt{\left(\frac{18\ \mu_l\ V_\infty}{g\ \Delta\rho}\ (1+0.15 Re_s^{0.687}) \right)} \qquad (7)$$

where: μ_l is the fluid viscosity, $\Delta\rho$ is the density difference between the two phases, and Re_s is the Reynolds number for a bubble swarm, calculated by:

$$Re_s = \frac{d_b V_{gl} \rho_l (1-\varepsilon_g)}{\mu_l} \qquad (8)$$

The estimation of the mean bubble diameter for a gas-water system is an iterative process, which includes the following steps (Dobby et al., 1988).

1. Estimate m.
2. Calculate V_∞ from equation (6).

3. Calculate d_b, iterating on d_b using equations (7) and (8).
4. Calculate m using equation (4) and compare with step 1; iterate on m if necessary.

In order to expand the drift-flux model to the gas-slurry system, the following assumptions were made.

1. The bubble diameter, d_b, is much larger than the particle diameter, d_p.

2. The slurry acts as a one phase fluid (i.e. liquid). The previously described liquid parameters (V_l, ρ_l, and μ_l) are then replaced by slurry parameters (V_{sl}, ρ_{sl}, and μ_{sl}).

The slurry density, ρ_{sl} can be estimated by the tailings density, if pressure differential is taken near the bottom of the column. However, the tailings density will be higher, due to the higher particle settling velocity relative to the liquid. This assumption can only be used if the solids are very fine. The slurry density can be calculated from:

$$\rho_{sl} = \phi_l \rho_l + (1-\phi_l)\rho_p \qquad (9)$$

where: Φ_l is the liquid volume fraction, $(1 - \Phi_l)$ is the solids volume fraction, and ρ_p is the solids density. The liquid volume fraction, can be determined using mean residence times (τ) and superficial velocities for both the solid and liquid phases, as follows:

$$\phi_l = \frac{V_l \tau_l}{V_l \tau_l + V_p \tau_p} \qquad (10)$$

It has been shown that the solids residence time, τ_p can be expressed by:

$$\tau_p = \tau_l \left[\frac{(V_l+V_p)/(1-\varepsilon_g)}{(V_l+V_p)/(1-\varepsilon_g) + V_{p,\infty}} \right] \qquad (11)$$

where: $V_{p,\infty}$ is the particle settling velocity, and is given as follows for Stokes' flow:

$$V_{p,\infty} = \frac{g\, d_p^2\, (\rho_p-\rho_l)\, \phi_l^{3.7}}{18\mu_l} \qquad (12)$$

Note that if slurry viscosity is not known (or measured) it can be estimated by:

$$\mu_{sl} = \mu_l\, \phi_l^{-2.5} \qquad (13)$$

Similar to the bubble diameter calculations for the gas-liquid system, calculations for a gas-slurry system follow an iterative approach (Dobby et al., 1988), as follows:

1. Estimate the gas holdup, ε_g.
2. Solve for the volume fraction of liquid using equations (10) and (11).
3. Calculate the slurry density, ρ_{sl} using equation (9).
4. Then solve for gas holdup, using equation (1) and compare with step 1. If the desired tolerance is not reached then repeat steps 1-4 using the new value.

5. Estimate the slurry viscosity from equation (13).
6. Calculate the terminal bubble rise velocity and bubble diameter, as described for the gas-liquid system, but replacing the slurry viscosity and density.

Of the empirically determined models to estimate bubble diameter, two are presented here. The first model relates the bubble diameter to the superficial gas velocity (Dobby and Finch, 1986-a). The second model developed by Xu and Finch, 1988, is based on the sparger type and surface area, as well as the superficial gas velocity. The first model is based on the fact that as the gas rate is increased, the bubble diameter also increases. The function of bubble diameter with respect to gas rate can be expressed by:

$$d_b = C V_g^n \qquad (14)$$

where: C and n are empirically determined constants. For typical column flotation gas rates, n=0.2-0.4 (Dobby and Finch, 1986-a), depending on the type of sparger. C is dependant on many factors, including the frother dosage.

The second model was an effort to characterize spargers, based on the relationship between gas holdup and superficial gas velocity, as shown below:

$$\varepsilon_g = \alpha V_g^{\beta} \qquad (15)$$

where: α and β are empirical constants. The value of β is based on the operation flow regime (for bubbly flow, $0.7 \leq \beta$

≤ 1.0). The gas holdup however is also a sensitive measure of bubble diameter, and therefore a similar relationship can be established for bubble diameter (equation 16). By holding all parameters constant except the sparger type and size, a relationship was developed between bubble diameter and sparger, as follows:

$$d_b = C_1 [R_s \times V_g]^n \qquad (16)$$

where: R_s is the ratio of column cross-sectional area A_c to the sparger surface area A_s, and C_1 is a constant. The volumetric gas rate per unit of sparger surface area, R_s times V_g can be written as:

$$R_s \times V_g = \frac{A_c}{A_s} \times \frac{Q_g}{A_c} = \frac{Q_g}{A_s} \qquad (17)$$

The values of the constants n and C_1 were estimated using regression analysis, with the best fit being n=0.25 and C_1=1 (Xu and Finch, 1988), shown in figure 2.1

2.1.1.2 PARTICLE COLLECTION

Kinetic studies have shown that the rate constant, k for column flotation, assuming first order kinetics can be expressed by (Dobby and Finch, 1986-a):

$$k = \frac{1.5\ V_g\ E_k}{d_b} \qquad (18)$$

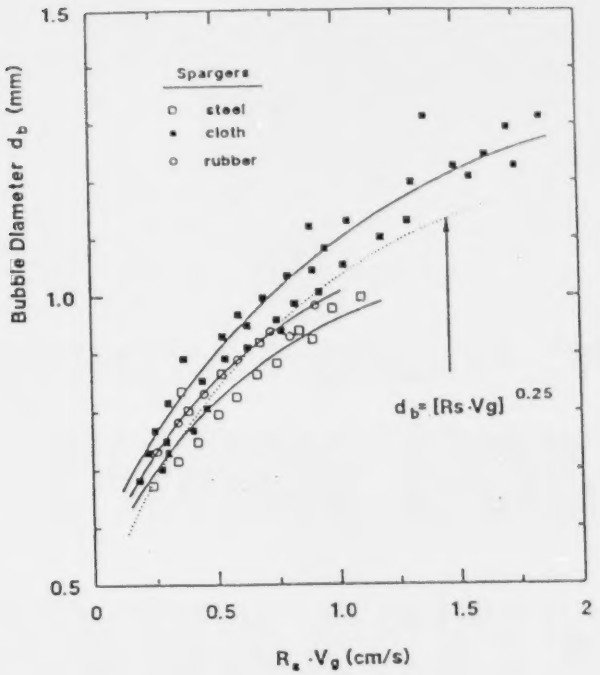

Figure 2.1 Bubble diameter versus gas flow rate per unit area of sparger (adapted from Xu and Finch, 1988).

where: E_k is the probability of particle capture, or collection efficiency. This equation was developed by investigating the collection process. The collection process can be described as the collision of a mineral particle with bubble, followed by particle attachment. The attachment can occur in two ways: due to the hydrophobic nature of the particle surface, or due to entrainment.

Considering a single bubble system; collision efficiency, E_c, is defined as the fraction of all particles that collide with the bubble, and attachment efficiency, E_a, is defined as the fraction of colliding particles that attach to the bubble (Dobby and Finch, 1986-a). Entrainment and detachment are not considered for a single bubble system, so E_k is expressed as:

$$E_k = E_c * E_a \qquad (19)$$

Collision modelling, for a single bubble system, has shown that the smaller the bubble diameter, the higher the collection efficiency. For bubble diameters less than 1.3 mm, E_c is approximately proportional to $1/d_b$ (Dobby and Finch, 1986-a). Attachment modelling compares the particle-bubble contact time, t_c with induction time t_i (the time required for film thinning and particle attachment). Note that the more rigid the bubble surface (due to the excessive presence of surface active reagents) the lower the attachment rate, and ultimately the recovery (Joseph, 1985). Figure 2.2 shows the relationship between contact time, and particle and bubble size.

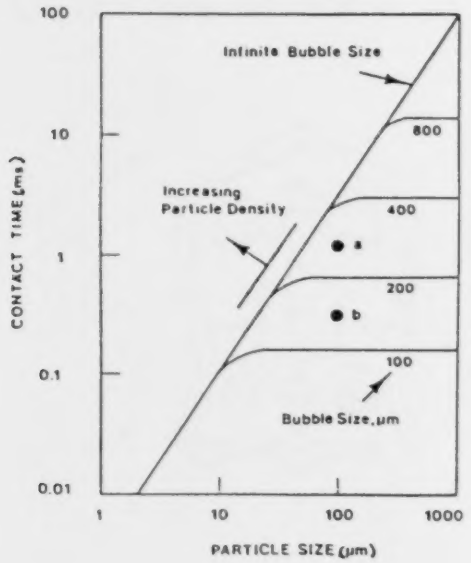

Figure 2.2 Calculated contact time with respect to particle and bubble size, for particle specific gravity of 2.6 (adapted from Ye and Miller, 1989).

The distribution of contact times is the result of particles colliding between the top (θ = 0°) and the graze angle (θ = 60 to 70°) of the bubble. Angle θ is measured from the bubble centre with respect to the vertical, as shown in figure 2.3. E_a is the fraction of colliding particles with contact time greater than the induction time, ie. $t_c > t_i$ (Dobby and Finch, 1986-a).

There is some evidence that as the bubble diameter decreases, the induction also decreases, although this effect is not accounted for in this model. This may be due to the higher internal pressures, compounded by a larger contact angle, relative to a larger bubble with the same particle collision path (Dobby and Finch, 1986-a).

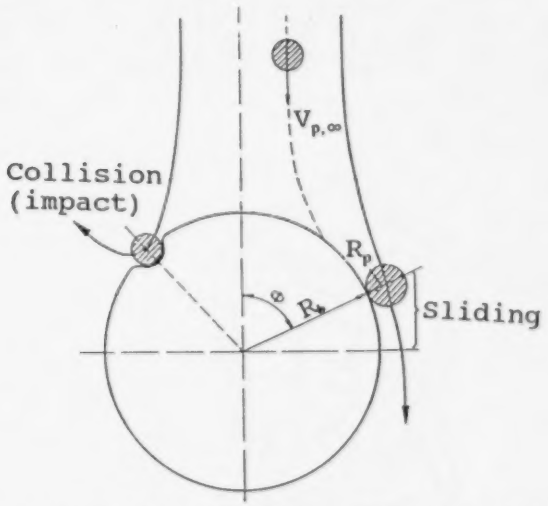

Figure 2.3 Schematic diagram of particle bubble collisions (adapted from Schulze et al., 1989).

"Collection efficiency, E_k is defined as the fraction of all particles swept out by the projected area of the bubble that collide with, attach to and remain attached to the bubble until reaching the cleaning zone" (Dobby and Finch, 1986-b).

It is dependant upon many factors including: particle and bubble diameters, and the particle surface characteristics.

For an operating system, the relationship between collection efficiency and flotation rate is given in equation (18). From this equation, it can be seen that decreasing bubble size while retaining the same gas flux, V_g will increase the flotation rate. However, there is an upper limit on gas flux, $V_{g,max}$, that is dependant on the bubble diameter, specifically the terminal bubble rise velocity, V_∞. The limiting gas rate can be estimated by using equations (2) and (3). Operation of the column above the maximum gas flux, will result in 'flooding' at the gas inlet. Smaller gas bubbles, and higher liquid flux, will both work to decrease the maximum gas flux possible. Operating as close to the maximum gas flux as possible will result in the maximum flotation rate, although increasing the gas flux will also increase the bubble diameter. This requires that an optimal gas flux be found in order to operate at the maximum flotation rate (Dobby and Finch, 1986-a).

The measurement of the rate constant can be done by performing a series of tests, using fixed flow rates for each test. For the first test, the tailings and concentrate are collected. The tailings are re-used for the next test as the feed, and the concentrate is kept for analysis. The mean retention time for each test is used to plot recovery versus time to obtain an estimate of the flotation rate constants. Two additional constraints are required: the bubble carrying capacity must be close to or at 100%, and the gangue entrainment must be near zero (Dobby and Finch, 1986-b).

2.1.2 MIXING CHARACTERISTICS

There are two flow regimes considered in flotation modelling: bubbly flow and turbulent flow. Figure 2.4 presents a graphical representation of these two flow regimes, by plotting gas holdup, ε_g versus superficial gas velocity V_g.

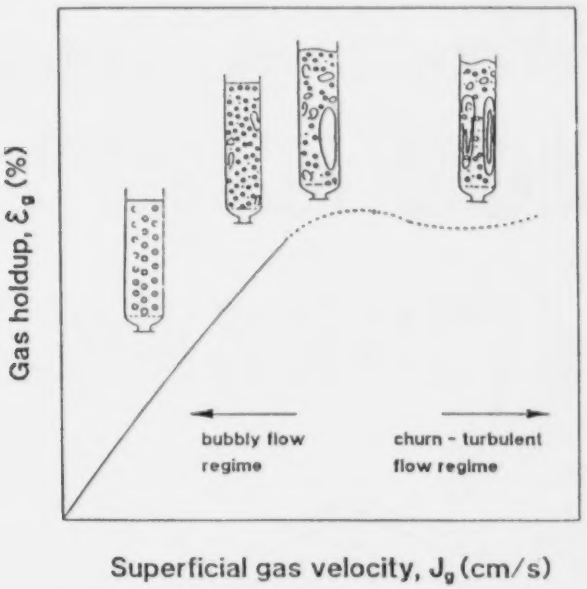

Figure 2.4 Flow regimes as a function of gas holdup and superficial gas rate (adapted from Finch and Dobby, 1990).

The bubbly flow regime offers the best operating conditions for column flotation. It consists of a homogeneous distribution of uniform sized bubbles, which in turn have uniform rise velocities (Finch and Dobby, 1990). In the turbulent flow regime, the gas holdup ε_g becomes very unstable, especially for high superficial gas velocities. This gives rise to large bubbles, coalescence, and wide variations in bubble size distribution. This creates the undesirable

conditions of high mixing, and lower the collection efficiency due to less bubble surface area (Finch and Dobby, 1990).

The product recovery in a flotation column depends upon the mixing conditions of the collection zone, as well as the particle retention time, and rate constant, (Dobby and Finch, 1986-b). The recovery can be expressed by the following:

$$R = 1 - \frac{4ae^{\frac{1}{2N_d}}}{(1+a^2)e^{\left(\frac{a}{2N_d}\right)} - (1-a^2)e^{-\left(\frac{a}{2N_d}\right)}} \qquad (20)$$

where: N_d is the vessel dispersion number, and a is expressed as:

$$a = \sqrt{(1 + 4k\tau_p N_d)} \qquad (21)$$

where: k is the rate constant, and τ_p is the particle residence time (equation 11). Therefore, it is important to understand these factors in order to predict column flotation performance.

The mixing behaviour of the collection zone is usually represented by a dimensionless vessel dispersion number, N_d. The vessel dispersion number is a indication of the degree of mixing. It will lie between the two extremes of mixing: plug flow, and perfect mixing. Plug flow is defined as all particles having the same residence time, therefore creating a concentration gradient of floatable particles along the vertical axis of the column. Perfect mixing is defined as a distribution of particle resident times, therefore the

concentration of floatable particles is homogeneous throughout the length of the collection zone (Dobby and Finch, 1986-b). The mixing conditions for laboratory scale columns approaches plug flow conditions, while for plant columns they are between plug and homogeneous flow regimes. The vessel dispersion number is given by (Yianatos et al., 1988):

$$N_d = \frac{E_d}{H_{col}\,(V_l + V_{p,\infty})} \qquad (22)$$

where E_d is the axial dispersion coefficient, which describes the turbulent eddies, and diffusion conditions. For plug flow, the axial dispersion coefficient is equal to zero, and equation (20) can be rewritten as:

$$R = 1 - \exp^{-k\tau_p} \qquad (23)$$

where τ_p is the particle retention time.

For perfect mixing, the axial dispersion coefficient is equal to infinity, and equation (20) can be rewritten as:

$$R = \frac{k\,\tau_p}{1 + k\,\tau_p} \qquad (24)$$

Liquid residence times can be measured by injecting a tracer pulse along with the feed. Using the distribution of these residence times (RTD), a mass transport equation can be developed to describe tracer concentration C, at an axial

distance x from the injection point, with respect to time, as follows (Mavros et al., 1989):

$$E_d \cdot \frac{\delta^2 C}{\delta x^2} = \frac{V_l}{(1-\varepsilon_g)} \cdot \frac{\delta C}{\delta x} + \frac{\delta C}{\delta t} \qquad (25)$$

This allows the axial dispersion coefficient to be quantified for specified flow rate conditions.

With the drift-flux relationships defined, the effects of the mixing process, and flow rates can be investigated. As can be seen from these relationships, the effect of increasing the gas flow rate is opposite to the effect of increasing the liquid flow rate. An increased gas flow rate will create a more turbulent regime, while increasing the liquid flow rate will allow the column to approach a plug flow regime (Mavros et al., 1989), although the latter may overload the column capacity.

One model proposed for the mixing conditions of columns is a series of 'mixed zones'. Figure 2.5 shows a schematic of this model. It involves two parameters: the number of zones, N_d and the ratio of backflow (from one zone to the previous one) to net liquid flow, λ. The backflow parameter, λ is an indication of the degree of mixing, with the degree of mixing increasing proportionally with the value of λ. The major advantage of this form of modelling is its structured record of the column contents (Mavros et al., 1989).

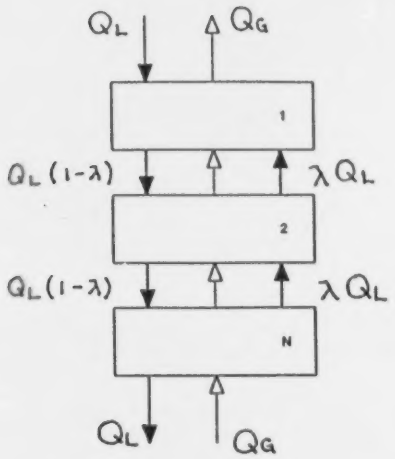

Figure 2.5 Schematic diagram of a N_d mixed zones model (adapted from Mavros et al., 1989).

2.1.3 CARRYING RATE

The carrying rate is dependant on the bubble surface area rate and the solids loading per unit area of bubble (Finch and Dobby, 1990). For a given gas rate and bubble loading, there is a certain mass rate that can be carried. The carrying rate, C_r is defined as: the mass of solids per unit time per unit column cross-sectional area. The carrying rate can be expressed by:

$$C_r = K_1 \frac{\pi d_p \rho_p V_g}{d_b} \qquad (26)$$

where: K_1 is the fraction of the bubble surface area covered by a monolayer of particles.

The theoretical maximum carrying rate, $C_{r,max}$ can be expressed for either: a given gas rate, V_g and the minimum bubble diameter $d_{b,min}$ under those conditions, or for a given bubble diameter, and the maximum gas rate, $V_{g,max}$ for that bubble size, as follows:

$$C_{r,max} = \frac{\pi}{2} \frac{d_p \rho_p V_g}{d_{b,min}} = \frac{\pi}{2} \frac{d_p \rho_p V_{g,max}}{d_b} \qquad (27)$$

The maximum carrying rate allows the operator to choose the optimum conditions, depending on product specifications. For example, the grade increases as the column becomes carrying capacity limited (bubbles are almost completely loaded, therefore only the fast floating fractions will be preferentially captured). This allows for some degree of selectivity in the collection zone.

2.2 FROTH ZONE

The use of wash water provides two important benefits to column flotation: entrained particle are removed from the froth, at the same time the froth is stabilized. The froth zone in flotation columns prevents the entrainment of hydrophylic particles by maintaining a net downward flow (bias) of water across the interface (Yianatos et al., 1986). The bias water also continuously replaces the naturally draining water film surrounding the bubbles, which promotes froth stability. This fact is shown by the increased froth depths possible in column flotation (Finch and Dobby, 1990). A stable froth is required to carry the particles to the collection point (Espinosa-Gomez et al., 1988-b). Bubble coalescence can cause operating problems, that need to be addressed. A method of quantifying coalescence, using the

changes in gas holdup and calculated bubble diameter was developed by Espinosa-Gomez, Finch, and Bernert, 1988.

2.2.1 FROTH STRUCTURE

The size distribution changes as the distance from the froth-collection interface increases, due the coalescence of bubbles. Using photographic techniques, it was determined that the mean bubble diameter did not vary significantly from the collection zone to the froth zone (Pal and Masliyah, 1989). However, as the distance from the interface increased, the bubble bed changed from an expanded bubble bed (where all of the bubbles are of a uniform size), to a packed bubble bed. A packed bubble bed (where bubble coalescence is beginning) is a very efficient method of preventing or minimizing entrainment (Dobby and Finch, 1986). It leads to a wider distribution of bubble sizes, skewed towards larger sizes (Yianatos et al., 1986). As the distance from the interface increases, larger bubbles start to form, it is more closely approximated by a gamma distribution (Yianatos et al., 1986). The froth structure is shown in figure 2.6.

2.2.1.1 ENTRAINMENT AND CLEANING MECHANISMS

One model proposed to characterize the entrainment and cleaning mechanism was developed by Yianatos, Finch and Laplante, 1987. It is based on the worst case scenario: feed water entrainment. The entrainment factor X_f, represents the mass percentage of the feed water entrained in the froth water. It can be expressed as follows:

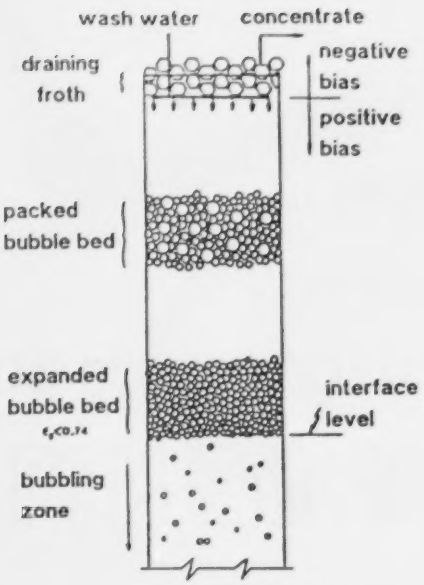

Figure 2.6 Froth structure (adapted from Yianatos et al., 1986).

$$X_f(z) = \frac{\left(\int_0^x C_{(t,z)}\,dt\right)\cdot Q_f \cdot 100}{W_{tr}} \qquad (28)$$

where: $C_{(t,z)}$ is the tracer concentration, in the froth zone at level z and time t. W_{tr} is the total mass of tracer added to the feed, and Q_f is the volumetric feed rate. Tracer concentration was related to its conductivity, K, using a corrected conductivity profile. The measured conductivity profile needed to be normalized to zero gas holdup conditions, in order to see the tracer conductivity, as shown below.

$$C_{(t,z)} = f\,[K_{(t,z)}] = f\left[\frac{K_{(0,z,0)}}{K_{(0,z,\varepsilon_g)}}\cdot K_{(t,z,\varepsilon_g)}\right] \qquad (29)$$

The effects of gas rate, bias rate and froth depth can now be analyzed in terms of feed water entrainment in the froth zone. The results from this study are as follows. The effect of increasing the gas rate, while holding all other parameters constant, increases the feed water entrainment, especially near the interface. Bias rate has two opposing forces at work in the froth zone. The advantage of increasing the bias rate (cleaning) is offset by the increased mixing in the froth attributed to wash water. For example, high bias rates will increase the liquid recirculation, channelling and bubble coalescence near wash water outlet. This will also lead to higher liquid holdup in froth due to the higher wash water flows required. These mixing conditions become even more critical at low froth depths (less than 50 cm). Therefore, lowering the bias rate will still provide efficient cleaning. Overall, the gas rate and froth depth have more significant effects on the cleaning action than bias rate.

One method of quantifying the cleaning efficiency is to use a mass transfer approach. Figure 2.7 shows a schematic diagram of the modelling parameters.

This approach allows the contamination of the froth by feed water to be simulated, and determines the number and height of transfer units, to determine average cleaning factor CF (slope of the operating line). Figure 2.8 shows the graphical determination of transfer units. Cleaning becomes progressively more difficult from the interface to the overflow, as seen by the increasing amount of transfer units. The main cleaning action occurs near the interface (within 10 cm) for moderate gas rates.

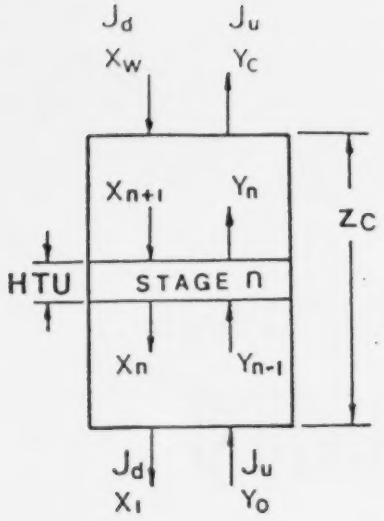

Modelling parameters for the froth cleaning in counter-current bubble bed (test L_2; J_g=1.8 cm/s). Symbols: HTU - height of transfer unit, J_d and J_u - superficial downward and upward flow rates, X_n - solute concentration in downward flow at stage n, X_w - initial solute concentration in wash water, Y_n - solute concentration in upward flow at stage n, Y_c and Y_0 - solute concentrations at concentrate and interface level.

Figure 2.7 Height of a transfer unit modelling of the froth zone (adapted from Yianatos et al. 1987).

2.2.1.2 BUBBLE COALESCENCE AND FROTH COLLAPSE

Bubble coalescence in collection zone is not related to froth stability, as both collection and froth zones have different dominating forces. In the collection zone bubble coalescence predominates, while in the froth zone bubble film stabilization prevails. This is evident from the fact that a froth may continue even with intense bubble coalescence in the collection zone (Espinosa-Gomez et al., 1988-b). The mechanisms of coalescence and froth collapse are slowed down by the use of frothers.

A new method of quantifying bubble coalescence in the collection zone is presented by Espinosa-Gomez, Finch, and Bernert, 1988. By monitoring the changes in gas holdup in the collection zone, coalescence and increased bubble diameter can

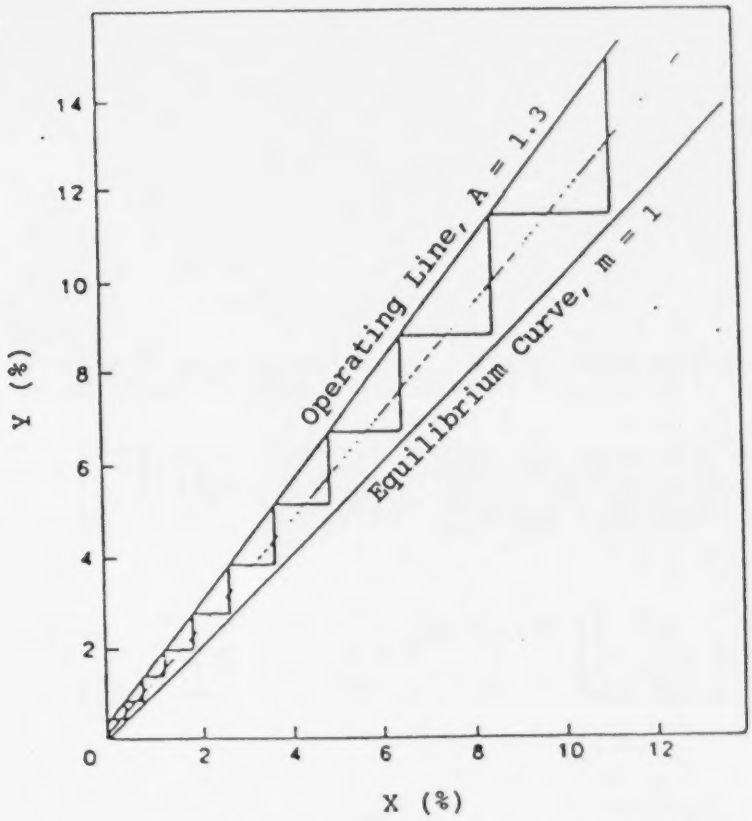

Figure 2.8 Graphical determination of transfer units and cleaning factor (adapted from Yianatos et al., 1987).

be quantified. For a constant gas rate and chemical environment, decreasing the gas holdup indicates an increasing bubble diameter, and therefore coalescence.

Coalescence and froth collapse is promoted by the overabundance of fatty acid (collector), and the presence of fine dispersed hydrophobic solids. Both of these will compete with the frother at the bubble surface, creating a hydrophobic coating on the bubble which leads to the drainage of the water film. The presence of a chemical dispersant will further amplify coalescence and collapse.

2.2.2 FROTH CARRYING CAPACITY

Similar to the mass carrying rate for the collection zone, the carrying capacity, C_a is dependant on bubble surface area, and solids loading. It can be expressed as:

$$C_a = K_1 \frac{\pi \rho_p d_p V_g}{d_{b0}} \qquad (30)$$

where d_{b0} is the bubble diameter at the top of the column. The carrying capacity becomes a more relevant parameter, than the corresponding carrying rate of the collection zone, since the overall capacity will be limited by the froth zone capacity (i.e. $d_b < d_{b0}$). Beyond a certain maximum gas rate, the relationship will degrade (Espinosa-Gomez et al, 1988-d). As with the collection zone, the bubble diameter in the froth zone can be related to the gas rate as follows:

$$d_{b0} \propto V_g^q \qquad (31)$$

where q is greater than 0.25. Thus equation (30) becomes:

$$C_a = K_1 \pi \rho_p d_p \, [V_g^{(1-q)}] \qquad (32)$$

This model predicts a linear relationship between the carrying capacity and the product of particle size, $d_{p,80}$ and density ρ_p. This model is valid only for the parameter ranges tested (Finch and Dobby, 1990). The upper limits on particle size, and column diameter for this model have not been found. Carrying capacity does not seem to be affected by the column diameter ($d_c \leq 100$ cm). This may be because there are much

better flow characteristics, compared with the dryer cell flotation froths. As well, the froth is allowed to overflow over the entire diameter of the column. The overflow lip length to area ratio does not become a performance controlling parameter for the current range of column diameters (Finch and Dobby, 1990). For initial design purposes, this model will give a reasonable estimate of the carrying capacity. Another method of estimating the froth carrying capacity is to increase the feed solids rate until the percent solids in the concentrate reaches a maximum value (Espinosa-Gomez et al., 1988-c).

The bubble residence time in a column is much longer than that of a conventional flotation cell, which means that the bubble surface area may be completely covered with particles when they reach the interface level. Therefore due to the cleaning action, there may be some degree of particle recycling between the froth and collection zones. Thus the total column recovery, R_T can be written in terms of the recoveries of the collection (R_{col}) and froth (R_{fr}) zones. Assuming that the recycled portion is included in the collection zone recovery, a relationship can be developed as follows (Dobby and Finch, 1986-b):

$$R_T = \frac{R_{col} \cdot R_{fr}}{1 - R_{col}\,(1 - R_{fr})} \qquad (33)$$

This relationship allows the amount of particles recycling back from the froth to be quantified. This in turn can be used to define the maximum carrying capacity.

2.3 CONTROL, MODELLING AND SIMULATION

There are two forms of control strategies: stabilizing and optimizing. Stabilizing control will keep the operating conditions stable with respect to the interface level and bias rate. Optimizing control strategies go one step further. The optimal conditions (grade and recovery) are defined by economics, and then the system is stabilized to achieve these objectives. In order to operate the column at the optimum economic conditions, the column will be at or near "overload" conditions. This will make performance more sensitive to fluctuations in the feed (Finch and Dobby, 1990). Therefore, prior modelling and the control strategy become integral components to column flotation operations.

One of the most important aspects of any model or control scheme is knowing the interactions that occur when a control variable is changed and the other control parameters are held constant. This information can be organized in terms of a process control matrix. Figure 2.9 shows a process control matrix for some of the important design parameters in column flotation.

2.3.1 ZONE INTERACTION

The behaviour of the collection and froth zones can be inter-related using the drift-flux analysis model. Assuming that the gas holdup is radially uniform for the cross-section, and the wall drag effects are negligible, it can be shown that the drift-flux divided by terminal bubble velocity (V_∞) can be represented by some function of the gas holdup. Equation 3 shows the general form of the drift-flux equation for the flotation column.

MANIPULATED VARIABLES	CONTROLED VARIABLES						
	Level	Froth Depth	Bias Rate	% Solids in Conc.	Gas Holdup	Grade	Recovery
WW Rate	+ S	- S	+ F	- M	+ S	+ - F	- + S
Tails Rate	- F	+ F	+ F		+ M	+ S	- S
Gas Rate	+(-) F	-(+) F	- S	- S	+ - F	- M	+ - M
Frother Dosage	+ - S	- + S	- S	- S	+ M	- S	+ S
Feed Rate	+ F	- F	- F	+ S	+ S	+ S	- S

+ control variable increased with increase in manipulated variables
- control variable decreased with increase in manipulated variables

Response speed: S slow; F fast; M moderately fast; blank no respose
( ) steady state response if different from dynamic response

Figure 2.9 Process control matrix (adapted from Finch and Dobby, 1990).

Providing that the bubbles behave as solid particles, one can estimate 1-m equal to 2.39. The drift flux can be determined experimentally by measuring the superficial gas and liquid velocities (flux), and the gas holdup (Pal and Masliyah, 1989).

Gas holdup can be determined using pressure differentials, for both the collection and the froth zones. The gas flux for the column is calculated from the known air flow rate, and divided by the cross-sectional area of the column. The liquid flux, however, must be determined separately for both zones, and then a net liquid flux can be

determined. For the collection zone, the liquid flux is calculated from the tailings flow rate divided by cross-sectional area.

For the froth zone, there are two components of liquid flow: the liquid that drains downward through the bubbles, due to gravity, and the entrained liquid that is carried upwards by the rising bubble bed. The rate of liquid drainage relative to a simultaneously rising bubble bed, $V_{dg}=-V_{gl}$, gives the relative velocity between the gas and liquid (Pal and Masliyah, 1989). The drift-flux for the froth zone then becomes:

$$V_{gl} = -V_{dg}\,\varepsilon_g\,(1-\varepsilon_g) \qquad (34)$$

Combining equations (34) and (35) gives the net liquid flux for the froth zone as:

$$V_l = \frac{V_g}{\varepsilon_g}\,(1-\varepsilon_g) + V_{dg}\,(1-\varepsilon_g) \qquad (35)$$

where: $V_g/\varepsilon_g(1-\varepsilon_g)$ is the upward liquid flux, and $V_{dg}(1-\varepsilon_g)$ is the liquid drainage flux, and V_l is the net liquid flux in the froth zone. Another method of calculating the net liquid flux in the froth zone, is by doing a water balance around the sprinkler system:

$$Q_{net} = Q_{conc} - Q_{ww} \qquad (36)$$

By dividing through by the column cross-sectional area, A_c, the net liquid flux can be calculated as:

$$V_l = \frac{Q_{net}}{A_c} = \frac{Q_{conc} - Q_{ww}}{A_c} \qquad (37)$$

Using the drift-flux relationships, the flow and holdup behaviours of the collection and froth zones can be inter-related (Pal and Masliyah, 1989). The performance level of the column will change, (according to the relationships developed above) for variations in the following operating parameters: V_g, V_l, and Q_{ww}. Knowing these inter-relationships, therefore allows the operating procedure to be optimized for any given situation.

2.3.2 CONTROL STRATEGIES

A summary of currently operating control methods, as well as a discussion of new methods based on temperature or electrical conductivity profiles within the froth zone will be presented. The four main objectives for a control system are (Moys and Finch, 1988):

1. To maintain the interface at a set level. If the level is too high, the froth volume will be insufficient to maintain the cleaning action, therefore decreasing the grade. If the level is too low, the collection zone volume may be insufficient to allow maximum recovery.

2. A positive bias rate must be maintained. However, there is an upper limit, beyond which there is very little improvement in the washing efficiency. Going beyond this limit will only serve to dilute the tailings stream.

3. Control of the bubble size through frother addition. If the bubble size is too large, the surface area and therefore the carrying capacity is reduced for the same gas rate. The lower limit on bubble size is imposed by both the maximum gas rate for a given bubble size and the economics of increased frother addition.

4. The gas rate must be set at a level that maximizes recovery. If the gas rate is too high, the gas holdup will increase, which will either decrease the slurry residence time or increase the bubble size. Either way it will result in a loss of recovery. Another adverse effect of very high gas rates is the increased turbulence in the collection zone which could prevent efficient recovery. This may also carry over into the froth zone, increasing entrainment and reducing the overall grade.

The third and fourth objectives can be achieved by the manipulation of the frother dosage and the gas rate. Frother dosages are usually pre-determined with bench scale cell flotation, and then modified as needed. The gas rate can be manipulated to maintain a certain gas holdup, within practical operating limits (Moys and Finch, 1988).

There are two controls presently in use to achieve the first two control objectives. They are shown schematically in figure 2.10. The first method involves setting the wash water rate to maintain a set grade point, and then manipulating the tailings flow rate to control the interface level and bias rate. The second method is somewhat more complex, as there are two control variables. The wash water rate is manipulated to maintain a set interface level. Then by measuring the feed rate, and keeping the tailings rate higher, a positive bias can be maintained. There are two ways of controlling the bias

rate: either maintain a constant bias ratio, BR or constant bias rate, Q_B:

$$BR = \frac{Q_t}{Q_f} \quad or \quad Q_B = Q_t - Q_f \tag{38}$$

This strategy tends to create internal looping within the control system, since one control variable (wash water or tailings rates) is used to control the parameter that the other's influence will dominate. For example, the tailings rate is used to control bias rate, and wash water rate is used to control the interface level (Moys and Finch, 1988).

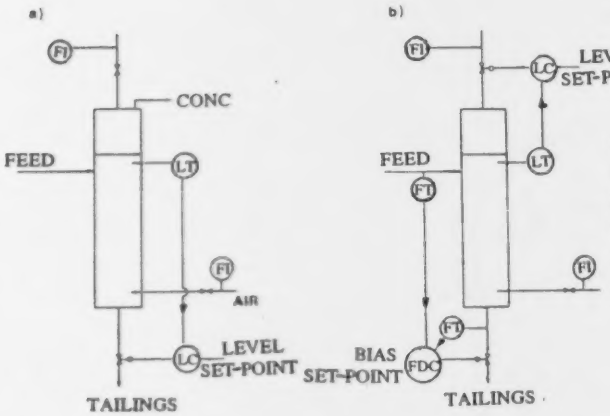

Symbols: FDC - flow difference controller (or FRC flow ratio controller); FT - flow signal transmitter; FI - flow indicator; LT - level signal transmitter; LC - level controller.

Figure 2.10 Stabilizing control schemes currently in use: a) level control and b) level and bias control (adapted from Finch and Dobby, 1990).

One disadvantage of both of these control strategies is that they are based on inaccurate or inferred measurements of bias flux and interface level. For example, the bias rate is assumed to be a good measure of the bias flux, however in cases of high solids removal in the concentrate, the bias

flux, V_B can be positive even when the calculated bias rate is negative, as shown below:

$$Q_{B_{est}} = Q_t - Q_f = Q_{ww} - Q_{conc}$$
$$Q_{B_{act}} = A_c V_B + \frac{Q_{conc}\chi_{conc}}{\rho_{p,conc}} \qquad (39)$$

Also the estimation of bias rate tends to propagate error. Any error in measuring two large and nearly equal flow rates (feed and tailings), will tend to be magnified in the bias rate estimation.

In summary, the control of flotation columns must consider both economics, and stability in operating conditions. The operating limitations imposed by operating in the bubbly flow regime (maximum gas rate, minimum bubble diameter), as well as feed characteristics (maximum grade and recovery) and mechanical limitations will determine the maximum carrying capacity (recovery), and the maximum cleaning rate (grade). By controlling the tailings rate, and maintaining the gas and wash water rates within the operating limits, stable operating conditions can be achieved. Economic requirements can be achieved to some degree by manipulating the gas and wash water rates, to control grade and recovery. In order to achieve the objectives, some control strategy must be put in place. The control strategies described above meet the basic control requirements, although there may be some inaccuracy due to measurement techniques and/or assumptions.

2.3.3 COLUMN FLOTATION SCALE-UP

The modelling and scale-up of lab columns to industrial columns utilizes kinetic data, mixing characteristics, and

carrying capacity (Dobby and Finch, 1986-b). The two zones are first modelled separately (as described above) and then combined to give an overall picture.

During scale-up procedures, from laboratory scale to industrial scale flotation columns, a number of observations can be made. Firstly, the mixing characteristics are quite different. Laboratory columns approach plug flow, while industrial columns operate somewhere between plug flow and completely mixed flow regimes. The mixing characteristics can be quantified using the vessel dispersion number, N_d, dispersion coefficient, E_d, and the mean residence time, τ. The two mixing parameters N_d and τ can be determined from either: experimental residence time distributions (RTD); or from a given column diameter, d_c, slurry feed rate, V_l, and gas rate, V_g. The RTD for the column can be determined experimentally, by injecting a tracer pulse in the feed stream and then measuring the tracer concentration over time in the tailings stream. Note the dispersion coefficient for solids are assumed the same as for liquid. The dispersion coefficient E_d is linearly dependant on the column diameter, as shown below:

$$E_{d,l} = E_{d,p} = 0.063\, d_c \left[\frac{V_g}{1.6}\right]^{0.3} \qquad (40)$$

From this equation, it can be seen that increasing the gas rate will result in an increased dispersion coefficient. The rate constant will also increase, but so will the mean bubble diameter which leads to a decreased collection efficiency. The net result is a maximum gas rate (based on k versus V_g).

Another observation, is that the gas hold up is not uniform radially for small diameter columns. The terminal bubble velocity, equation (6) can be modified to account for this fact, using two distribution coefficients, K_o and C_o (Dobby et al., 1988),:

$$V_\infty K_o = \frac{V_g}{\varepsilon_g(1-\varepsilon_g)^m} - C_o\frac{(V_g+V_l)}{(1-\varepsilon_g)^m} \qquad (41)$$

The coefficients can be determined by holding gas velocity constant, measuring gas holdup for varying liquid velocities. The slope is C_o, and the intercept is $V_\infty K_o$ for the plot of $V_g/\varepsilon_g(1-\varepsilon_g)^m$ versus $(V_g+V_l)/(1-\varepsilon_g)^m$. For large diameter columns, the distribution coefficients are assumed as equal to one. With this modification, large and small diameter columns can be compared.

Another area of interest is the optimal geometry of flotation columns. Based on three geometry dependant factors: degree of mixing N_d, volumetric bias and gas rates, Q_B and Q_g, the ratio of collection zone height, H_{col} to column diameter, d_c can be evaluated with respect to performance (Yianatos et al., 1988). Each of these factors will affect the overall performance of the column. Variations of the height to diameter ratio (H:D) will give the same retention times. However, the gas and bias rates will change as the diameter (and cross-sectional area) change. Mixing characteristics will also be affected by changing the ratio. Both the height and diameter will affect the mixing characteristics. Equation (22) shows that the vessel dispersion number, N_d is inversely proportional to the collection zone height, H_{col}, and directly proportional to the dispersion coefficient, E_d, which has been

empirically related to column diameter for a range of industrial column geometries as follows:

$$E_d = 0.063\, d_c \quad where; \quad \begin{array}{l} 50 \le d_c \le 100 \ (cm); \\ 10 \le H_{col} \le 12 \ (m); \\ 150 \le Q_f \le 600 \ (L/\text{min}) \end{array} \qquad (42)$$

By holding the volume of the collection zone constant, as well as the superficial gas and bias rates, the following conclusions can be drawn:

1. There is a trend towards increased recovery for increasing H:D ratios. There are three reasons for this increase: mixing characteristics, liquid and particle residence times. The mixing becomes less turbulent, due to the N_d decreasing both directly (equations 22 and 43) and indirectly due to increase in V_l for smaller cross-sections. The liquid residence time τ_l will increase, since volumetric bias rate, Q_B decreases as cross-section decreases. In addition, the particle residence time τ_p increases faster than τ_l (i.e. $\tau_p:\tau_l$ increases) due to the increasing V_l (equation 11).

2. As the H:D ratio continues to increase, the volumetric gas rate will continue to decrease, and the maximum carrying capacity of the gas will be reached, and therefore an upper limit is placed on the ratio. The upper limit imposed by the carrying capacity will be further reduced with decreasing particle size, and increasing feed pulp density and mineral content.

3. A lower limit on the H:D ratio is imposed by the increased mixing and the declining performance of the volumetric bias rate.

Figure 2.11 shows the effect of the H:D ratio on recovery, vessel dispersion number, and solids residence time, for a constant collection zone volume and feed rate. From this information, it can be seen that performance increases as the ratio increases, however these improvements start to level off. In addition, the carrying capacity becomes a factor. Figure 2.11 refers to a column, that is beneath its maximum solids carrying capacity, however if the H:D ratio continues to increase, while holding the gas and feed flow rates the same, the maximum carrying capacity will be reached, the performance will decline.

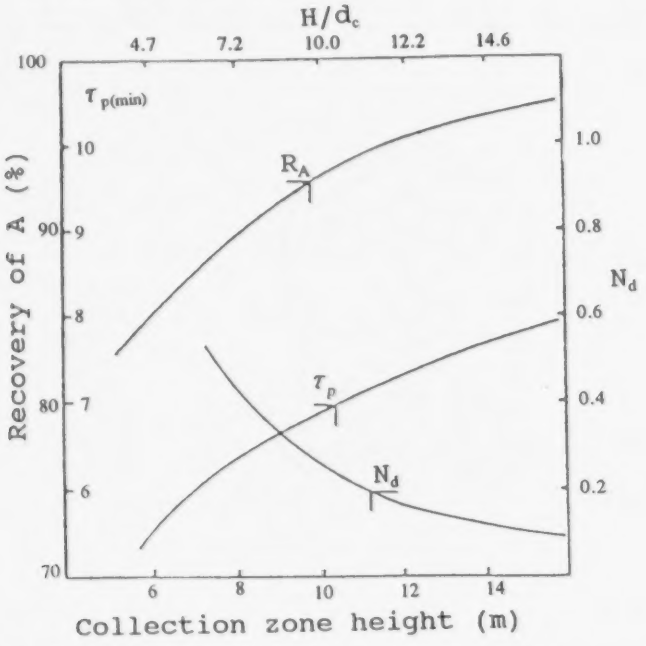

Figure 2.11 Effect of H:D and collection zone height on the recovery, vessel dispersion number, and mean particle residence time (adapted from Yianatos et al.,1988).

Figure 2.12 shows the relationship of grade and recovery, with respect to feed rate, and the H:D ratio. For typical operating conditions, a H:D ratio of approximately 10:1 is found to be ideally located between the upper and lower limits described above (Yianatos, et al., 1988).

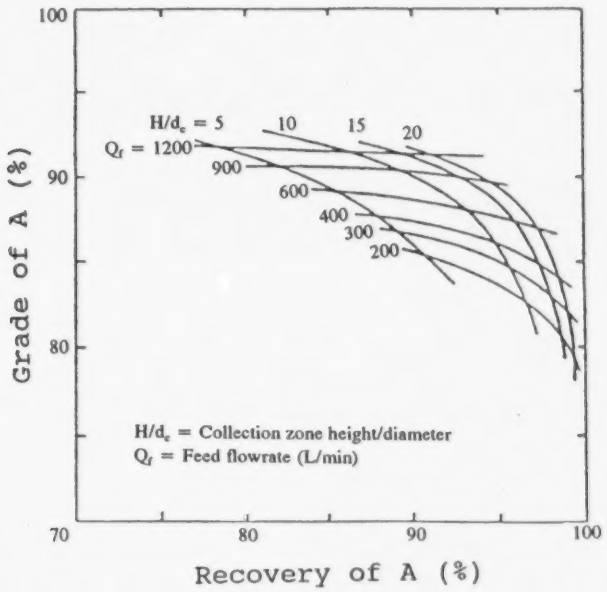

Figure 2.12 Grade-recovery relationship with H:D ratio and feed rate (adapted from Yianatos et al., 1988).

3.0 EXPERIMENTAL

3.1 EQUIPMENT SETUP

Figure 3.1 shows the schematics of the laboratory flotation column set-up used in this project. The column was setup to operate on a semi-continuous basis, under manual control (Ofori, 1988). The column is 3.6 m in height with an inside column diameter of 6.35 cm. It is made of transparent lucite to permit visual observations during experiments. The equipment setup consists of a 370 ℓ baffled feed tank, equipped with a large mixer and a recirculating moyno pump to keep the particles in suspension.

The feed slurry was pumped from the feed tank into the column using a variable speed moyno pump. The feed stream enters the column at approximately two thirds the height (2.6m). The feed flow rate is measured volumetrically using a magnetic flow meter with a range of 0 to 8 ℓ/min. The flow meter is located on the outlet line of the feed pump. Calibration of the flow meters on the feed, wash water, and gas streams were detailed by Ofori, 1988.

Frother was injected directly into the feed line using a Ruska piston pump. A specific frother flow rate is achieved by shifting gears on the pump. Using the first gear range, flow rates between 2.5 and 8.75 mℓ/hr can be achieved. This translates to frother concentrations between 14 and 49 ppm based on a feed slurry flow rate of 3.0 ℓ/min. The collector was added directly to the feed tank before each experimental run.

The wash water stream enters through a spray nozzle located one to two centimeters below the overflow lip.

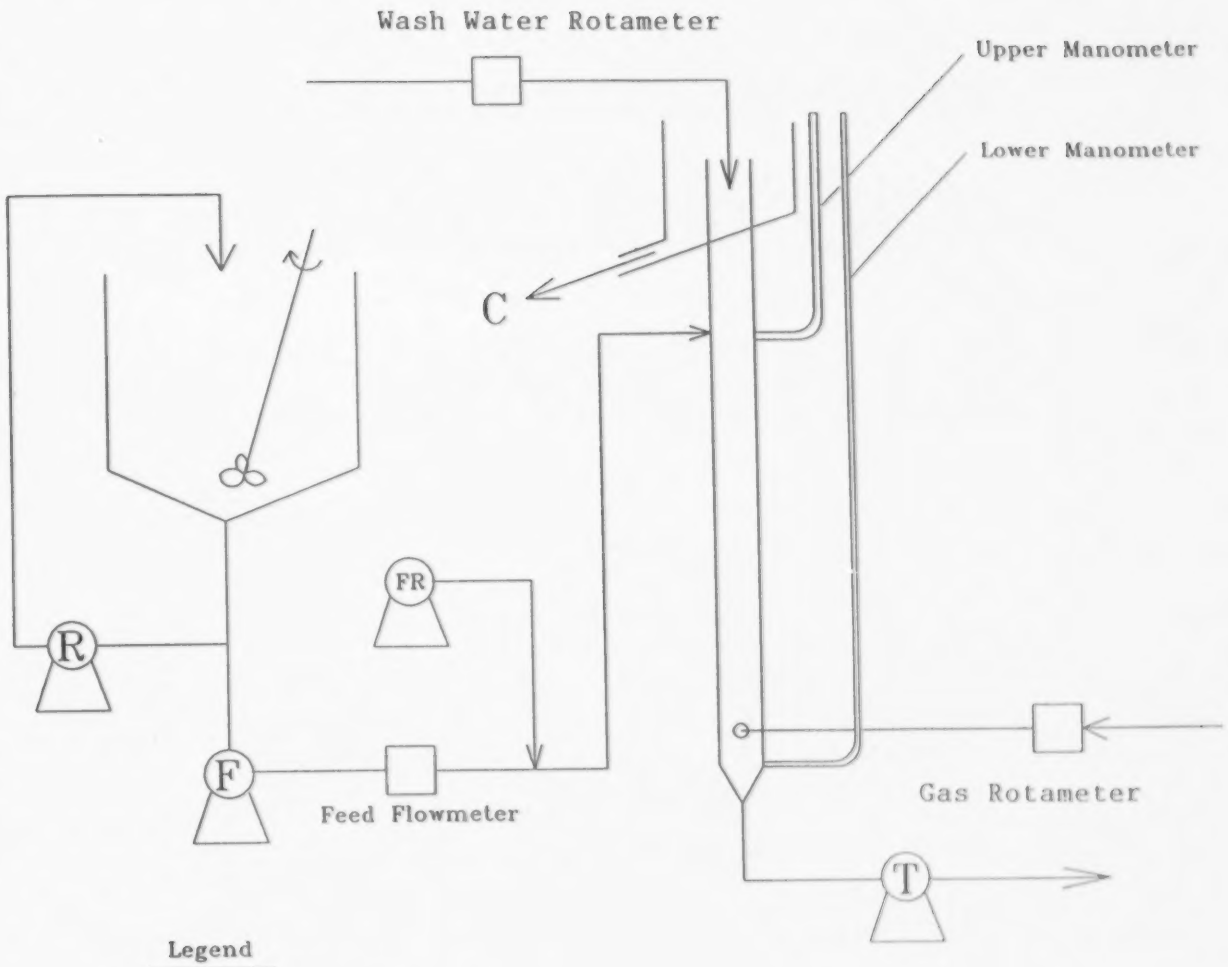

Legend

R: Recirculating Pump
F: Feed Pump
FR: Frother Pump
C: Concentrate
T: Tailings Pump

Figure 3.1 Flotation column set-up.

Edmonton tap water was used for all column experiments. The wash water flow rate is measured volumetrically with a rotameter calibrated between 0 and 2 ℓ/min.

The gas stream enters the column through a porous steel sparger located near the bottom of the column. The sparger is 25 mm in length by 15 mm diameter, with an air inlet diameter of 3.2 mm. The average pore size is 2 μm. The gas flow rate is measured volumetrically by a rotameter calibrated between 0 and 2.4 ℓ/min at standard temperature and pressure (STP).

The tailings are pumped from the bottom of the column using a variable speed moyno pump. The concentrate stream overflows from the column into a launder. The concentrate and tailings flow rates can be estimated either by timed samples taken at their exit point from the column or calculated from the material balances after the experimental analysis.

3.1.1 MATERIAL BALANCES

There are three material balances to be considered for the column: ash, percent solids, and the overall balance. Figure 3.2 shows a schematic diagram of all the input and output streams for the system.

The overall material balance for the column can be written as:

$$Q_f + Q_{ww} + Q_{(g,in)} = Q_t + Q_c + Q_{(g,out)} \qquad (43)$$

where: Q denotes the mass flow rate and f, ww, t, c, and g indicate the feed, wash water, tailings, concentrate and gas

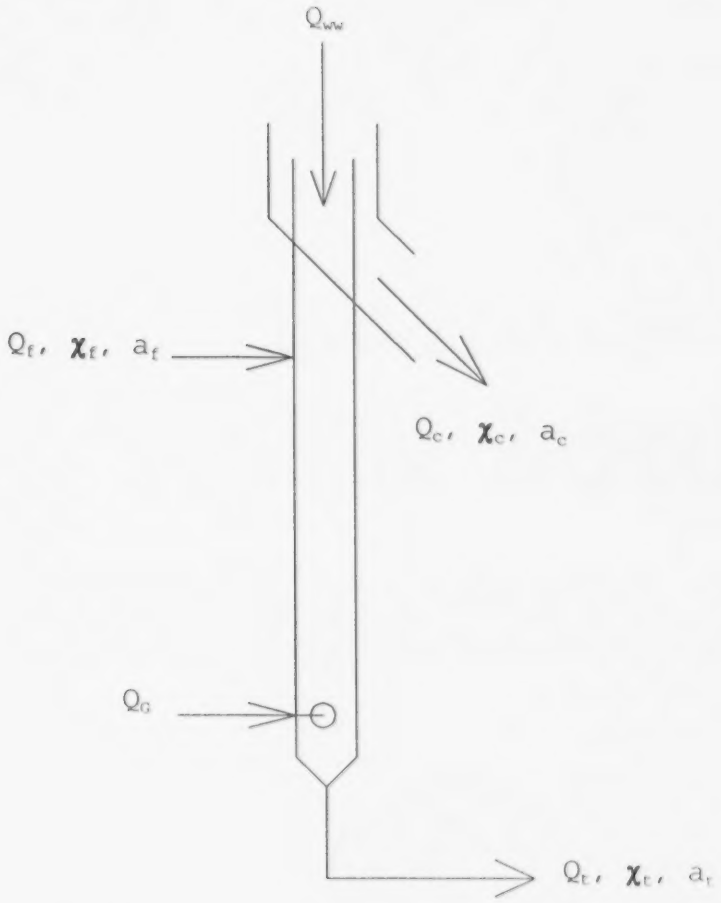

Figure 3.2 Material Balances around the column.

streams respectively (Note: $Q_{g,in}=Q_{g,out}$). The solids balance is written as:

$$Q_f * \chi_f = Q_t * \chi_t + Q_c * \chi_c \qquad (44)$$

where: χ_f, χ_t, and χ_c denote the solids fraction in the each of the corresponding stream.

The ash balance is written as follows:

$$Q_F * a_F = Q_T * a_T + Q_C * a_C \qquad (45)$$

where: a_i is the percent ash in the corresponding stream i.

3.1.2 GAS HOLDUP AND INTERFACE LEVEL

The gas holdup of the column was measured by the two manometer method. The first manometer is located just below the sparger inlet and the second is located just above the feed inlet. The length between the starting point of each manometer is defined as ΔL. The height difference between the two level readings is defined as Δh. The average gas holdup, ε_g, for the collection zone is calculated using equation 1.

The interface level of the column was measured using the first manometer. This method gives the hydrostatic head and will need to be divided by $(1-\varepsilon_g)$.

3.2 SAMPLE ANALYSES

3.2.1 FEED SAMPLE PREPARATION

A sample of approximately 1 tonne run-of-mine (ROM) coal was received from Smokey River Coal Limited on March 7, 1991. The coal is a low volatile bituminous coking coal, with an average ash content of 14% ranging from 12% to 16%. The mean density is 1.35 g/cm^3. The entire coal sample was ground down to -50 mm to facilitate better handling, and then split using the riffler into four representative samples (approximately 250 kg each). This particle size was chosen since it is still above the mechanically imposed particle size limit. Two of these samples were further ground to represent the coarse (d_{50}

= 250μm) and the fine (d_{50} = 35μm) size distributions (qualitatively defined). The remaining material was stored as spare feed material.

Both of the feed coal samples was analyzed for particle size and ash distribution. Two size analysis techniques were used: microtrac (light scattering technique), and wet sieving. The sieving technique requires a significantly larger sample, and therefore is more statistically accurate. The disadvantages of sieving are: it requires more work and the minimum particle size measurable is 38 μm. The microtrac is limited by an upper size limit of 1000 μm. Screen and microtrac analysis were combined to obtain a complete size range of the coal samples.

The fine particle size distribution has a maximum particle size of 300μm, with d_{80} and d_{50} sizes of 75μm and 35μm. Figure 3.3 shows the particle size distribution for the fine sample. The sample was ground down to a passing size of approximately 300μm in two grinding steps. The first step employed the Holmes Hammermill with a 600μm grate, followed by the Holmes pulverizer with a 250μm slitted grate.

The coarse sample has a maximum particle size of 850μm, with d_{80} and d_{50} sizes of 500μm and 250μm respectively. Figure 3.4 shows the particle size distribution for this sample. The sample was ground down to a passing size of approximately 850μm using two screening and two grinding steps. The first screening step removes the +600μm material. This oversize material is then ground using the Holmes Hammermill with a 600μm grate. The second screening step removes +850μm material from the ground product of the first step. The oversize material from this second screening is further ground using the Holmes pulverizer, with a 250μm slitted grate.

3.2.2 SIZE AND ASH DISTRIBUTION

During each experiment, one feed sample and two samples each from the tailings and concentrate streams were taken. The physical analysis of each sample included: percent ash, percent solids, slurry density, mean particle size and a brief particle size distribution. Below is a brief description of the sample analysis techniques that were used.

Wet sieving was used to separate the samples into size fractions. The wet sieving procedure is detailed in appendix A. The screen sizes chosen were based on the size distribution of the starting feed. The samples from fine experiments were divided into three size fractions: +100, -100+40, and -40 micron size fractions. The screen sizes of 106 and 40 microns approximately correspond to d_{90} and d_{55} of the fine feed (refer to figure 3.3). The samples from coarse experiments were divided into four size fractions: +600, -600+250, -250+75, and -75 microns. These screen sizes correspond to d_{90}, d_{55}, and d_{25} (refer to figure 3.4).

An ash assay was performed on a sub-sample of each size fraction from each sample. The ash assay procedure is described in appendix A. The ash for the whole sample, a_s, is calculated using a weighted average, as follows:

$$a_s = \frac{\sum_i W_i * a_i}{100\ \%} \qquad (46)$$

where: W_i and a_i are the percent weight and percent ash of the size fraction i.

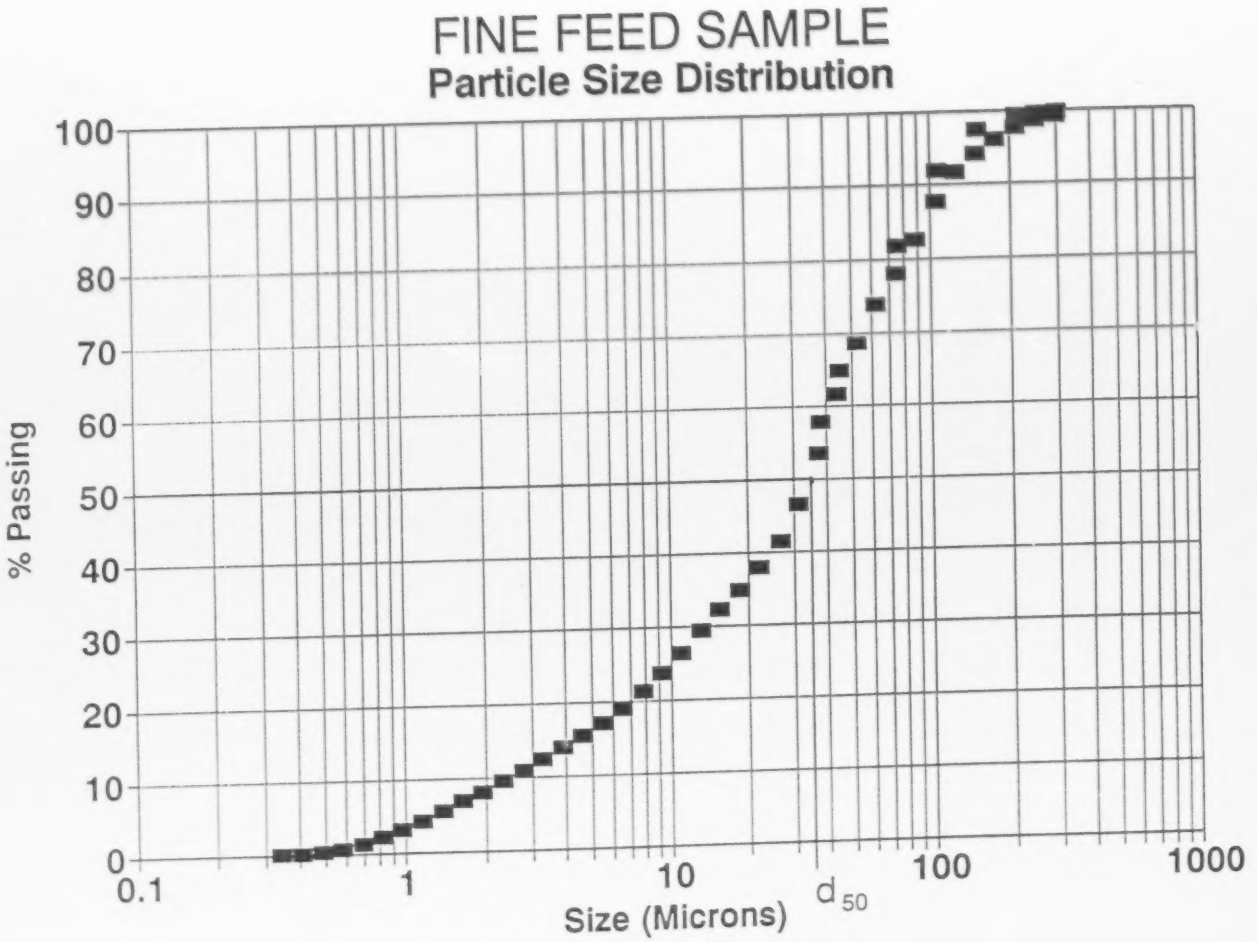

Figure 3.3 Fine particle size distribution.

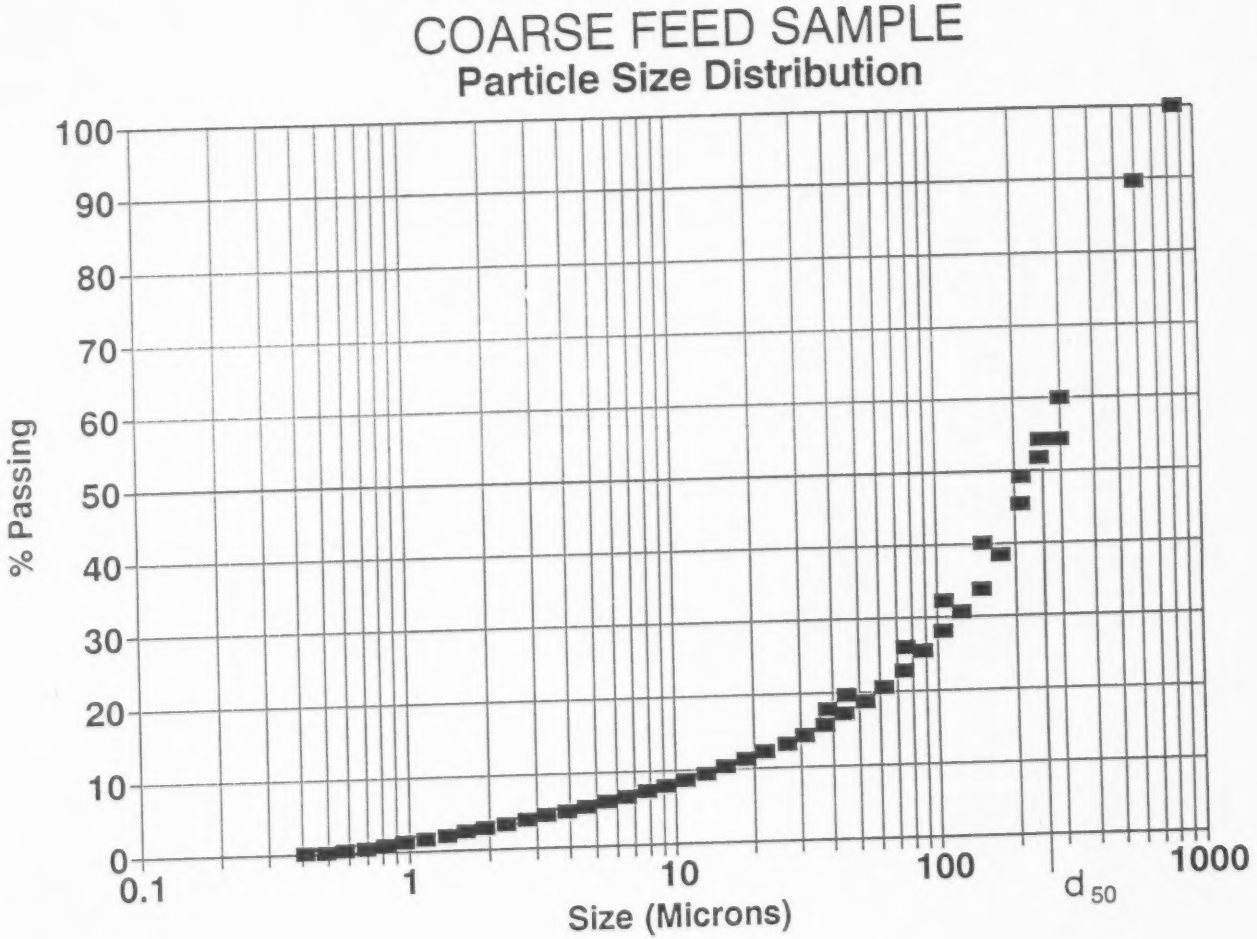

Figure 3.4 Coarse particle size distribution.

3.2.3 YIELD AND GRADE

The yield and concentrate grade will be used to evaluate the performance of the flotation column. Yield is defined as the fraction of the feed that reports to the concentrate launder. Two estimates of yield will be calculated from the material balances. The first yield Y_1, estimates the percent of the feed slurry reporting to the concentrate, and was calculated using the material balance for ash (equation 45), as follows:

$$Y_1\ (\%) = \frac{Q_c}{Q_f} * 100\% = \frac{a_t - a_f}{a_t - a_c} * 100\% \qquad (47)$$

The second yield Y_2, estimates the percent of feed solids that report to the concentrate, and was calculated from the solids fraction in each stream (equation 44), as follows:

$$Y_2\ (\%) = \frac{Q_c * \chi_c}{Q_f * \chi_f} * 100\% = \frac{\chi_c * (\chi_f - \chi_t)}{\chi_f * (\chi_c - \chi_t)} * 100\% \qquad (48)$$

The concentrate grade is defined as the average percent ash of the concentrate stream, as calculated using equation 46. The optimal operating conditions are achieved when the percent yield is maximized, and the concentrate ash content is minimized. A balance must be established between the product grade and the yield since they are inversely preportional. The degree of liberation of ash from coal increases with decreasing particle size. This allows for a lower product ash content, while maintaining a similar yield, as compared with a coarser particle size distribution.

3.3 EXPERIMENTAL DESIGN

In order to have consistent results for all experiments, all input parameters were held constant over each set of experiments, except for the design variables described in the section below.

Percent solids in the feed slurry were made up at approximately 4.5% and 3.5% solids by weight, for the fine and coarse samples respectively. The coarse sample was kept at a lower percent solids because of difficulty in maintaining the solids in suspension. Kerosene was used as the collector, at a dosage of 2ℓ/tonne$_{coal}$. Dowfroth 250 was used as the frother. A feed flow rate of 3ℓ/min or J_f=1.58 cm/s was maintained. The interface level was set and maintained by adjusting the tailings flow rate. The set interface level varied according to the gas flow rate (gas holdup). Except in the case of zero wash water, the tailings flow rate was greater than the feed flow rate to maintain a net downward flow of water or positive bias.

During the course of an experiment two concentrate and tailings sample sets were taken. These sample sets were taken simultaneously. The first sample set was taken when steady state conditions are reached. By dividing the feed flow rate by the average collection zone volume, the *approximate* column retention time of 4 minutes was determined. To reach steady state conditions after operating variables have been changed a period of 12 minutes (based on three residence times) was observed. In addition, a steady interface level was maintained for several minutes before the first sample set and throughout the remainder of the experiment. The second sample set was taken after waiting one full retention time from the time of the first sample. A feed tank sample was taken between the first and second samples, using a tubular sampling device.

3.3.1 DESIGN VARIABLES

The experimental design includes four variables: coal feed particle size distribution, wash water flow rate, gas flow rate, and frother dosage. The effects of the coal size distribution on the performance parameters was investigated. Two particle size distributions qualitatively defined as coarse and fine were used. A relationship between the performance parameters (yield and ash) and coal particle size was developed.

Particle size has effect on many elements of the flotation process. The effects of decreasing the coal particle size include:

1. The probability of mechanical entrainment in the froth increases as particle size decreases, particularly for hydrophylic particles (Kirjavainen, 1989).

2. There will be less middling particles, (greater liberation of coal from minerals) so a lower concentrate ash content is possible.

3. Finer bubbles are required in order to maintain the same particle collection rate (Trahar, 1981).

4. The amount of collector required increases, based on particle surface area. However, larger particles will need to be more hydrophobic to float the same quality of coal particle (Bustamante and Warren, 1984).

These effects were investigated by holding experimental conditions constant, and varying the coal particle size distribution. An individual particle size cannot be investigated, however narrow size ranges can be analyzed. The

overall size distribution of the feed can be varied by controlled grinding procedures. As well, a few operating variables will affect the role of particle size. These variables include: bubble size (mainly controlled by gas rate, gas holdup, and frother dosage), and the degree of particle entrainment in the froth (controlled by wash water flow rate).

The effect of particle size on column flotation performance for variations of three operating parameters were also studied. The operating parameters studied are: wash water flow rate, gas flow rate, and frother dosage. Relationships between operating parameters and coal particle size, and column performance indicators were developed.

The effect of wash water flow rate on the particle size distribution in the concentrate should indicate which particle sizes will preferentially detach under high washing conditions.

Variations in the superficial gas rate and frother dosage will create a corresponding change in the mean bubble diameter (bubble size can be estimated). This in turn should affect the relative rates of flotation for different size ranges. With this information, the optimal bubble size for a particle size range can be determined.

The wash water flow rate was set at four levels 0.0, 0.5, 1.0, and 1.5 ℓ/minute (superficial velocity range: 0.0 cm/s < J_{ww} < 0.79 cm/s). Gas flow rate was set at four levels of 0.5, 1.0, 1.5, and 2.0 ℓ/minute (0.26 cm/s < J_g < 1.05 cm/s). Frother dosage was set at 14, 17, 21, and 28 ppm based on feed flow rate. All other process variables were held constant.

3.3.2 LATIN SQUARES

A latin square is a multilevel, multivariable experimental design (Diamond, 1981 and Lindman, 1990). The use of a Latin Square experimental design was chosen because it allows several multilevel variables to be studied simultaneously, while greatly reducing the number of experiments required compared with a full factorial design. The advantages of this type of design are obvious (time, effort and cost are minimized). The disadvantage is that it assumes that there is no interaction between input variables. For this experiment, the three operating variables gas, frother, and wash water will each have four set levels. The design was repeated for both the coarse and the fine particle size distributions.

This is accomplished by using a fully crossed block design. Each variable will be tested at all the levels of the other two variables. Both other variables will be changed simultaneously, therefore, there are four experiments that correspond to a given variable level. Likewise, each experiment will be used three times, once for each variable.

For example, A_1 (level 1 of variable A) is tested at each level of B and C, although both are changed simultaneously. Each set point (A_1) for each variable will have four (n) corresponding samples. The mean result for A_1 will be calculated using the four tests containing A_1. The mean results of A_1, A_2, A_3, and A_4 will be used to determine the trend of the A. Each mean result is taken over the same range of B and C variables (although they are ordered differently), and therefore their effects will cancel.

The basic form of this design is shown in table 3.1 for three variables A,B,C at four levels (X_1, X_2, X_3, X_4 for each

of A, B, and C) crossed with one variable D at two levels (D_1, D_2). Sampling is required at each of the 32 condition sets.

Table 3.1 Latin Square Design

		B_1	B_2	B_3	B_4
D_1	C_1	A_1	A_2	A_3	A_4
	C_2	A_2	A_3	A_4	A_1
	C_3	A_3	A_4	A_1	A_2
	C_4	A_4	A_1	A_2	A_3
D_2	C_1	A_1	A_2	A_3	A_4
	C_2	A_2	A_3	A_4	A_1
	C_3	A_3	A_4	A_1	A_2
	C_4	A_4	A_1	A_2	A_3

Variables A B and C correspond to gas flow rate, frother dosage, and wash water flow rate respectively. Variable D is the repeated variable corresponding to particle size distribution. By rearranging each unique set of conditions into a test, the experimental plan is as shown in table 3.2.

Using this plan, the effects of particle size distribution on the flotation process (yield and ash) can be determined. The information obtained from this experimental design were used to decide if changes to a variable significantly effects the result. The fine and coarse particle size distributions shown in figures 3.3 and 3.4 were used. Both size distributions were tested at the same operating conditions. This allows the interaction between particle size and each of the three operating variables to be determined.

Table 3.2 Experimental Plan.

Variable / Test#	Gas (ℓ/min)	Frother (ppm)	WW (ℓ/min)	Size Distribution
1	0.5	17	0.0	Coarse
2	1.0	14	0.0	Coarse
3	1.5	21	0.0	Coarse
4	2.0	28	0.0	Coarse
5	1.0	17	0.5	Coarse
6	1.5	14	0.5	Coarse
7	2.0	21	0.5	Coarse
8	0.5	28	0.5	Coarse
9	1.5	17	1.0	Coarse
10	2.0	14	1.0	Coarse
11	0.5	21	1.0	Coarse
12	1.0	28	1.0	Coarse
13	2.0	17	1.5	Coarse
14	0.5	14	1.5	Coarse
15	1.0	21	1.5	Coarse
16	1.5	28	1.5	Coarse
17	0.5	17	0.0	Fine
18	1.0	14	0.0	Fine
19	1.5	21	0.0	Fine
20	2.0	28	0.0	Fine
21	1.0	17	0.5	Fine
22	1.5	14	0.5	Fine
23	2.0	21	0.5	Fine
24	0.5	28	0.5	Fine
25	1.5	17	1.0	Fine
26	2.0	14	1.0	Fine
27	0.5	21	1.0	Fine
28	1.0	28	1.0	Fine
29	2.0	17	1.5	Fine
30	0.5	14	1.5	Fine
31	1.0	21	1.5	Fine
32	1.5	28	1.5	Fine

3.3.3 DATA ANALYSIS

Each test result can be thought of as a composition of several parts, the population mean, the effect of the independent variables, and an error distribution term (Lindman, 1992). Using a linear model each test result X_{ijkl} can be represented by the population mean μ, the effect terms

α_i, β_j, and γ_k, and an error term (population distribution about the universal mean) ε_{ijkl} as follows:

$$X_{ijkl} = \mu + \alpha_i + \beta_j + \gamma_k + \varepsilon_{ijkl} \qquad (49)$$
$$\varepsilon_{ijkl} \sim N_{(0,\sigma_e^2)}$$

where: X_{ijkl} represents the result at the i^{th} level of variable A, the j^{th} level of variable B, and the k^{th} level of variable C, with a random value l of the population variance σ_e^2 at test ijk, and α_i, β_j, and γ_k are estimated by the differences between the universal mean and the mean of the respective group, A, B, and C, as follows:

$$\hat{\alpha}_i = \hat{X}_{i...} - \hat{X}_{....}$$
$$\hat{\beta}_j = \hat{X}_{.j..} - \hat{X}_{....} \qquad (50)$$
$$\hat{\gamma}_k = \hat{X}_{..k.} - \hat{X}_{....}$$

The effect of a variable on the results can be computed using analysis of variance (ANOVA). Data analysis using ANOVA has three requirements that must be met:

1. Independence of results
2. Normal distribution of variance
3. Equal variances over all groups

The first requirement will have a large effect on the F ratio, if it is not met. The other two requirements can be bypassed by making some adjustments to the testing procedure.

To determine whether the difference is due to changes in input parameters, or just random error (chance) an F test is

performed. F can be calculated from the ratio of mean squares. A large F value (greater than 1) will indicate that the differences between the grouped means is larger than the variance can account for, and can therefore be attributed to the input parameters. Table 3.3 is a summary of the calculations required to test the significance of a latin square experiment. Abbreviations used in this table include: raw sum of squares RS; sum of squares SS; degrees of freedom df; mean sum of squares MS; and F is the calculated F-ratio. The p value (not shown in the table) is the calculated equivalent of a specified tolerance level α. The confidence level that can be held in the conclusions is 1-p. In the subscript column; a b and c refer to variables A, B, and C; m refers to the universal mean, rem refers to the remainder after specific effects have been removed, and t refers to the total.

Table 3.3 Latin Square F Table.

Sub	RS	SS	df	MS	F
m		T^2/N	1	SS_m/df_m	
a	$(\Sigma_i t_i^2)/I$	$RS_a - SS_m$	I-1	SS_a/df_a	MS_a/MS_{rem}
b	$(\Sigma_j t_j^2)/I$	$RS_b - SS_m$	I-1	SS_b/df_b	MS_b/MS_{rem}
c	$(\Sigma_k t_k^2)/I$	$RS_c - SS_m$	I-1	SS_c/df_c	MS_c/MS_{rem}
rem	$\Sigma_l X_{ijkl}^2$	$RS_{rem} - SS_m - SS_a - SS_b - SS_c$	N+2-3*I	SS_{rem}/df_{rem}	
t		$RS_{rem} - SS_m$	N-1	SS_t/df_t	

where: T is the total of all test results; t_i t_j and t_k are the totals of populations A B and C; N is the total number of experiments; and I is the number of set levels in each group.

The question being asked of the F-test is this: is there a difference between the results at different levels? To answer this the null hypothesis H_o and the alternative hypothesis are defined as:

$$\begin{array}{ll} H_o : \alpha_i = 0 & H_a : \alpha_i \neq 0 \\ \quad \beta_j = 0 & \quad \beta_j \neq 0 \\ \quad \gamma_k = 0 & \quad \gamma_k \neq 0 \end{array} \qquad (51)$$

This does not tell anything about the direction of the differences or where they are located. For this we need a trend analysis. The most obvious way to analyze the trends in data is graphically. This shows the trend visually.

Another method of analyzing the trend is to compare the effect terms (α_i β_j and γ_k) at the different set levels. This will give an indication of where the greatest difference occurs.

4.0 RESULTS AND DISCUSSION

This section is subdivided into three sections: fine results, coarse results, and comparison. A discussion follows the presentation of results in each section. All figures are held to the end of their respective sections.

4.1 FINE RESULTS

The experimental results for the fine sample are shown in table 4.1. The experiment number and operating conditions of each test are shown in the first four columns. The whole sample analysis of the feed, concentrate and tailings are given in the next six columns. Concentrate and tailings results are the average of the two samples taken. The calculated $yield_1$ and $yield_2$ are shown in the last two columns. Below the data is a summary of mean μ, variance σ^2, standard deviation σ, and the minimum and maximum values for each column.

The average feed percent solids is 4.21%, ranging from 3.71 to 4.67. The average feed ash is 14.42%, ranging from 13.21 to 15.68. The low level of variance for both the feed percent solids and ash indicates that the feed consistency was maintained for all experiments. The remaining columns of data all have high levels of variance with respect to their mean value. This indicates that the changes in operating conditions have significantly affected the results. The significance level of these results will be analyzed in the following sections.

Table 4.1 Experimental results for the fine experiments.

#	Gas	Fr	WW	FEED (%)		CONC.(%)		TAILS (%)		$YIELD_1$ (%)	$YIELD_2$ (%)
				SOLIDS	ASH	SOLIDS	ASH	SOLIDS	ASH		
1	0.5	17	0.0	4.19	15.68	20.22	5.89	3.80	17.02	12.11	11.35
2	1.0	14	0.0	4.67	14.41	28.56	6.29	1.66	19.45	38.31	68.43
3	1.5	21	0.0	4.52	13.73	25.96	7.33	0.74	33.64	75.70	86.08
4	2.0	28	0.0	4.39	14.14	18.43	10.13	0.42	46.15	88.87	92.54
5	1.0	17	0.5	4.38	14.60	20.57	8.87	0.94	36.16	79.01	82.31
6	1.5	14	0.5	4.38	14.15	11.88	7.85	0.61	35.22	76.98	90.73
7	2.0	21	0.5	4.30	13.67	10.98	9.12	0.46	43.80	86.90	93.21
8	0.5	28	0.5	4.25	13.63	10.52	7.89	1.79	25.04	66.55	69.65
9	1.5	17	1.0	4.01	15.08	15.59	8.63	0.62	43.30	81.39	88.09
10	2.0	14	1.0	4.16	13.97	7.75	9.41	0.47	58.70	90.74	94.42
11	0.5	21	1.0	3.88	15.32	23.96	7.45	1.27	24.18	52.97	70.99
12	1.0	28	1.0	3.86	15.17	16.33	8.20	0.82	34.72	73.73	82.99
13	2.0	17	1.5	4.22	14.14	8.42	7.92	0.64	44.47	82.98	91.83
14	0.5	14	1.5	3.71	13.21	17.18	5.79	2.10	16.34	29.61	49.31
15	1.0	21	1.5	4.26	15.15	10.56	6.31	1.59	23.98	49.97	73.73
16	1.5	28	1.5	4.24	14.69	8.60	7.00	1.07	30.49	67.24	85.30
μ				4.21	14.42	15.97	7.76	1.19	33.29	65.82	76.94
σ^2				0.06	0.47	40.54	1.56	0.71	134.37	497.74	425.37
σ				0.24	0.69	6.37	1.25	0.85	11.59	22.31	20.62
Min	0.5	14	0.0	3.71	13.21	7.75	5.79	0.42	16.34	12.11	11.35
Max	1.5	28	1.5	4.67	15.68	28.56	10.13	3.80	58.70	90.74	94.42

4.1.1 LATIN SQUARE ANALYSIS OF FINE RESULTS

All three performance parameters have wide ranges of results. The average concentrate ash is 7.76%, ranging from 5.79 to 10.13. The average $yield_1$ is 65.82%, ranging from 12.11 to 90.74. The average $yield_2$ is 76.94%, ranging from 11.35 to 94.42. It can be seen that $yield_2$ and $yield_1$ are both very similar. Consequently, only the statistical analysis for the $yield_1$ and concentrate ash will be shown.

4.1.1.1 ANOVA ANALYSIS

Tables 4.2 and 4.3 show the ANOVA analysis for the concentrate ash and yield$_1$ respectively. Both tables are organized in a similar fashion. The latin square conditions of wash water rate (ww), frother dosage (fr), and gas rate (gas) and the results are shown in the upper left corner in bold. The total, mean, and effect terms of the wash water and frother surround the square in their corresponding row or column. The gas results are located beneath the frother results. The results of the ANOVA F-test are shown at the bottom.

Based on the results of the F-test in the two tables, the ANOVA analysis ranks the importance of the input variables in decreasing order of significance as: gas, wash water, and frother. The confidence levels that the results are significant for concentrate ash are 1-p, or 99.34% for gas, 96.62% for wash water, and 76.19% for frother. The confidence levels for yield$_1$ are 99.37% for gas, 92.47% for wash water, and 56.36% for frother. The confidence levels for yield$_2$ are also calculated at 98.59% for gas, 78.35% for wash water, and 53.66% for frother.

A fifty percent level of significance for any input variable means that there is a 50-50 chance of making a correct conclusion. Since the level of significance for the frother is only 56.36% and 53.66% in the ANOVA analysis of yield$_1$ and yield$_2$ respectively, this variable can be regarded as insignificant with respect to yield.

The two ANOVA analyses indicate that both gas and wash water flow rates are significant factors in the performance of fine coal during column flotation, and that frother has only a small significance to the results, although it has more

effect on the percent ash. Using averages, the data has been further analyzed with respect to gas flow rate, frother dosage and wash water flow rate to show the average trends in the data.

Table 4.2 ANOVA analysis of concentrate ash for fine experiments.

	fr_1	fr_2	fr_3	fr_4	$t_{..k}$	$X_{..k}$	γ_k
ww_1	gas_1 5.89	gas_2 6.29	gas_3 7.33	gas_4 10.13	29.64	7.41	-0.38
ww_2	gas_2 8.87	gas_3 7.85	gas_4 9.12	gas_1 7.89	33.73	8.43	0.64
ww_3	gas_3 8.63	gas_4 9.41	gas_1 7.45	gas_2 8.17	33.66	8.42	0.63
ww_4	gas_4 8.51	gas_1 5.79	gas_2 6.31	gas_3 7.00	27.61	6.90	-0.89
$t_{.j.}$	31.9	29.34	30.21	33.19	T =	**124.64**	
$X_{.j.}$	7.98	7.34	7.55	8.30	X =	**7.79**	
β_j	0.19	-0.46	-0.24	0.51			

	gas_1	gas_2	gas_3	gas_4
$t_{i..}$	27.02	29.64	30.81	37.17
$X_{i..}$	6.76	7.41	7.70	9.29
α_i	-1.04	-0.38	-0.09	1.50

RS	SS	df	MS	F	p
m	970.95	1			
gas 984.87	13.92	3	4.64	11.936	0.0066
fr 973.17	2.22	3	0.74	1.9038	0.2381
ww 977.89	6.94	3	2.31	5.9510	0.0338
rem 996.36	2.33	6	0.39		
t	25.42	15			

Table 4.3 ANOVA analysis of $yield_1$ for fine experiments.

	fr_1	fr_2	fr_3	fr_4	$t_{..k}$	$X_{..k}$	γ_k
ww_1	gas_1	gas_2	gas_3	gas_4			
	12.11	38.31	75.70	88.87	214.99	53.75	-12.11
ww_2	gas_2	gas_3	gas_4	gas_1			
	79.01	76.98	86.90	65.88	308.77	77.19	11.34
ww_3	gas_3	gas_4	gas_1	gas_2			
	81.39	90.74	52.97	73.64	298.74	74.69	8.83
ww_4	gas_4	gas_1	gas_2	gas_3			
	84.36	29.61	49.97	67.24	231.18	57.80	-8.06
$t_{.j.}$	256.87	235.64	265.54	295.63	T =	1053.68	
$X_{.j.}$	64.22	58.91	66.39	73.91	X =	65.86	
β_j	-1.64	-6.95	0.53	8.05			

	gas_1	gas_2	gas_3	gas_4
$t_{i..}$	160.57	240.93	301.31	350.87
$X_{i..}$	40.14	60.23	75.33	87.72
α_i	-25.71	-5.62	9.47	21.86

RS	SS	df	MS	F(3,6)	p
m	69390.1	1			
gas	74431.9	5041.77	3	1680.59	12.105	0.0063
fr	69854.3	464.15	3	154.72	1.1144	0.4364
ww	71062.4	1672.25	3	557.42	4.0149	0.0753
rem	77401.3	833.02	6	138.84		
t		8011.19	15			

4.1.1.2 GAS ANALYSIS

The averaged results for each level of gas flow rate are shown in table 4.4. The table also includes the estimated gas holdup data. The results of gas analysis are shown graphically in figures 4.1, 4.2 and 4.3 for $yield_1$, $yield_2$ and concentrate ash respectively. The trend for increasing gas flow rates is

a corresponding (approximately linear) increase in all three performance parameters.

Table 4.4 Gas analysis for fine experiments.

GAS (ℓ/m)	FEED (%)		CONC. (%)		TAILINGS (%)		$YIELD_1$ (%)	$YIELD_2$ (%)	ε_g (%)
	SOLIDS	ASH	SOLIDS	ASH	SOLIDS	ASH			
0.5	4.00	14.46	17.97	6.76	2.24	20.65	40.31	50.32	6.00
1.0	4.29	14.83	19.00	7.42	1.25	28.58	60.26	76.87	10.83
1.5	4.29	14.41	15.51	7.70	0.76	35.66	75.33	87.55	13.60
2.0	4.27	13.98	11.39	9.15	0.50	48.28	87.37	93.00	14.24

The results are wide ranging over the range of gas flow rates studied. The concentrate ash increases from 6.76% at low gas flow rate to 9.15% for high gas flow rate. $Yield_1$ increases from 40.31% to 87.37% for increasing gas flow rate, and $yield_2$ increases from 50.32% to 93.00%. These results are in agreement with the increasing gas holdup with gas flow rate. The increasing gas holdup leads to increased particle recovery, and consequently concentrate ash increases as more middling particles are captured.

Another aspect affecting the results is the flow regime under which the column is operating. Figure 4.4 shows the relationship between the gas holdup and the superficial gas flow rate. This figure shows that the column is operating in the bubbly flow regime over the first three gas levels, and tending towards the turbulent flow regime at the highest gas rate. This is observed in table 4.4 in the sense that for a 30% increase in gas flow rate from 1.5 ℓ/min to 2.0 ℓ/min the corresponding increase in gas holdup is insignificant at 4.7%. Bubbly flow regime is characterized by small uniform bubbles with similar rise velocities. In turbulent flow, larger bubbles begin to form and disrupt the homogeneous flow. The effects of moving into the turbulent flow regime can also be

seen in the $yield_2$ and ash data. The $yield_2$ rate begins to level off, and the ash rate increases significantly. These results can be attributed to three factors:

1. For a constant gas flow rate, as larger bubbles are produced the overall bubble surface area decreases. This in turn decreases the overall carrying capacity in both the collection and the froth zone, and therefore the solids yield declines. For an increasing gas flow rate, the rate of $yield_2$ will drop, as the bubble surface area will not increase at the same rate when larger bubbles are being formed. Since the column is already operating near full carrying capacity the rate of $yield_2$ (slope) will drop. The mean bubble sizes are shown in Appendix C.

2. The large bubbles (and non-uniform size distribution) create turbulence in the froth zone. This in turn creates higher ash entrainment, as larger bubbles have higher rising velocities, and can carry entrained particles to the launder before washing occurs.

3. Although increasing the gas rate increases the collection zone gas holdup, it decreases gas holdup in froth zone due to increased entrainment of collection zone water (Finch and Dobby, 1990). This is shown in table 4.4 by the decreasing percent solids in concentrate samples as the gas flow rate increases above 1.0 ℓ/min. This phenomenon can lead to the loss of the interface and a negative bias. The bias flow rate calculations shown in Appendix D, verified the shift to negative bias as the gas flow rate increases.

In general, the cleaning or washing efficiency of the column in terms of ash rejection is quite good throughout the range of gas flow rates studied. The ash content of above 14%

in the feed is reduced to below 7.7% in the concentrate at the gas flow rates below 1.5 ℓ/min. As the gas flow rate is increased to 2.0 ℓ/min, the ash content in the concentrate increases significantly to 9.15%. This can be attributed to the shift in flow regime from bubbly flow to turbulent flow, thus causing increased entrainment of ash particles. In striking a balance between yield and concentrate ash, the results suggest that a gas rate of 1.5 ℓ/min is optimum with a resultant $yield_2$ of 87.55% and a concentrate ash content of 7.70%. This optimum gas flow rate of 1.5 ℓ/min translates to a superficial gas velocity of 0.79 cm/s.

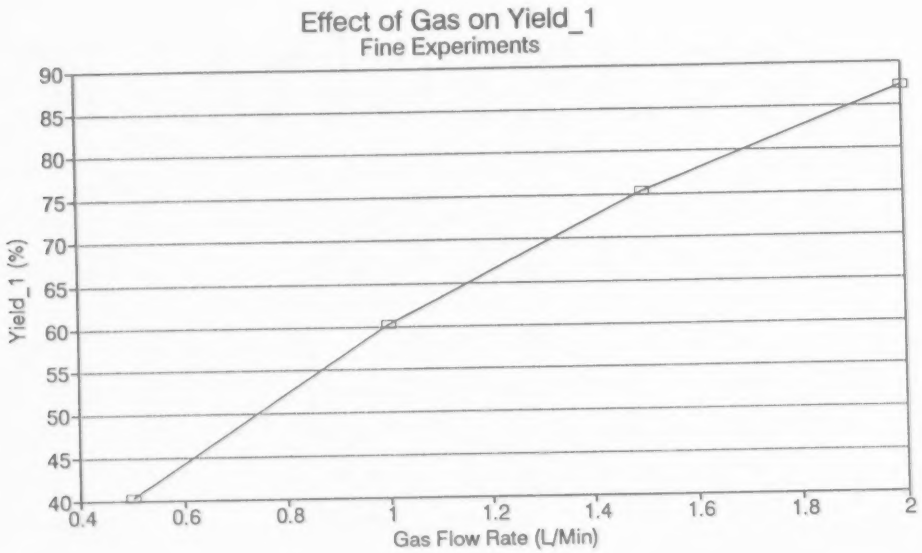

Figure 4.1 Effect of gas flow rate on $yield_1$ for fine experiments.

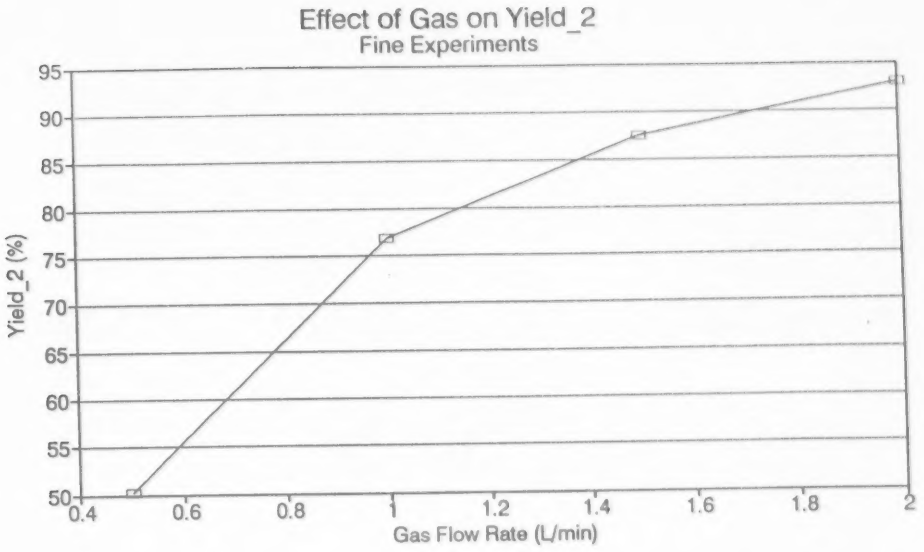

Figure 4.2 Effect of gas flow rate on yield$_2$ for fine experiments.

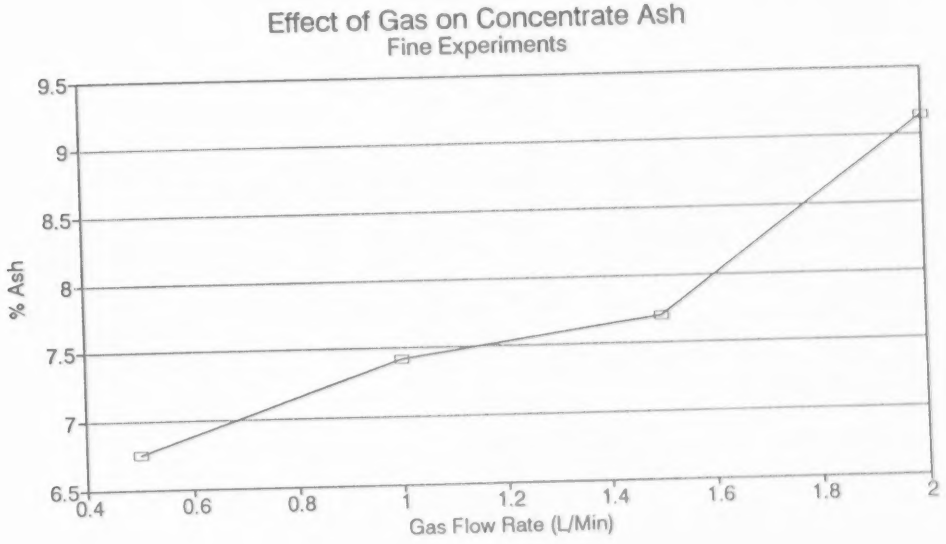

Figure 4.3 Effect of gas flow rate on concentrate ash for fine experiments.

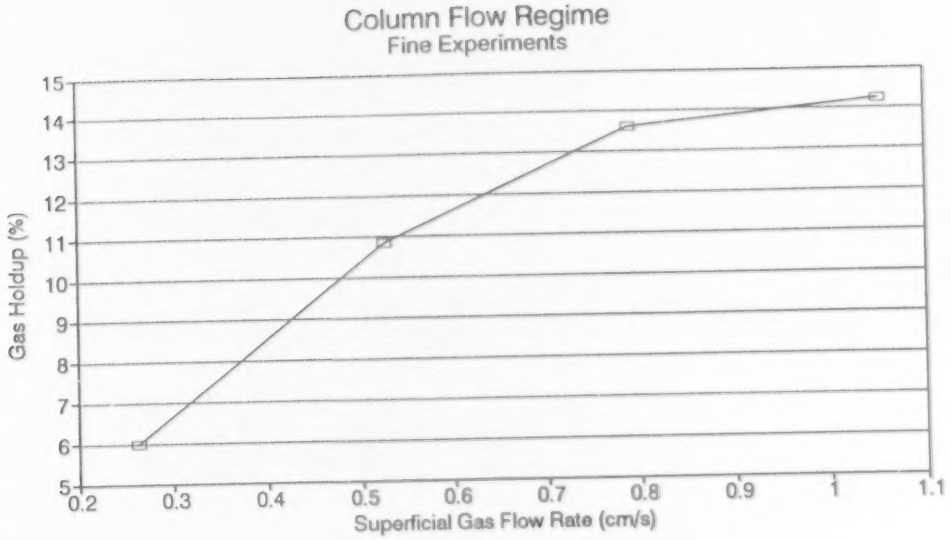

Figure 4.4 Gas holdup as a function of gas flow rate for fine experiments.

4.1.1.3 WASH WATER ANALYSIS

The averaged results for each level of wash water flow rate are shown in table 4.5. The results of wash water analysis are shown graphically in figures 4.5, 4.6 and 4.7 for $yield_1$, $yield_2$ and concentrate ash respectively. In contrast to the effect of gas flow rate on the performance parameters, increasing wash water flow rates leads to a maximum in the performance parameters, followed by a decline at wash water flow rates above 1.0 ℓ/min.

Table 4.5 Wash water analysis for fine experiments.

WW (ℓ/m)	FEED (%)		CONC. (%)		TAILINGS (%)		$YIELD_1$ (%)	$YIELD_2$ (%)
	SOLIDS	ASH	SOLIDS	ASH	SOLIDS	ASH		
0.0	4.44	14.49	23.29	7.41	1.66	29.07	53.75	64.60
0.5	4.33	14.01	13.49	8.43	0.95	35.06	77.36	83.97
1.0	3.98	14.89	15.91	8.42	0.79	40.23	74.71	84.12
1.5	4.11	14.30	11.19	6.76	1.35	28.82	57.45	75.04

A similar trend is seen in all three figures. With no wash water the percentages are low, over the two middle flow rates the percentages are high and almost level, and then at high wash water the percentages drop off again. This trend is also seen in the bias flow rates (appendix D). These results can be explained as follows:

1. In the case of zero wash water, the produced froth is dry and unstable. This means that less froth is recovered in the concentrate launder. The inverse relationship between recovery and ash indicates that the recovery of ash will be proportionally low due to selective flotation. The cleanest particles will tend to be recovered preferentially, and middlings particles will be excluded by limitations in the froth carrying capacity. This leads to a low yield as well as low ash content as shown in figures 4.5, 4.6, and 4.7.

2. As the wash water flow rate is increased to between 0.5 ℓ/min and 1.0 ℓ/min, the yield is observed to increase significantly from zero wash water. The solids yield (2) increases from 64.6% to 84.12%. The concentrate ash content only increases from 7.41% at zero wash water to 8.42% at a wash water rate of 1.0 ℓ/min. The observed concentrate ash, $yield_1$, and $yield_2$ were similar for wash water rates of 0.5 ℓ/min and 1.0 ℓ/min. Considering the fine size distribution of the feed coal these results suggest excellent washing efficiencies at these two wash water flow rates.

3. When the wash water flow rate was increased to 1.5 ℓ/min, the yield dropped significantly from 84.12% to 75.04%. The concentrate ash content also decreased to 6.76%, from 8.42% at a wash water flow rate of 1.0 ℓ/min.

In the case of the relatively high wash water flow rate of 1.5 ℓ/min, the wash water nozzle acts like a jet spray which creates mixing and channelling in the froth. This disrupts the plug flow regime, and a high shear zone is created in the froth. The high wash water flow rate washes away the entrained particles, and some of the valuable particles which were weakly attached to the rising bubbles. Consequently, the yield and ash content decline as indicated in figures 4.5, 4.6, and 4.7.

Plug flow conditions, along with moderate wash water rates permits the maximum efficiency to be achieved in the froth zone. Considering a trade-off between recovery and concentrate ash content, the optimum wash water flow rate for cleaning fine particles in the column will be between 0.5 ℓ/min and 1.0 ℓ/min. This corresponds to a superficial wash water velocity in the range of 0.26 cm/s to 0.53 cm/s, and bias flow rate is between -0.2 ℓ/min and +0.5 ℓ/min.

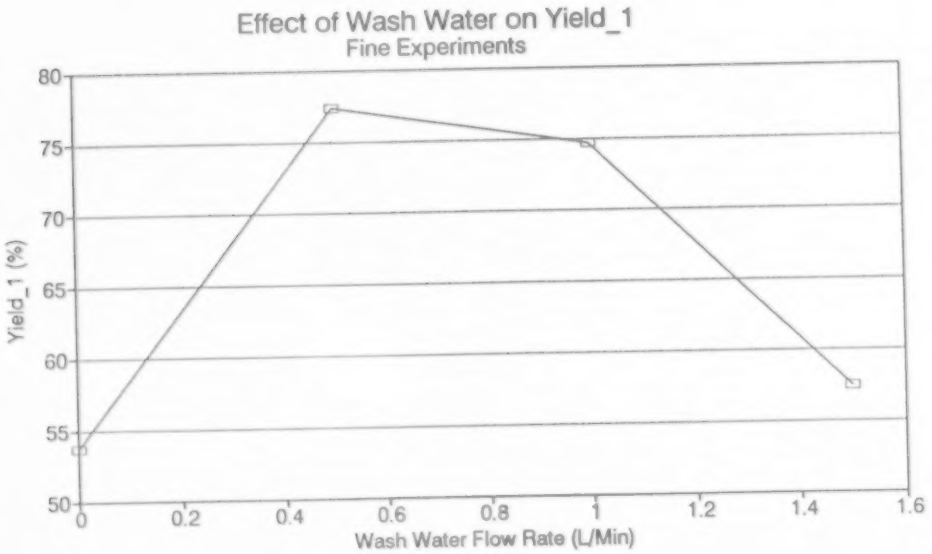

Figure 4.5 Effect of wash water flow rate on yield$_1$ for fine experiments.

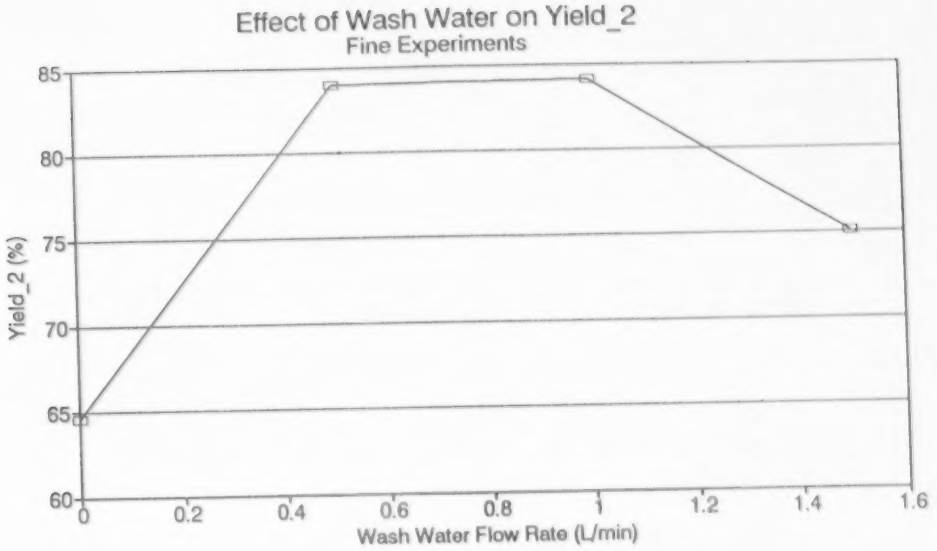

Figure 4.6 Effect of wash water flow rate on yield$_2$ for fine experiments.

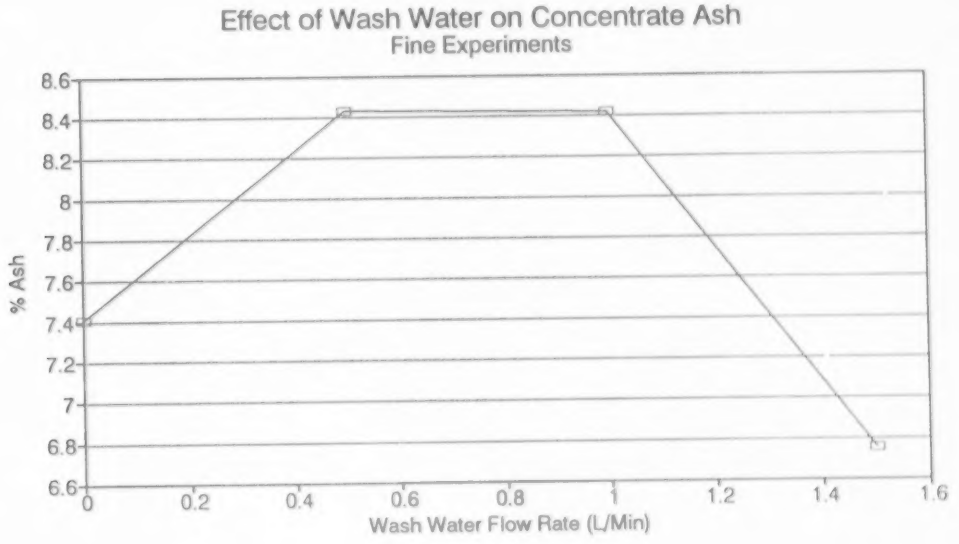

Figure 4.7 Effect of wash water flow rate on concentrate ash for fine experiments.

4.1.1.4 FROTHER ANALYSIS

The averaged results for each level of frother dosage are shown in table 4.6. The table also includes the estimated gas holdup data. The results of frother analysis indicate that increasing the dosage also increases the performance parameter. The relationship between frother dosage and $yield_1$ is almost linear, as shown in figure 4.8. The effect of frother dosage on $yield_2$ and concentrate ash are shown in figures 4.9 and 4.10 respectively.

Table 4.6 Frother analysis for fine experiments.

FR. (ppm)	FEED (%)		CONC. (%)		TAILINGS (%)		$YIELD_1$ (%)	$YIELD_2$ (%)	ϵ_g (%)
	SOLIDS	ASH	SOLIDS	ASH	SOLIDS	ASH			
14	4.23	13.94	16.34	7.34	1.21	32.43	58.91	75.72	8.42
17	4.20	14.88	16.20	7.83	1.50	35.24	63.87	68.39	12.31
21	4.24	14.47	17.87	7.55	1.02	31.40	66.39	81.00	10.69
28	4.18	14.41	13.47	8.31	1.03	34.10	74.10	82.62	13.25

The results indicate that the effect of increasing frother dosage on the performance parameters is much less than that observed for gas flow rates and wash water flow rates. For increasing frother dosage from 14 ppm to 28 ppm, the concentrate ash content only increased from 7.34% to 8.31%. $Yield_1$ only increased from 58.91% to 74.10%, and $yield_2$ increased from 75.72% to 82.62%. The fluctuations in $yield_2$ and concentrate ash are over a narrow range of results, and the standard deviations are high, therefore the fluctuations are less significant than they appear.

The limited effect of frother dosage on the performance parameters was predicted in the ANOVA analysis discussed in section 4.1.1.1. Although gas holdup increased from 8.42% at a frother dosage of 14 ppm to 13.25% at a dosage of 28 ppm,

thus indicating a smaller average bubble size (as shown in Appendix C), the performance parameters were not proportionately increased. This observation of a limited effect of frother dosage on the performance parameters could be due to several factors. One factor may be that the feed coal is highly hydrophobic and very floatable. A second factor may be that the minimum frother dosage of 14 ppm used in this study is already within the optimum concentration range necessary for cleaning the coal sample used, hence increasing the concentration beyond 14 ppm does not translate to significant improvements in the performance parameters. Which ever of these factors is responsible for the observed results will be a subject of further studies. However, the ANOVA multivariate analysis discussed earlier accurately predicted the observed effect of the frother dosage range used on the performance parameters for cleaning this fine coal sample in the column.

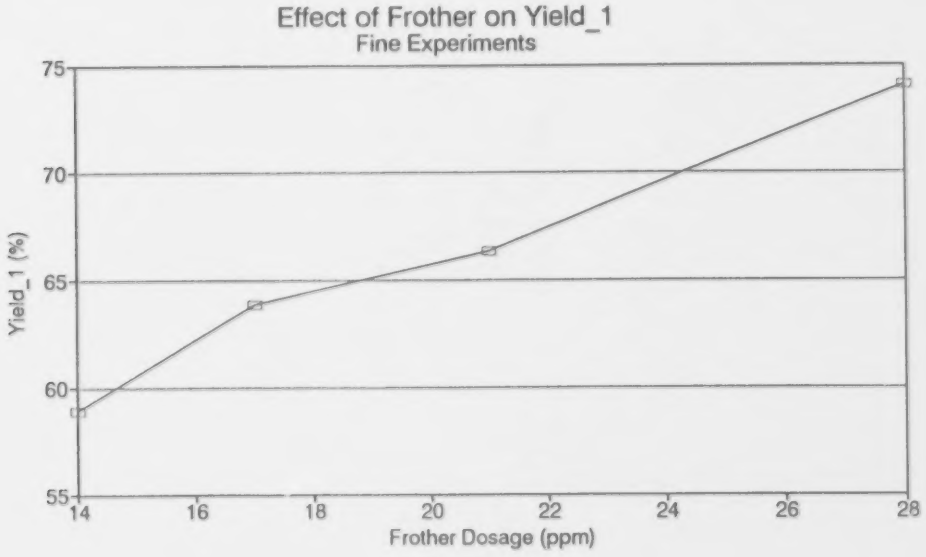

Figure 4.8 Effect of frother dosage on $yield_1$ for fine experiments.

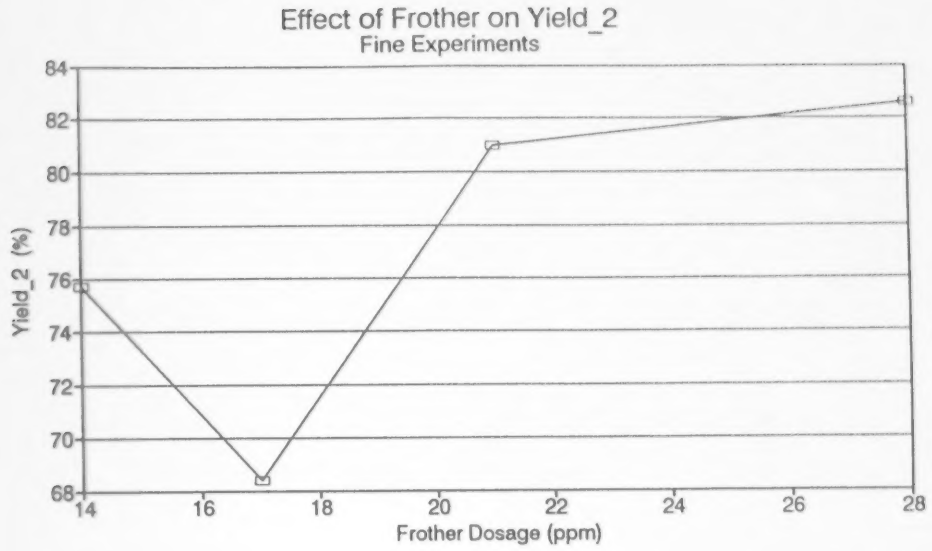

Figure 4.9 Effect of frother dosage on yield$_2$ for fine experiments.

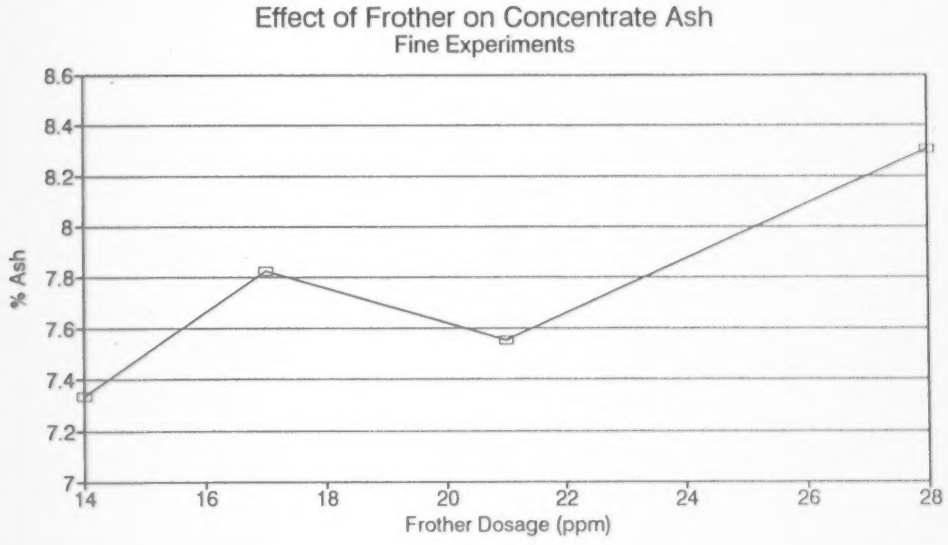

Figure 4.10 Effect of frother dosage on concentrate ash for fine experiments.

4.1.2 ANALYSIS OF INDIVIDUAL FINE RESULTS

As discussed in the previous section, the ANOVA analysis for the fine coal experiments indicated that both gas and wash water had significant effects on the performance parameters, and that the effect of frother is minimal. The effects and interaction of wash water and gas for the individual experimental data, as opposed to the averaged data, are shown three dimensionally in figures 4.11, 4.12, and 4.13 for $yield_1$, $yield_2$, and concentrate ash respectively.

Figure 4.11 shows that for gas flow rates within the bubbly flow regime (i.e. below 1.5 ℓ/min), the wash water flow rates gives a maximum concentrate yield at about 0.8 ℓ/min. This maxima becomes more pronounced as the gas flow rate decreases from 1.5 ℓ/min to 0.5 ℓ/min. In contrast, the yield maxima is virtually eliminated above a gas flow rate of 1.5 ℓ/min. This is an indication that as the column flow regime tends towards transition from bubbly to turbulent flow, the effectiveness of the wash water in cleaning the concentrate in the froth is decreased significantly. Thus at this high gas flow rate, the concentrate ash should increase as observed in the experimental data in table 4.4. On the other hand, for the gas flow rates within the bubbly flow regime, increasing the wash water rate beyond 0.8 ℓ/min leads to a significant decline in the concentrate yield due to the detachment of floated particles from the bubbles by the excessive wash water stream. These trends are also observed in figure 4.12 for the effect of gas and wash water flow rates on $yield_2$, and in figure 4.13 for the effect of the same two variables on concentrate ash. These individual results for the fine coal sample agree well with those obtained from the Latin Square experimental design and ANOVA analysis, thus verifying the analytical accuracy of this multivariate analysis technique.

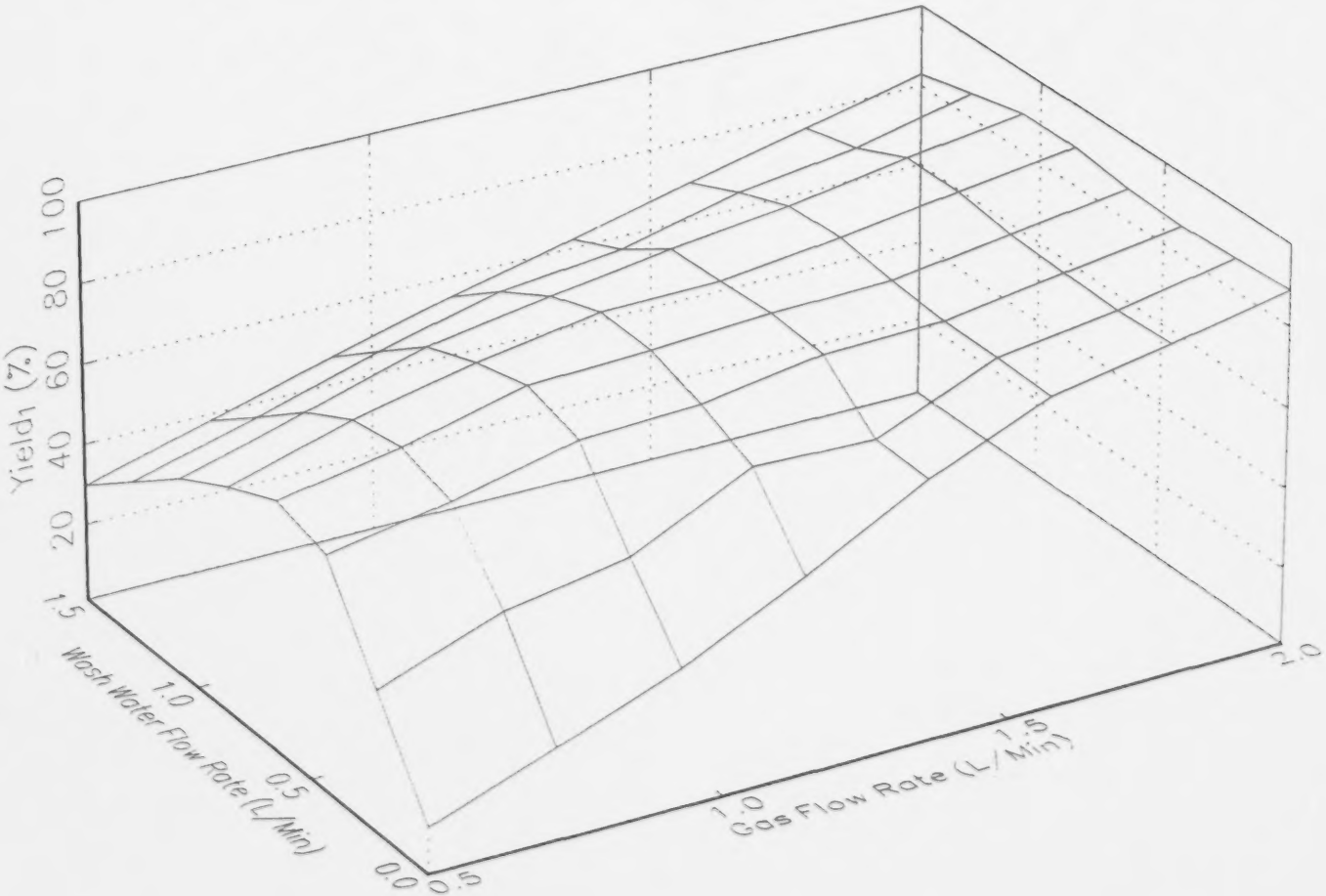

Figure 4.11 Effects of gas and wash water on yield$_1$ for fine experiments.

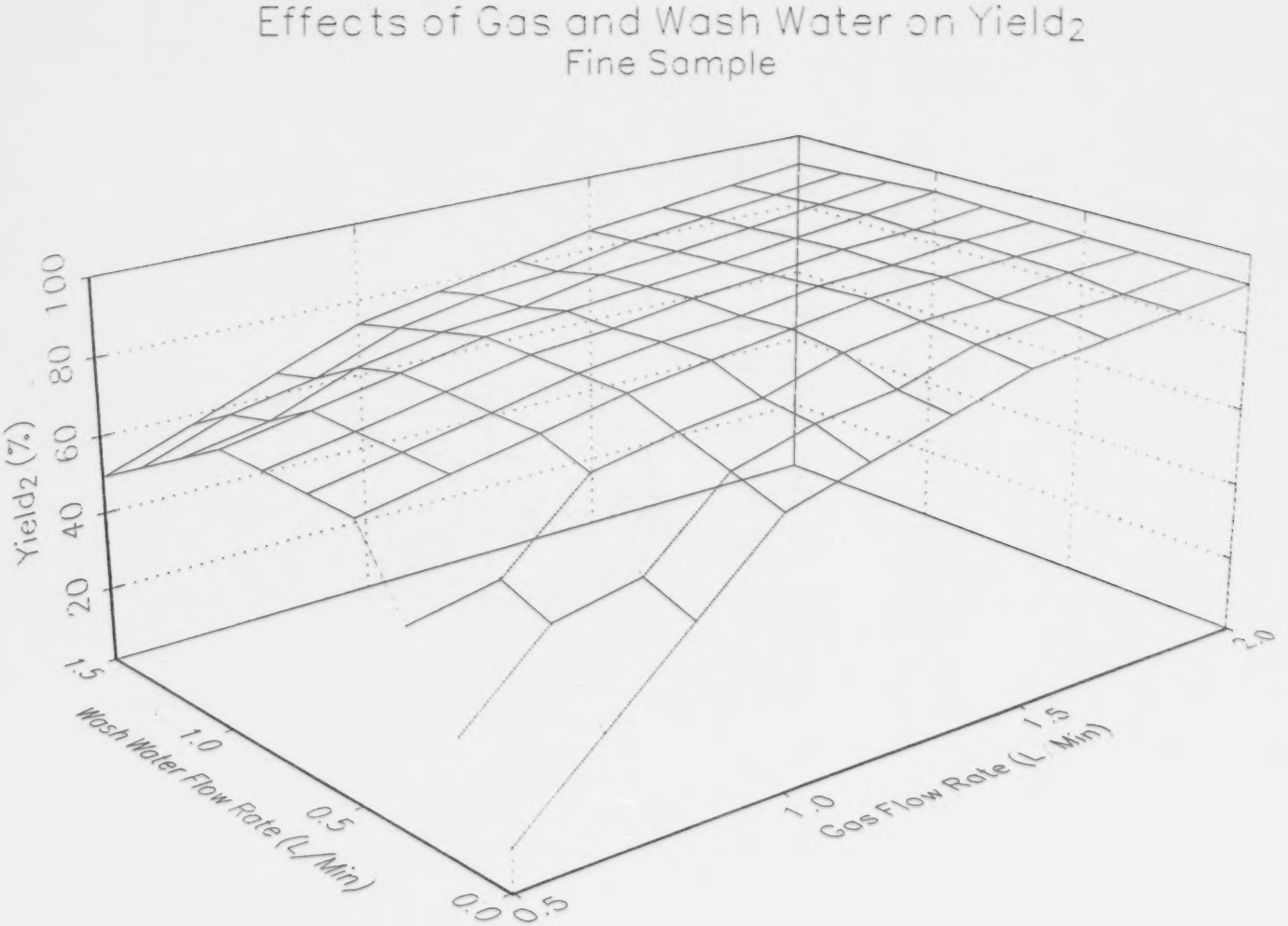

Figure 4.12 Effect of gas and wash water on $yield_2$ for fine experiments.

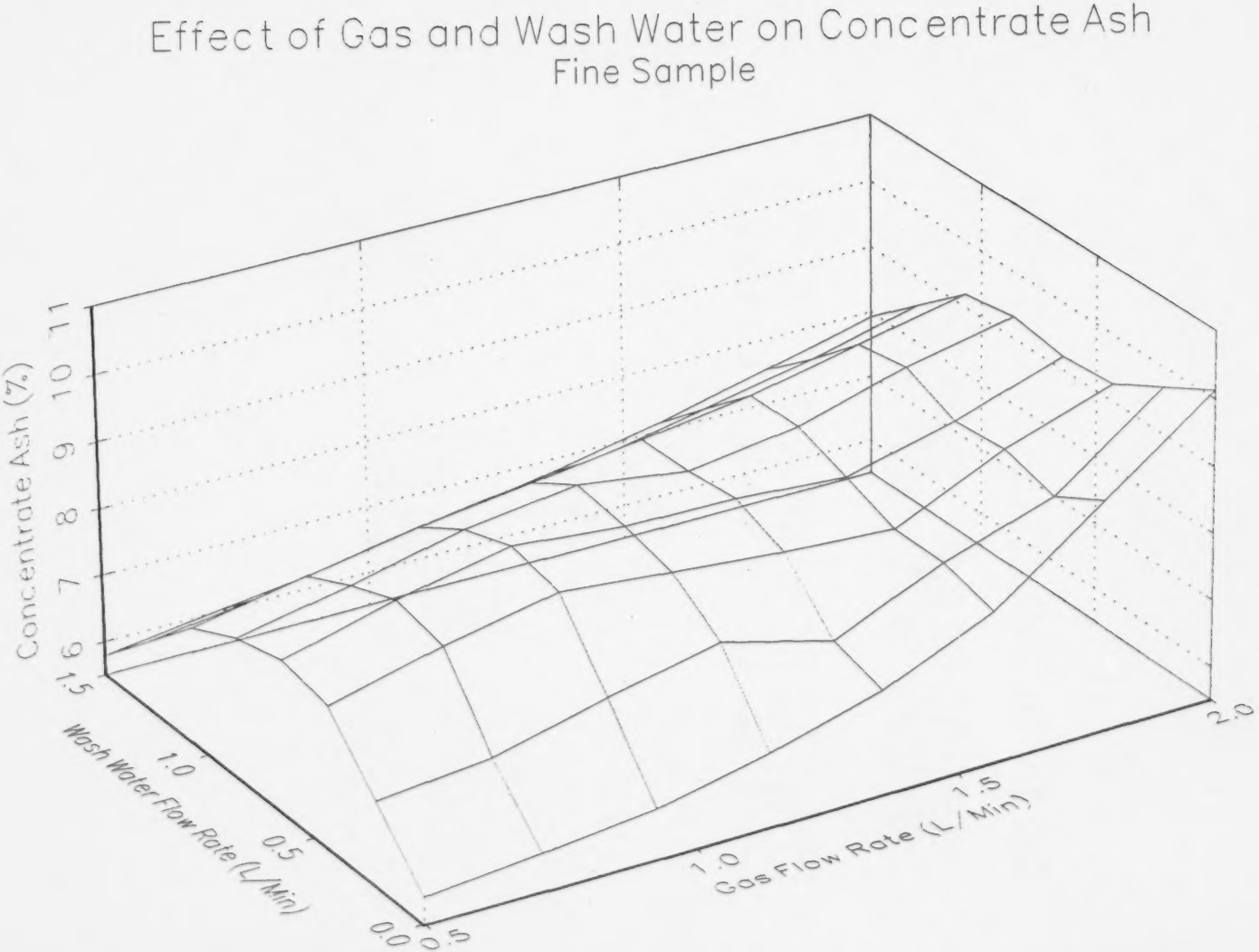

Figure 4.13 Effect of gas and wash water on concentrate ash for fine experiments.

4.2 COARSE RESULTS

The experimental results for the coarse samples are shown in table 4.7. The experiment number and operating conditions for each test are shown in the first four columns. The whole sample analysis of the feed, concentrate and tailings are given in the next six columns. Concentrate and tailings results are the average of the two samples taken. The calculated $yield_1$ and $yield_2$ are shown in the last two columns. Below the data is a summary of mean, variance, standard deviation, minimum and maximum for each column.

The average feed percent solids is 3.44% ranging from 3.00 to 4.05. The average feed ash is 13.65% ranging from 12.21 to 15.41. The consistency of the coarse feed stock was considerably more difficult to maintain even with the use of the recirculating pump. This is shown by the high variance of the feed analyses. However, the differences are still small enough to conclude that feed consistency was maintained. The remaining columns all have high levels of variance with respect to their mean value. This indicates that the changes in operating conditions have an effect on the results, although to a lesser degree than for the fine sample. The significance level of the results will be analyzed in the following sections.

4.2.1 LATIN SQUARE ANALYSIS OF COARSE RESULTS

The three performance parameters have wide ranging results, although not as marked as for the fine experiments. The average concentrate ash is 8.31%, ranging from 6.53 to 9.49. The average $yield_1$ is 87.11%, with a minimum of 62.89 and a maximum of 95.51. The average $yield_2$ is 89.24%, with a minimum of 75.21 and a maximum of 95.54. As in the fine

results section, only $yield_1$ and concentrate ash will be statistically analyzed.

Table 4.7 Experimental results for coarse experiments.

#	Gas	Fr	WW	FEED (%)		CONC. (%)		TAILINGS (%)		$YIELD_1$ (%)	$YIELD_2$ (%)
				SOLIDS	ASH	SOLIDS	ASH	SOLIDS	ASH		
1	0.5	17	0.0	3.40	15.07	42.72	9.30	0.55	48.91	85.45	84.90
2	1.0	14	0.0	3.87	12.96	30.16	7.62	0.47	58.32	89.47	89.32
3	1.5	21	0.0	3.16	12.59	33.07	7.69	0.57	58.87	90.42	83.29
4	2.0	28	0.0	3.23	12.35	33.27	8.34	0.33	63.08	92.69	90.70
5	1.0	17	0.5	3.24	14.61	21.13	8.68	0.25	62.91	89.06	93.33
6	1.5	14	0.5	3.00	12.40	17.20	9.13	0.32	68.33	94.48	91.17
7	2.0	21	0.5	3.33	12.49	20.53	9.44	0.26	77.41	95.51	93.44
8	0.5	28	0.5	3.75	14.70	13.58	6.53	0.67	47.60	80.12	86.37
9	1.5	17	1.0	4.05	15.41	17.69	7.73	0.49	49.96	81.80	90.49
10	2.0	14	1.0	3.20	12.21	22.54	9.49	0.17	69.14	95.44	95.54
11	0.5	21	1.0	3.56	15.11	20.57	7.02	1.01	28.81	62.89	75.21
12	1.0	28	1.0	3.40	13.60	21.11	8.72	0.308	70.02	92.04	92.30
13	2.0	17	1.5	3.60	14.49	22.54	8.68	0.32	65.76	89.82	92.44
14	0.5	14	1.5	3.05	13.41	22.14	7.58	0.58	35.01	78.72	83.17
15	1.0	21	1.5	3.91	13.70	25.87	8.11	0.35	45.44	85.02	92.30
16	1.5	28	1.5	3.32	13.29	24.30	8.84	0.23	57.42	90.84	93.91
μ				3.44	13.65	24.28	8.31	0.43	56.69	87.11	89.24
σ^2				0.09	1.15	50.09	0.73	0.04	164.35	64.53	26.78
σ				0.31	1.07	7.08	0.85	0.21	12.82	8.03	5.17
Min	0.5	14	0.0	3.00	12.21	13.58	6.53	0.17	28.81	62.89	75.21
Max	2.0	17	1.5	4.05	15.41	42.72	9.49	1.01	77.41	95.51	95.54

4.2.1.1 ANOVA ANALYSIS

Tables 4.8 and 4.9 show the ANOVA analysis for the concentrate ash and $yield_1$ respectively. Both tables are organized the same as in the fine section, with the latin square conditions and results shown in the upper left corner in bold. The total, mean, and effect terms of the wash water and frother surround the square in their corresponding row or

column. The gas results are located beneath the frother results. The results of the ANOVA F-test are shown at the bottom.

Table 4.8 ANOVA analysis of concentrate ash for coarse experiments.

	fr_1	fr_2	fr_3	fr_4	$t_{..k}$	$X_{..k}$	γ_k
ww_1	gas_1	gas_2	gas_3	gas_4			
	9.30	7.62	7.69	8.34	32.95	8.24	-0.07
ww_2	gas_2	gas_3	gas_4	gas_1			
	8.68	9.13	9.44	6.53	33.78	8.45	0.14
ww_3	gas_3	gas_4	gas_1	gas_2			
	7.73	9.49	7.02	8.72	32.96	8.24	-0.07
ww_4	gas_4	gas_1	gas_2	gas_3			
	8.68	7.58	8.11	8.84	33.21	8.30	0.00
$t_{.j.}$	34.39	33.82	32.26	32.43	T =	132.90	
$X_{.j.}$	8.60	8.46	8.07	8.11	X =	8.31	
β_j	0.29	0.15	-0.24	-0.20			

	gas_1	gas_2	gas_3	gas_4
$t_{i..}$	30.43	33.13	33.39	35.95
$X_{i..}$	7.61	8.28	8.35	8.99
α_i	-0.70	-0.02	0.04	0.68

	RS	SS	df	MS	F	p
m		1103.90	1			
gas	1107.72	3.82	3	1.27	1.1073	0.438
fr	1104.72	0.82	3	0.27	0.2374	NA
ww	1104.01	0.11	3	0.04	0.0329	NA
rem	1115.55	6.90	6	1.15		
t		11.65	15			

Table 4.9 ANOVA analysis of $yield_i$ for coarse experiments.

	fr_1	fr_2	fr_3	fr_4	$t_{..k}$	$X_{..k}$	γ_k
ww_1	gas_1 85.45	gas_2 89.47	gas_3 90.42	gas_4 92.69	358.03	89.51	2.40
ww_2	gas_2 89.06	gas_3 94.48	gas_4 95.51	gas_1 80.12	359.17	89.79	2.68
ww_3	gas_3 81.80	gas_4 95.44	gas_1 62.89	gas_2 92.04	332.17	83.04	-4.07
ww_4	gas_4 89.82	gas_1 78.72	gas_2 85.02	gas_3 90.84	344.40	86.10	-1.01
$t_{.j.}$	346.13	358.11	333.84	355.69	T =	**1393.77**	
$X_{.j.}$	86.53	89.53	83.46	88.92	X =	**87.11**	
β_j	-0.58	2.42	-3.65	1.81			

	gas_1	gas_2	gas_3	gas_4
$t_{i..}$	307.18	355.59	357.54	373.46
$X_{i..}$	76.80	88.90	89.39	93.37
α_i	-10.32	1.79	2.27	6.25

RS	SS	df	MS	F	p
m	121412.2	1			
gas 122027.8	615.58	3	205.19	6.0435	0.0325
fr 121503.3	91.14	3	30.38	0.8948	0.4975
ww 121534.2	122.03	3	40.68	1.1981	0.4131
rem 122444.7	203.72	6	33.95		
t	1032.47	15			

According to the ANOVA multivariate analysis of concentrate ash, as illustrated by the F-test results, the only input variable having any significant effect is gas flow rate. Both the wash water flow rate and the frother dosage were relatively ineffectual. The level of confidence for gas is only 56.2% which indicates a little significance. Therefore, the level of significance of all three operating

variables relative to the concentrate ash is low for the coarse coal sample as compared to the observed results for the fine sample discussed earlier.

The ANOVA analysis of $yield_1$ ranks the order of importance of the input variables as gas, wash water and frother. Only the F-test for the gas flow rate shows a value significantly above 1.0. The level of confidence is 96.75% for gas, 58.69% for wash water, and 55.25% for frother. Wash water flow rate and frother dosage can also be regarded as having no significant effect on $yield_1$.

The two ANOVA analyses show that gas flow rate has a significant effect on $yield_1$ and a minor effect on concentrate ash. Wash water and frother have limited effect on $yield_1$ and concentrate ash content. The results indicate that to determine the effects of any of these variables with high degree of certainty a more rigorous experimental plan would be required. They also indicate that the system is extremely stable over the range of operating conditions used, in spite of the difficulty in maintaining the feed slurry characteristics.

4.2.1.2 GAS ANALYSIS

The averaged results for each level of the gas flow rate are shown in table 4.10. The estimated gas holdup data is also shown in the table. The results of gas analysis are shown graphically in figures 4.14, 4.15 and 4.16 for $yield_1$, $yield_2$ and concentrate ash respectively. The trend for increasing gas flow rates is a general but limited increase in all three performance parameters. The range of results is much narrower than for the fine samples over the same gas range.

Table 4.10 Gas analysis of coarse experiments.

GAS (ℓ/m)	FEED (%)		CONC. (%)		TAILINGS (%)		$YIELD_1$ (%)	$YIELD_2$ (%)	ε_g (%)
	SOLIDS	ASH	SOLIDS	ASH	SOLIDS	ASH			
0.5	3.44	14.57	24.75	7.61	0.70	40.08	76.80	82.41	13.29
1.0	3.61	13.72	24.57	8.28	0.34	59.17	88.90	91.81	14.59
1.5	3.38	13.42	23.06	8.35	0.40	58.65	89.39	89.72	16.16
2.0	3.34	12.88	24.72	8.99	0.27	68.85	93.37	93.03	16.13

The concentrate ash increases from 7.61% at low gas flow rate to 8.99% for high gas flow rate. $Yield_1$ increases from 76.80% to 97.37% for increasing gas flow rate, and $yield_2$ increases from 82.41% to 93.03%. There are fluctuations in all parameters, although the range is small.

The column is operating in the bubbly flow regime over the first three gas levels, however at the high gas rate (2.0 ℓ/min) the flow regime is into the transition flow regime. This can be seen graphically in figure 4.17, as the gas holdup increases linearly and then levelled out completely between 1.5 ℓ/min and 2.0 ℓ/min of gas flow rate. The mean bubble sizes are shown in Appendix C. The bias flow rate calculations are shown in Appendix D.

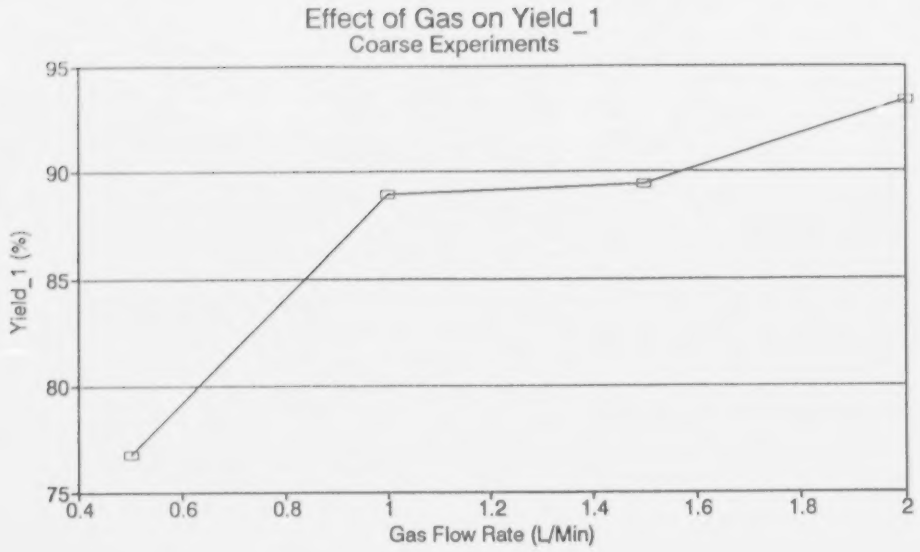

Figure 4.14 Effect of gas flow rate on yield$_1$ for coarse experiments.

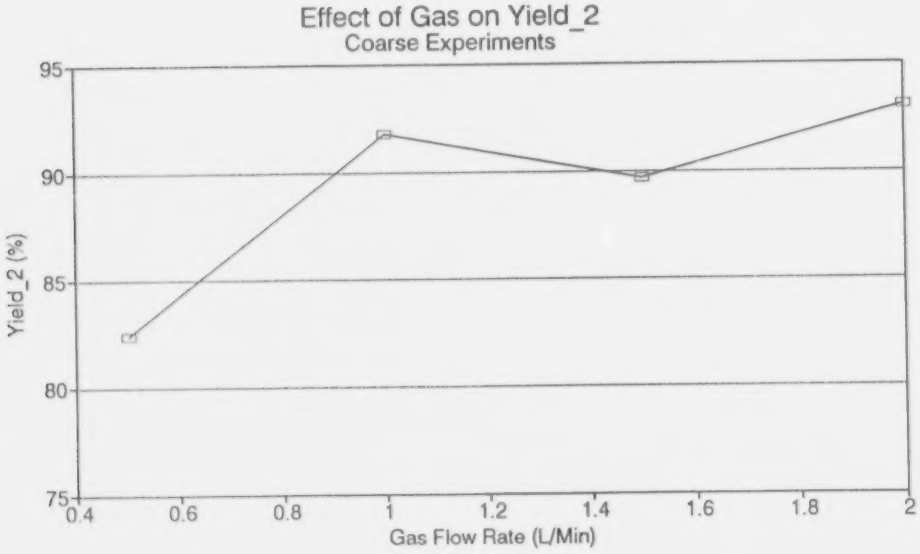

Figure 4.15 Effect of gas flow rate on yield$_2$ for coarse experiments.

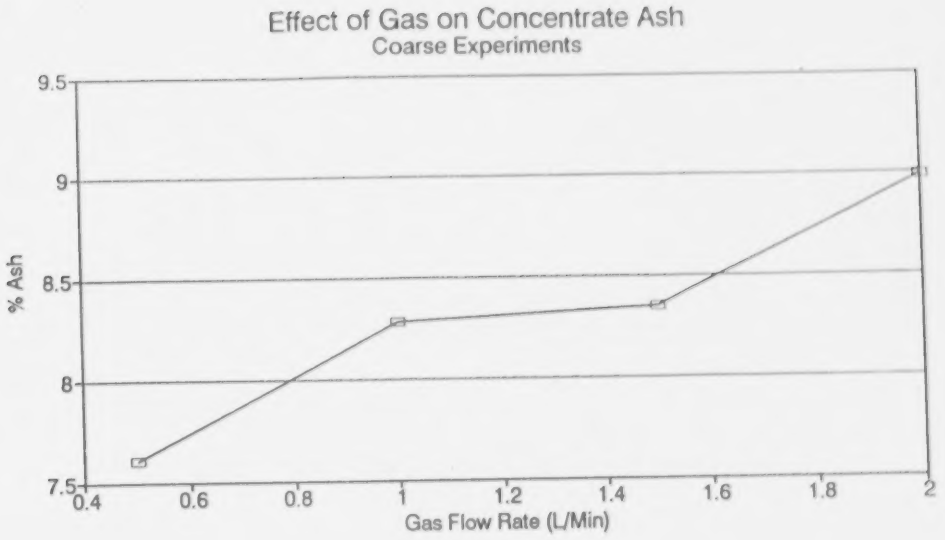

Figure 4.16 Effect of gas on concentrate ash for coarse experiments.

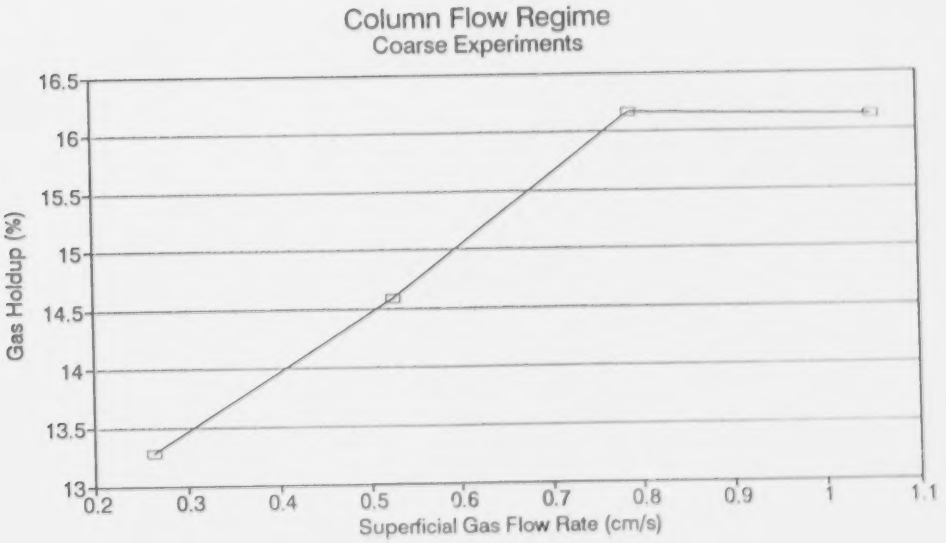

Figure 4.17 Gas holdup as a function of gas flow rate.

4.2.1.3 WASH WATER ANALYSIS

The averaged results are shown in table 4.11 for each level of the wash water flow rate. The results of wash water analysis are shown graphically in figures 4.18, 4.19 and 4.20 for $yield_1$, $yield_2$ and concentrate ash respectively.

Table 4.11 Wash water analysis of coarse experiments.

WW (ℓ/m)	FEED (%)		CONC. (%)		TAILINGS (%)		$YIELD_1$ (%)	$YIELD_2$ (%)
	SOLIDS	ASH	SOLIDS	ASH	SOLIDS	ASH		
0.0	3.42	13.24	34.80	8.24	0.48	57.30	89.51	87.05
0.5	3.33	13.55	18.11	8.45	0.37	64.06	89.79	91.08
1.0	3.55	14.08	20.48	8.24	0.49	54.48	83.04	88.39
1.5	3.47	13.72	23.71	8.30	0.37	50.91	86.10	90.46

Similar to the results for gas analysis, the wash water results remain relatively constant over the range of flow rates studied. The $yield_2$ only increased from 87.05% to 90.46% when the wash water flow rate increased from zero to 1.5ℓ/min. For the same wash water range, the $yield_1$ and concentrate ash also remain relatively constant. The ANOVA analysis correctly predicted these results. In contrast, the calculated bias flow rate (Appendix D) increases dramatically with increasing wash water. This indicates that the continuing increase in the bias flow rate does not significantly affect either the yield or the concentrate ash.

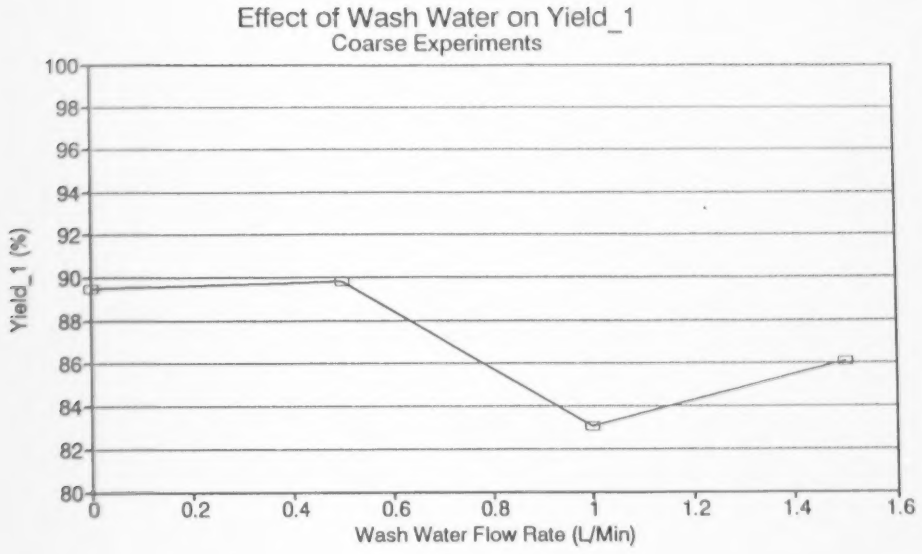

Figure 4.18 Effect of wash water flow rate on yield$_1$ for coarse experiments.

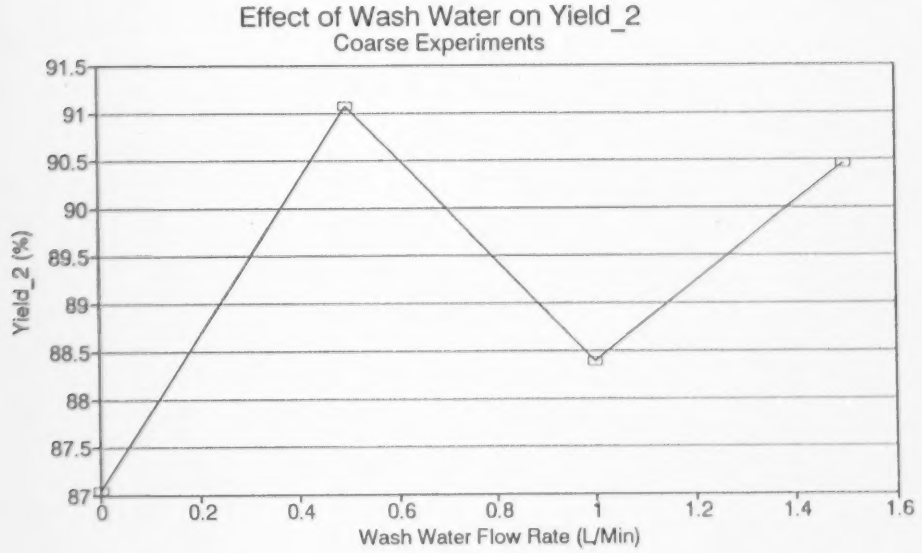

Figure 4.19 Effect of wash water flow rate on yield$_2$ for coarse experiments.

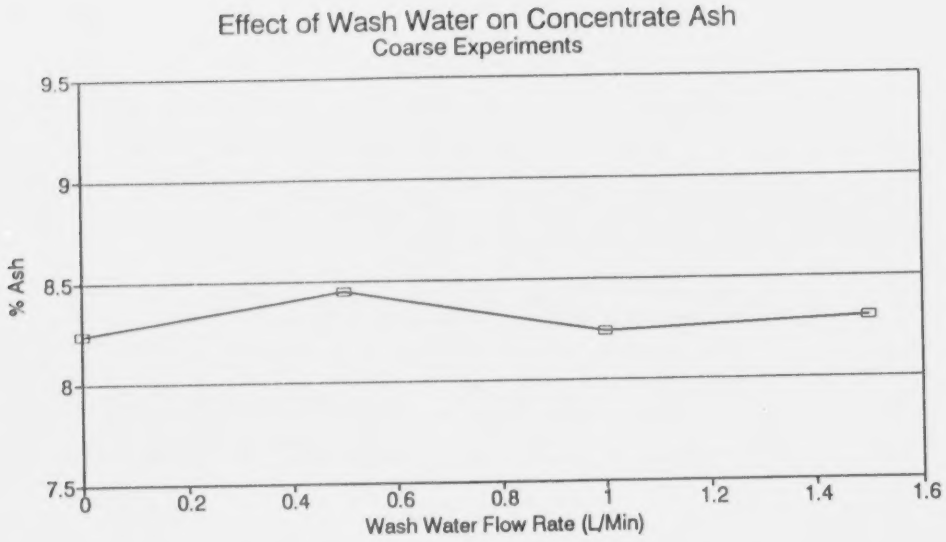

Figure 4.20 Effect of wash water flow rate on concentrate ash for coarse experiments.

4.2.1.4 FROTHER ANALYSIS

The averaged results are shown in table 4.11 for each level of the frother dosage. The results of frother analysis are shown graphically in figures 4.21, 4.22 and 4.23 for $yield_1$, $yield_2$ and concentrate ash respectively.

Table 4.12 Frother analysis of coarse experiments.

FR. (ppm)	FEED (%)		CONC. (%)		TAILINGS (%)		$YIELD_1$ (%)	$YIELD_2$ (%)	ε_g (%)
	SOLIDS	ASH	SOLIDS	ASH	SOLIDS	ASH			
14	3.28	12.74	23.01	8.46	0.38	57.70	89.53	89.80	17.92
17	3.57	14.90	26.02	8.60	0.40	56.89	86.53	90.29	13.25
21	3.49	13.47	25.01	8.07	0.55	52.63	83.46	86.06	14.66
28	3.43	13.49	23.07	8.11	0.39	59.53	88.92	90.82	14.34

As in the wash water analysis, the results show an almost constant value for all three parameters, thus indicating no

significant effect due to frother. The concentrate ash ranged from 8.07% to 8.60%. $Yield_1$ ranged from 89.53% to 83.46%, and $yield_2$ ranged from 89.90% to 90.82%. Appendix C shows the mean bubble size for each frother dosage. Each of these ranges is well within their standard deviation for the experiments. Again, the ANOVA analysis correctly predicted the insignificance of the frother concentrations range on the performance parameters for the flotation of the coarse sample.

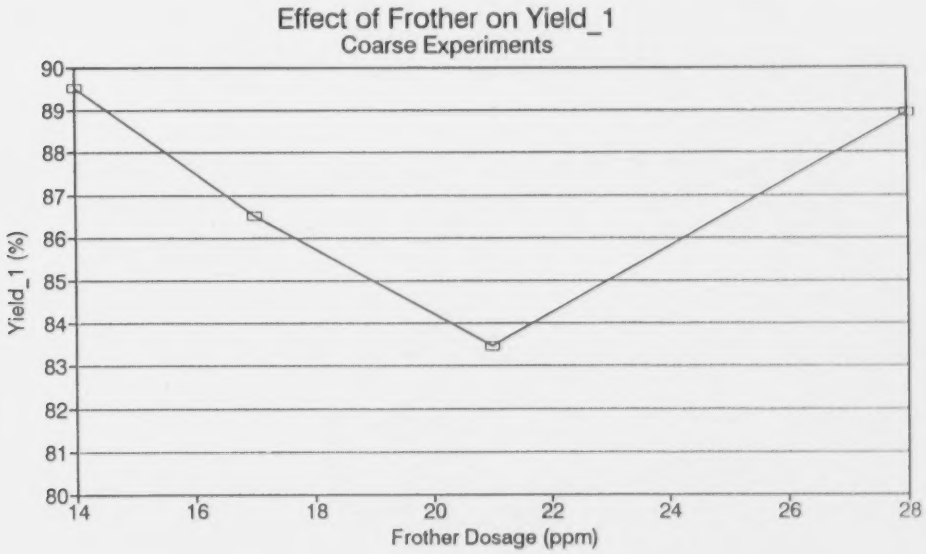

Figure 4.21 Effect of frother dosage on $yield_1$ for coarse experiments.

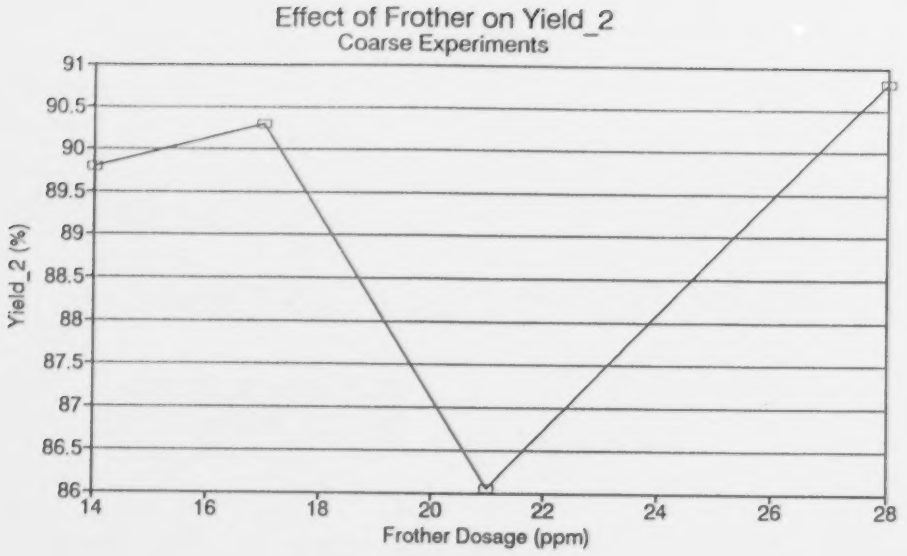

Figure 4.22 Effect of frother dosage on $yield_2$ for coarse experiments.

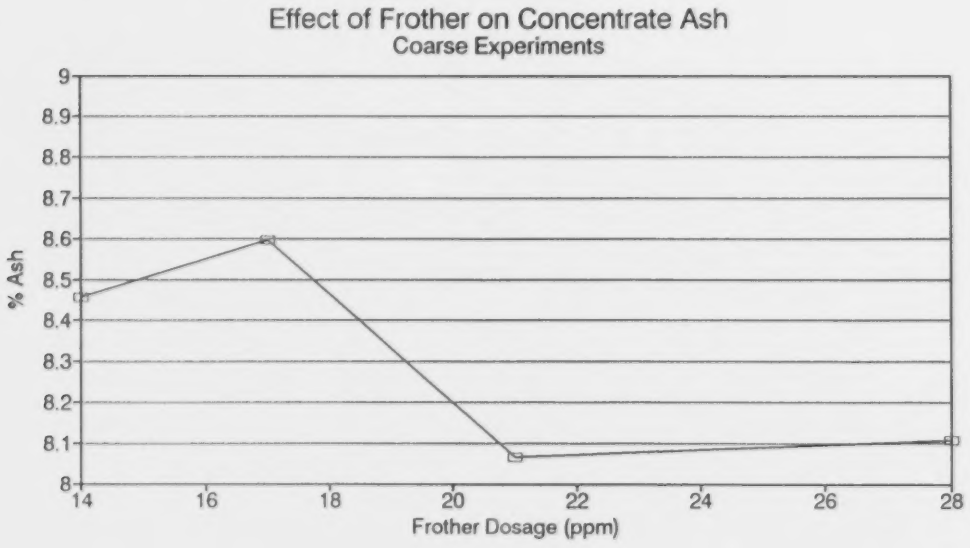

Figure 4.23 Effect of frother dosage on concentrate ash for coarse experiments.

4.3 COMPARISON

The use of the Latin Square experimental design and ANOVA analysis were effective in evaluating the significance of the three input variables relative to the performance parameters for both the fine and coarse coal samples used in this study.

The average concentrate ash for the fine experiments was 7.76%, ranging from 5.79% to 10.13%, compared with 8.31% for the coarse experiments, ranging from 6.53% to 9.49%. This indicates that the fine coal sample has better ash liberation, thus yielding a cleaner overall product. As well the washing of entrained ash particles from the fine coal product can be performed with greater ease. Appendix E shows the screen and ash analyses of the concentrate samples, in relation to particle size and the amount of wash water used. For the fine experiments, the percent ash was reduced in all size fractions as the wash water flow rate was increased, while only the -40μ size fraction lost recovered percent weight. The loss of percent weight is due to the large portions of entrained particles that originated in the -40μ size fraction. In contrast, for the coarse experiments, the percent ash was only reduced significantly in the -75μ size fraction, as wash water flow rates were increased, however the recovered percent weight dropped overall. This is due to the lack of liberated coal and ash particles in the upper size fractions, thus part of the middling material is being removed which results in lower yield, but approximately constant ash content.

The average $yield_1$ for the fine experiments was 65.82%, ranging from 12.11 to 90.74, compared with 87.11%, with a minimum of 62.89 and a maximum of 95.51 for the coarse experiments. The average $yield_2$ for the fine experiments was 76.94%, ranging from 11.35% to 94.42%, compared with 89.24%, with a minimum of 75.21% and a maximum of 95.54% for the

coarse experiments. It should be noted that for the coarse sample experiments, the observed yields were consistently above 82%, irrespective of the operating conditions. The concentrate ash content was also relatively constant at about 8.0% as compared to the coarse feed ash content average of 13.65%. In contrast, the fine coal clearly indicated a good level of dependence on the operating conditions, particularly with respect to the gas flow rate and the wash water flow rate. These results suggest that the column flotation of fine coal requires much more rigorous control of the operating conditions to achieve a good performance, as compared to the flotation of coarse coal samples which provides a very stable operating system, for which a wide range of operating conditions can result in acceptable performance.

5.0 CONCLUSIONS

5.1 SUMMARY OF RESULTS

1. The use of the Latin Square experimental design and ANOVA analysis was effective in evaluating the significance of the three input variables relative to the performance parameters for both the fine and coarse coal samples used in this study, and accurately predicted the significance of the input variables.

2. The ANOVA analyses of the coarse experiments show that gas flow rate has a significant effect on $yield_1$ and a minor effect on concentrate ash. Wash water and frother have no significant effect on either the yield or the concentrate ash content. The coarse experimental system was extremely stable over the range of operating conditions used, in spite of the difficulty in maintaining the feed slurry characteristics. Thus, the coarse experiment performance parameters remained relatively constant over the range of conditions studied.

3. The ANOVA analyses of the fine experiments indicate that both gas and wash water flow rates are significant factors in the performance of fine coal during column flotation, and that frother has only a small significance to the results, although it has more effect on the percent ash.

4. The fine coal results suggest that a gas flow rate of 1.5 ℓ/min (or a superficial gas velocity of 0.79 cm/s) is the optimum with a resultant $yield_2$ of 87.55% and a concentrate ash content of 7.70%. This ensures that the column operates in the bubbly flow regime. In general, the cleaning or washing efficiency of the column in terms of ash rejection is quite good throughout the range of gas flow rates studied.

5. Plug flow conditions, along with moderate wash water rates permits the maximum efficiency to be achieved in the froth zone. The optimum wash water flow rate for cleaning fine particles in the column will be between 0.5 ℓ/min and 1.0 ℓ/min. This corresponds to a superficial wash water velocity in the range of 0.26 cm/s to 0.53 cm/s.

6. The fine coal sample has excellent ash liberation, thus yielding a cleaner overall product, as well the washing of entrained ash particles from the fine coal product can be performed with greater ease.

7. Interaction between wash water and gas flow rates within the bubbly flow regime (below 1.5 ℓ/min), indicates that wash water reaches a maximum concentrate yield at about 0.8 ℓ/min. This maxima becomes less pronounced as the gas flow rate increases from 0.5 ℓ/min to 1.5 ℓ/min. In the transition to the turbulent regime (above 1.5 ℓ/min) the yield maxima is virtually eliminated, indicating that the effectiveness of the wash water is decreased significantly causing the concentrate ash to increase. On the other hand, for the gas flow rates within the bubbly flow regime, increasing the wash water rate beyond 0.8 ℓ/min leads to a significant decline in the concentrate yield due to the detachment of floated particles from the bubbles by the excessive wash water stream.

8. The results from the individual analysis for the fine coal sample agree well with those obtained from the Latin Square experimental design and ANOVA analysis, thus verifying the analytical accuracy of this multivariate analysis technique.

9. The fine coal clearly indicated a good level of dependence on the operating conditions, particularly with respect to the gas flow rate and the wash water flow rate.

These results suggest that the column flotation of fine coal requires much more rigorous control of the operating conditions to achieve a good performance, as compared to the flotation of coarse coal samples which provide a very stable operating system, for which a wide range of operating conditions can result in acceptable performance.

5.2 COMPARISON OF COLUMN AND CELL FLOTATION

The results from several batch cell flotation experiments on the fine coal sample are shown in Appendix B. The batch cell flotation dosage tests achieved yields between 77 and 81 percent, during a one minute collection period, for frother dosages between 25 ppm to 150 ppm. The corresponding concentrate ash content was between 7.69 and 10.55 percent. A batch cell flotation rate test conducted at 25 ppm frother, indicated that the maximum yield obtainable is 88.28%, with concentrate ash content of 8.26%.

Using the optimum flow rates for gas (1.5 ℓ/min) and wash water (0.8 ℓ/min) yielded between 88 and 90 percent, based on experiments 6, and 9. The corresponding concentrate ash content is between 7.85 and 8.63 percent. Comparing the two methods, shows that column flotation gives a moderately higher yield and a comparable ash content. This indicates that column flotation is a feasible alternative for the flotation of fine coal particles.

5.3 AREAS FOR FUTURE WORK

Over the course of completing this thesis project several areas for future work were identified.

One area to examine is the effect of the frother dosage. This can be done by expanding the range of frother dosages

used in the experiments. This would make the trends more evident. As well, experiments could be conducted with frother dosage as the only input variable.

Another area for future examination, is to determine the practical feasibility of utilizing column flotation for the treatment of processed coal tailings. This project has shown that column flotation is an effective method of treating fine coal particles. The next step is to use actual plant tailings material (or simulated high ash tailings). This will present some new problems, including the oxidation of coal particles, and the presence of other reagents. The effects of these new problems will be somewhat balanced by the lower percent solids in the tailings stream.

REFERENCES

Bahr, A., R. Imhoff, and H. Luedke, 1985, "Application and Sizing of a New Pneumatic Flotation Cell", 15th Congres International De Mineralurgie, Eds. Compte and Rendu, Vol. 2, pp. 314-325.

Bensley, C.N., T. Roberts, and S.K. Nicol, 1985, "Column Flotation for the Treatment of Fine Coal", Proceedings: 3 Australian Coal Preparation Conference, Wollongong, NSW, Australia, Nov. 18-21, 1985.

Bustamante, H. and L.J. Warren, 1984, "The Joint Effect of Rank and Grain Size on the Flotation of Australian Bituminous Coals", International Journal of Mineral Processing, Vol. 13, No. 1, pp. 13-28.

Degner, V.R. and J.B. Sabey, 1988, "WEMCO/Leeds Flotation Column Development", Column Flotation '88, Ed. K. Sastry, SME, Littleton, Colorado, pp. 267-280.

Diamond, William J., 1981, Practical Experimental Designs for Engineers and Scientists. Wadsworth Inc., Belmont, California.

Dobby, G.S. and J.A. Finch, 1986-a, "Particle Collection in Columns - Gas Rate and Bubble Size Effects", Canadian Metallurgical Quarterly, Vol. 25, No. 1, pp. 9-13.

Dobby, G.S. and J.A. Finch, 1986-b, "Flotation Column Scale-up and Modelling, CIM Bulletin, Vol. 79, May., pp. 89-96.

Dobby, G.S., J.B. Yianatos, and J.A. Finch, 1988, "Estimation of Bubble Diameter in Flotation Columns from Drift Flux Analysis", Canadian Metallurgical Quarterly, Vol. 27, No. 2, pp. 85-90.

Espinosa-Gomez, R., J.A. Finch, and W. Bernert, 1988-b, "Coalescence and Froth Collapse in the Presence of Fatty Acid", Colloids and Surfaces, Vol. 32, pp. 197-209.

Espinosa-Gomez, R., J. Yianatos, J.A. Finch, and N.W. Johnson, 1988-c, "Carrying capacity limitations in flotation columns", Column Flotation '88, Ed. K. Sastry, SME, Littleton, Colorado, pp. 143-148.

Espinosa-Gomez, R., J.A. Finch, J.B. Yianatos, and G.S. Dobby, 1988-d, "Flotation Column Carrying Capacity: Particle Size and Density Effects", Minerals Engineering, Vol. 1, No. 1, pp. 77-79.

Finch, J.A., and G.S. Dobby, 1990, Column Flotation, Pergamon Press, Toronto, Canada.

Groppo, J., 1986, "Fine Coal Cleaning with Column Flotation", Proceedings of Coal Prep 86, Coal Mining, Chicago, Ill., pp. 381-392.

Jameson, G.J., 1988, "A new concept in flotation column design", Column Flotation '88, Ed. K. Sastry, SME, Littleton, Colorado, pp. 281-286.

Joseph, S., 1985, Hydrodynamic and Mass Transfer Characteristics of a Bubble Column, Ph.D. Thesis, University of Pittsburgh, Pittsburgh, U.S.A.

Kirjavainen, V.M., 1989, "Application of a Probability Model for the Entrainment of Hydrophylic Particles in Froth Flotation", International Journal of Mineral Processing, Vol. 27, pp. 63-74.

Lindman, H.R., 1992, Analysis of Variance in Experimental Design. Springer-Verlag

Mavros, P., N.K. Lazaridis, and K.A. Matis, 1989, "A Study and Modelling of Liquid-Phase Mixing in a Flotation Column", International Journal of Mineral Processing, Vol. 26, pp. 1-16.

Moys, M.H. and J.A. Finch, 1988, "Developments in the Control of Flotation Columns", International Journal of Mineral Processing, Vol. 23, pp. 265-278.

Ofori, P.K., 1988, Column Flotation of Coal and A Froth Model, M.Sc. Thesis, Dept. of Mining, Metallurgy, and Petroleum Engineering, University of Alberta, Edmonton, Alberta.

Pal, R. and J. Masliyah, 1989, "Flow Characterization of a Flotation Column", The Canadian Journal of Chemical Engineering, Vol. 67, Dec., pp. 916-923.

Parekh, B., J. Groppo, and A. Bland, 1986, "A Parametric Study of Fine Coal Cleaning Using Column Flotation", Proceedings: AICHE Winter Annual Meeting, New York, pp. 1-31.

Schneider, J.C. and G. Van Weert, 1988, " Design and Operation of the Hydrochem Flotation Column", Column Flotation '88, Ed. K. Sastry, SME, Littleton, Colorado, pp. 287-292.

Schulze, H.J., B. Radoev, Th. Geidel, H. Stechemesser, and E. Topper, 1989, "Investigations of the Collision Process between Particles and Gas Bubbles in Flotation - A Theoretical Analysis", International Journal of Mineral Processing, Vol. 27, pp. 263-278.

Trahar, W.J., 1981, "A Rational Interpretation of the Role of Particle Size in Flotation", International Journal of Mineral Processing, Vol. 8, pp. 289-327.

Wills, B.A., 1985, Mineral Processing Technology, 3rd Edition, Pergamon Press, Oxford, England.

Xu, M. and J.A. Finch, 1989, "Effect of Sparger Type and Surface Area on Bubble Size in a Flotation Column", Canadian Metallurgical Quarterly, Vol. 28, No. 1, pp. 1-6.

Yang, D.C., 1988, "A New Packed Column Flotation System", Column Flotation '88, Ed. K. Sastry, SME, Littleton, Colorado, pp. 257-266.

Ye, Y. and J.D. Miller, 1989, "The Significance of Bubble/Particle Contact Time During Collision in the Analysis of Flotation Phenomena", International Journal of Mineral Processing, Vol. 25, pp. 199-219

Yianatos, J.B., J.A. Finch, and A.R. Laplante, 1986, "Hold-up Profile and Bubble Size Distribution of Flotation Column Froths", Canadian Metallurgical Quarterly, Vol. 25, No. 1, pp. 23-29.

Yianatos, J.B., J.A. Finch, and A.R. Laplante, 1987, "Cleaning Action in Column Flotation Froths", Transactions of the Institute of Mining and Metallurgy, Section C - Mineral Processing and Extractive Metallurgy, Vol.96, Dec.

Yianatos, J.B., R. Espinosa-Gomez, J.A. Finch, A.R. Laplante, and G.S. Dobby, 1988, "Effect of Column Height on Flotation Column Performance", Minerals and Metallurgical Processing, Feb., pp. 11-14.

Zhou, Z., 1992, Surfactant Effects on Bubbles and Column Flotation of Coal, M.Sc. Thesis, Dept. of Mining, Metallurgy, and Petroleum Engineering, University of Alberta, Edmonton, Alberta.

Zipperian, D.E. and U. Svensson, 1988, "Plant Practice of the FLOTAIRE Column Flotation Machine for Metallic, Nonmetallic, and Coal Flotation", Column Flotation '88, Ed. K. Sastry, SME, Littleton, Colorado, pp. 43-54.

APPENDIX A

Analyses Procedures

Procedure for wet screen analysis

1. Arrange the screens in the wet screening device, with the largest aperture on top down to the smallest. Place a clean bucket at bottom to catch the undersize material.

2. Pour the sample into the top screen, washing all of the particles out the sample beaker. Turn on a moderate level of vibration. Use a gentle water spray to wash the particles through the screens. When the flow of particles through the screen ceases, begin washing the next screen until all screens have been washed.

3. Remove the screens starting from the top, rinsing down the area below the screen into the next screen (or bucket for last screen). Using pre-weighed trays (W_T), put the screens the drying oven. Filter the undersize material in the catch pail before drying.

4. Remove the dried samples from the drying oven and allow to cool. Empty the screen into the tray using a brush to loosen all particles in the screen and on the walls. Record the weight of the tray plus sample (W_{T+S}). Subtraction of the tray weight gives the weight of the size fraction, W_i. The dry weight for the whole sample is the sum of all its size fractions.

Procedure for ash analysis

1. Clean and weigh the required number of crucibles. Record the crucible name and weight to one thousandth of a gram (W_{CR}).

2. Subsample approximately 1.0 gram of sample into the crucible, and record the weight of the crucible plus the sample (W_{CR+S}). Ensure sample in crucible is representative of the entire sample.

3. Arrange the filled crucibles in the furnace, and start the automatic timer. The furnace will heat to 750°C and remain at that temperature for the preset time (8 hours).

4. Weigh the crucibles immediately after they have cooled to room temperature, so the samples do not pick up moisture from the air. Record the weights as crucible plus ash(W_{CR+A}).

5. Calculate the percentage ash from the following formula:

$$A\,(\%) = \frac{W_{CR+A} - W_{CR}}{W_{CR+S} - W_{CR}} \times 100\%$$

Procedure for Denver Cell Flotation

1. Add the first 1ℓ of tap water to the cell, and weigh out the coal (W_f) required to make up the desired percent solids. Mix coal into water with spatula. Once all of the coal is wetted, lower the impeller into the cell. Turn on the impeller and add the remainder of the water to the cell.

2. Allow the slurry to mix for about 5 minutes to ensure all particles are wetted. Add the proper regent dosages, and allow 2 minutes for reagents to mix. Place the first collector pan under overflow lip.

3. Turn on the air, while starting stop watch. Scoop froth over overflow lip into collector pan. Rinse down particles of the edges of the cell, and impeller with a wash bottle. Add tap water if necessary to maintain the fluid level.

4. After one minute, turn off the air and the impeller. Lift the impeller out of the tailings and rinse thoroughly with water until completely clean.

5. Filter the tailings sample, and then dry and weigh both the concentrate (W_{conc}) and tailings (W_t) samples.

6. Complete an ash analysis of both samples. The yield can be calculated directly using the following formula:

$$Y = \frac{W_{conc}}{W_f} \times 100\%$$

APPENDIX B

Additional Experimental Results

Column Flotation Verification Experiments

Table B.1 Results for the fine verification experiments.

#	Gas	Fr	WW	FEED (%)		CONC.(%)		TAILS (%)		$YIELD_1$ (%)	$YIELD_2$ (%)
				SOLIDS	ASH	SOLIDS	ASH	SOLIDS	ASH		
FV1	1.5	21	0.5	4.15	14.35	17.70	9.20	0.63	45.27	85.72	87.85
FV2	1.5	21	1.0	4.13	14.54	8.04	9.35	0.61	48.88	86.87	92.16
FV3	1.5	14	1.0	4.13	14.44	15.76	8.59	0.61	43.53	83.28	88.69
FV4	1.0	14	1.0	3.32	15.04	25.38	7.92	0.79	32.06	70.49	78.74
FV5	0.5	21	1.0	3.31	13.77	21.73	7.51	1.00	26.43	66.93	73.13
FV6	1.0	28	1.0	3.39	14.24	16.78	8.48	1.02	41.76	82.69	74.29
FV7	0.5	14	1.5	3.22	13.22	15.62	5.37	1.88	15.52	22.69	47.27
FV8	1.5	21	1.5	4.03	14.19	15.35	7.36	0.82	32.78	73.14	84.23
μ				4.05	14.36	16.33	7.83	1.10	34.12	67.70	77.39
σ^2				0.15	0.41	34.77	1.52	0.54	127.55	468.51	343.67
σ				0.39	0.64	5.90	1.23	0.74	11.29	21.65	18.54
Min	0.5	14	0.0	3.22	13.21	7.75	5.37	0.42	15.52	12.11	11.35
Max	1.5	28	1.5	4.67	15.68	28.56	10.13	3.80	58.70	90.74	94.42

Table B.2 Results for coarse verification experiments.

#	GAS	FR	WW	FEED (%)		CONC. (%)		TAILINGS (%)		$YIELD_1$ (%)	$YIELD_2$ (%)
				SOLIDS	ASH	SOLIDS	ASH	SOLIDS	ASH		
CV1	2.0	21	0.5	2.69	11.00	19.47	9.17	0.17	70.21	97.01	94.53
CV2	0.5	21	1.0	2.66	11.83	20.93	7.99	0.33	44.08	89.37	88.98
CV3	0.5	14	1.5	4.43	14.75	33.00	6.83	0.82	33.36	70.13	83.50
μ				3.41	13.47	24.31	8.26	0.43	55.51	86.86	89.21
σ^2				0.19	1.55	48.00	0.77	0.05	183.64	74.88	25.76
σ				0.44	1.24	6.93	0.88	0.22	13.55	8.65	5.08
Min	0.5	14	0.0	2.66	11.00	13.58	6.53	0.17	28.81	62.89	75.21
Max	2.0	17	1.5	4.43	15.41	42.72	9.49	1.01	77.41	97.01	95.54

The verification of the fine coal results include a series of experiments that show the effect of wash water for a constant gas flow rate of 1.5 ℓ/min and a constant frother

dosage of 21 ppm. The experiment numbers in order of increasing wash water are: #3, #FV1, #FV2, and #FV8. These results are shown in figures B.1, B.2, and B.3.

A second series of the fine coal verification experiments show the effect of frother dosage for a constant gas flow rate of 1.5 ℓ/min and a constant wash water flow rate of 1.0 ℓ/min. The experiment numbers in order of increasing frother dosage are: #FV3, #9, and #FV2. These results are shown in figures B.4, B.5, and B.6.

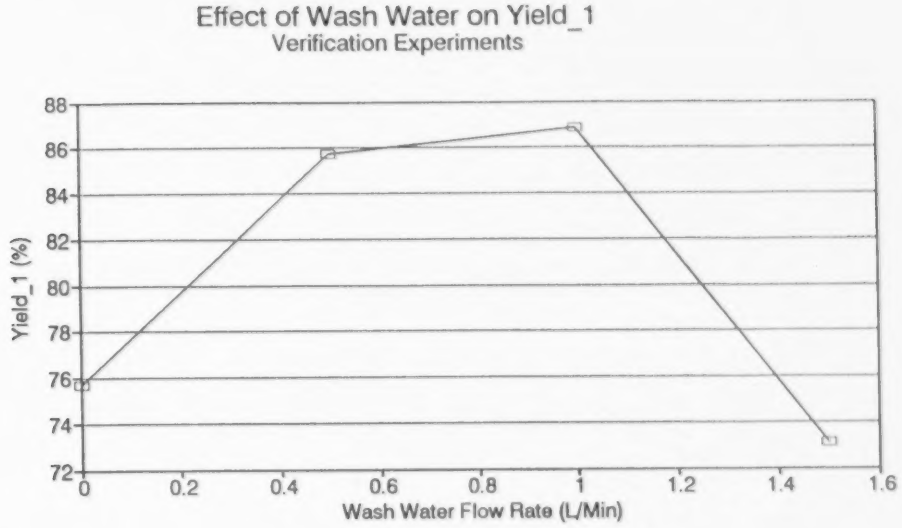

Figure B.1 Effect of wash water on yield$_1$ for fine verification experiments, with a gas flow rate of 1.5 ℓ/min and a frother dosage of 21 ppm.

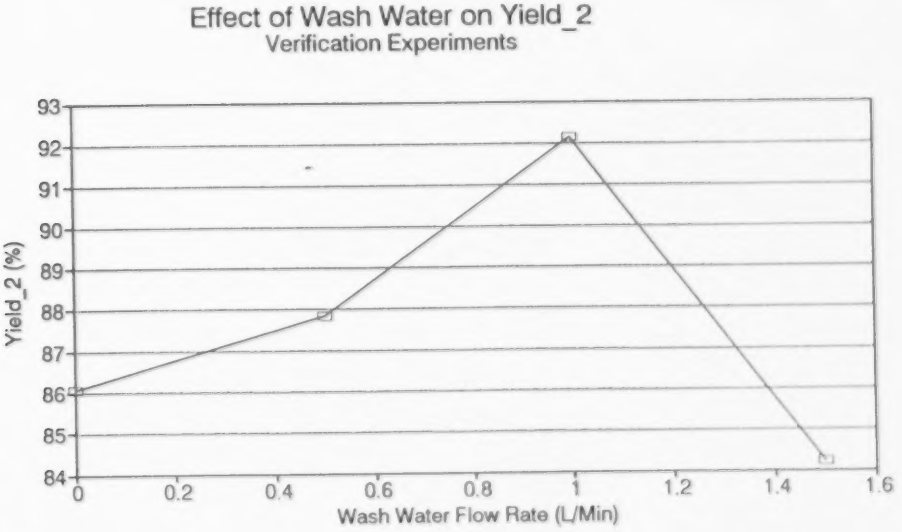

Figure B.2 Effect of wash water on yield$_2$ for fine verification experiments, with a gas flow rate of 1.5 ℓ/min and a frother dosage of 21 ppm.

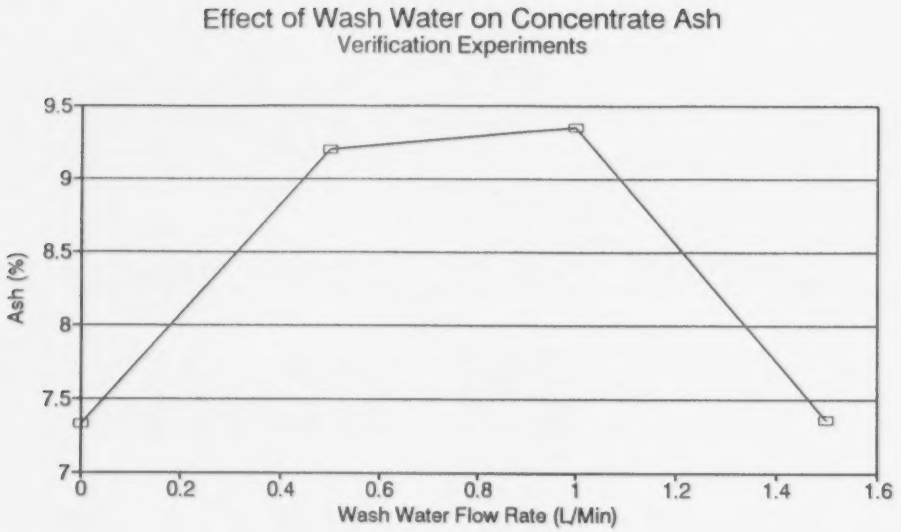

Figure B.3 Effect of wash water on concentrate ash for fine verification experiments, with a constant gas flow rate (1.5 ℓ/min) and a constant frother dosage (21 ppm).

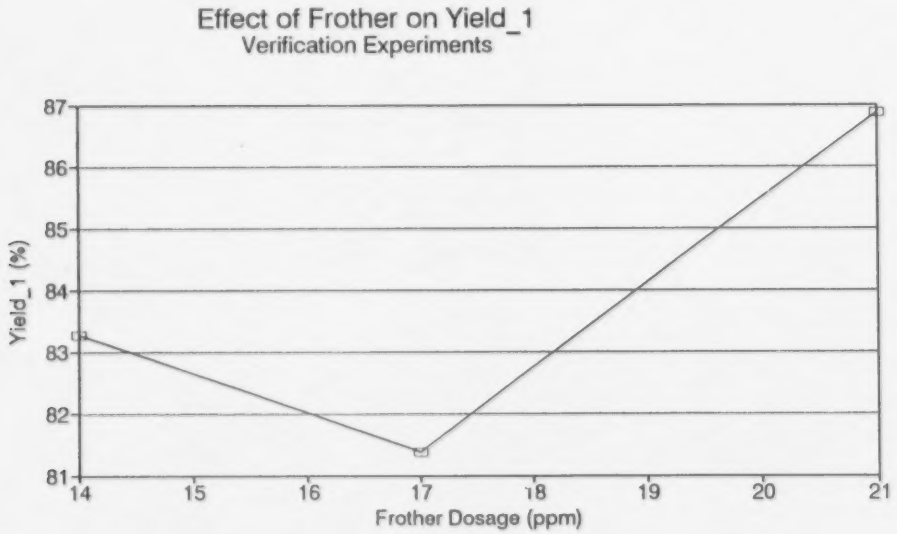

Figure B.4 Effect of frother on $yield_1$ for fine verification experiments, with constant flow rates for gas (1.5 ℓ/min) and wash water (1.0 ℓ/min).

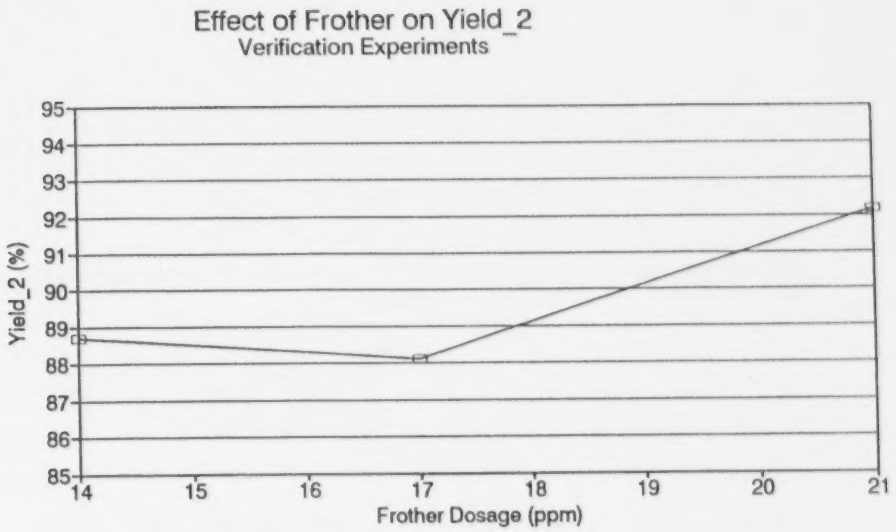

Figure B.5 Effect of frother on $yield_2$ for fine verification experiments, with constant flow rates for gas (1.5 ℓ/min) and wash water (1.0 ℓ/min).

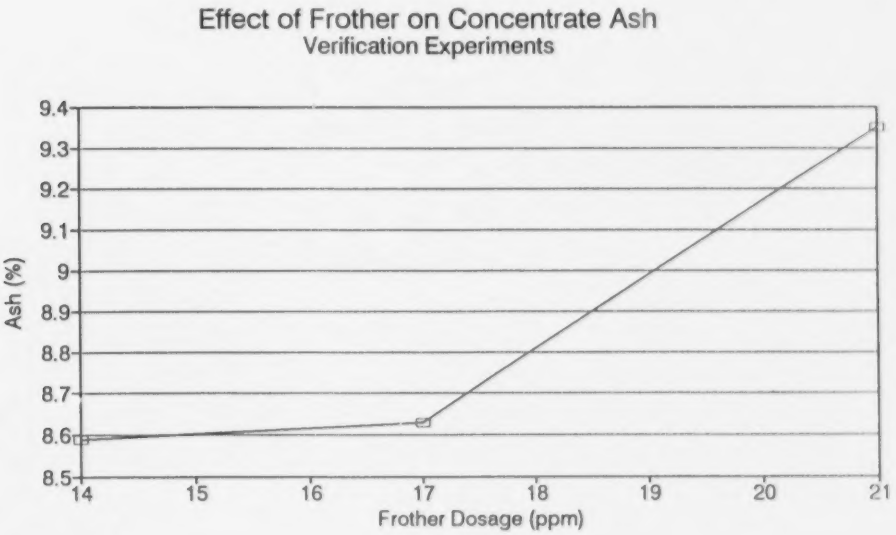

Figure B.6 Effect of frother on concentrate ash for fine verification experiments, with constant flow rates for gas (1.5 ℓ/min) and wash water (1.0 ℓ/min).

Batch Denver Cell Flotation Results

Two categories of batch cell flotation tests were performed on the fine coal sample: dosage tests, and rate tests. Table B.3 shows the results from the dosage tests. The procedure for the batch cell flotation tests is outlined in Appendix A. The reagent dosage is the combination of both the collector and frother, in the specified ratio. The frother dosage ranges from 25 ppm to 150 ppm.

Table B.3 Denver cell flotation dosage test for the fine coal sample.

10% solids
Feed ash 14.3%
1 Kerosene:1 Dowfroth
1 minute sample

Dosage (ℓ/tonne$_c$)	Yield (%)	C. Ash (%)	T. Ash (%)
0.5	77.41	7.69	38.99
1	78.18	9.27	36.23
1.5	78.84	9.12	35.36
2	79.34	9.40	35.86
2.5	81.13	10.55	35.64
3	81.16	9.43	33.91

Table B.4 shows the results from a rate test. The frother dosage for this test is 25 ppm (0.5 ℓ/tonne$_c$). This dosage level exhibited the highest flotation efficiency, while it is also within the range used for the column flotation experiments. The final tailings weight was 11.72% with an ash content of 58.24%.

Table B.4 Denver cell flotation rate test for the fine coal sample.

10% solids
Feed ash 14.12%
1 Kerosene:1 Dowfroth
0.5 ℓ/tonne$_c$

Time (Minutes)	Cumulative Yield (%)	Ash (%)
0.0 - 0.25	22.95	6.60
0.25 - 0.5	53.34	7.09
0.5 - 0.75	70.28	7.41
0.75 - 1.0	78.13	7.67
1.0 - 1.5	84.86	8.00
1.5 - 2.0	88.28	8.26

APPENDIX C

Bubble Size Calculations

Sample Bubble Size Calculations

Bubble size calculations follow the drift flux procedure outlined in Chapter 2. The average slurry properties for the fine coal experiments were used for each calculation. A sample calculation for the averaged gas flow rate of 0.5 ℓ/min is shown below. The factor to convert from volumetric to superficial velocity is 0.526 cm-min/ℓ-s. The superficial gas flow rate, V_g and the gas holdup estimate, ε_g for the experiment are the two input variables in this procedure, along with an initial estimates of m, and bubble size.

Constants for all calculations:

$\Phi_l = 0.965$

$\rho_{sl} = 0.995$ g/cm^3

$\mu_{sl} = \mu_{water} * \Phi_l^{2.5} = 0.01$ g/cm-s $\cdot 0.965^{2.5} = 0.010875$ g/cm-s

$V_{sl} = 1.58$ cm/s

Constants of gas flow rate of 0.5ℓ/min:

$V_g = 0.26$ cm/s

$\varepsilon_g = 0.0600$

Calculate the drift-flux constant V_{gl} for the experimental conditions as follows:

$$V_{gl} = \frac{V_g}{\varepsilon_g} - \frac{V_{sl}}{(1-\varepsilon_g)}$$

$$= \frac{0.26}{0.06} - \frac{1.58}{(1-0.06)} = 2.652$$

Estimate m = 3.00, and calculate the terminal bubble rise velocity V_∞ as follows:

$$V_\infty = \frac{V_g}{\varepsilon_g (1-\varepsilon_g)^m} - \frac{(V_g + V_{sl})}{(1-\varepsilon_g)^m}$$

$$= \frac{0.26}{0.06 \cdot (1-0.06)^3} - \frac{(0.26+1.58)}{(1-0.06)^3} = 3.002$$

Estimate d_b = 0.1 cm, and calculate the Reynolds number for the bubble swarm as follows:

$$Re_s = d_b \cdot \frac{V_{gl}\, \rho_{sl}\, (1-\varepsilon_g)}{\mu_{sl}}$$

$$= 0.1 \cdot \frac{(2.652)\,(0.995)\,(1-0.06)}{0.010875} = (0.1)\,(228.153) = 22.815$$

Calculate d_b as follows:

$$d_b = \sqrt{\frac{18\,\mu_{sl} V_\infty}{g \Delta\rho}\,(1+0.15 Re_s^{0.687})}$$

$$= \sqrt{\frac{(18)\,(0.010875)\,(3.002)}{(981)\,(0.995-0.001)}\,(1+(0.15)\,(22.815)^{0.687})}$$

$$= \sqrt{(6.03\times10^{-4})\,(2.2859)} = 0.0371 cm$$

Begin iterations of Re_s and d_b as follows:

$$Re_s = (0.0371)\,(228.153) = 8.468$$

$$d_b = \sqrt{(6.03\times10^{-4})\,(1+0.15\,(8.468)^{0.687})} = 0.0315$$

$$Re_s = 7.196$$

$$d_b = 0.0309$$

$$Re_s = 7.044$$

$$d_b = 0.0308$$

Calculate a new value for m, using the last values of Re_s and d_b:

$$m = \left[4.45 + 18\frac{d_b}{d_c}\right] Re_s^{-0.1}$$

$$= \left[4.45 + 18\frac{0.0308}{6.35}\right] 0.7044^{-0.1} = 3.734$$

Calculate a new V_{∞} = 3.141, and continue iterations of Re_s and d_b as follows:

$$Re_s = (0.0308)\frac{(2.652)(0.995)(1-0.06)}{0.010875}$$

$$= (0.0308)(228.082) = 7.023$$

$$d_b = \sqrt{\frac{(18)(0.010875)(3.141)}{(981)(0.994)}(1+0.15(7.025)^{0.687})}$$

$$= \sqrt{(6.036\times10^{-4})(1.5724)} = 0.0315$$

$$Re_s = 7.182$$

$$d_b = 0.0316$$

$$Re_s = 7.202$$

The bubble size for this set of conditions is 0.316 mm, using the drift-flux calculation method.

After verifying the program results, a pascal computer program was used to do the remaining calculations. The speed of calculations allowed several starting estimates of m and d_b to be tested, to determine if the starting values affected the final bubble size value. It was determined that there is no effect due to these estimates. A listing of the source program, and a sample of its output are provided at the end of this section. Table C.1 shows the mean bubble size estimates for the averaged gas results. Table C.2 shows the mean bubble

size estimates for the averaged frother results, using the average gas flow rate of 1.25 ℓ/min.

Table C.1 Mean bubble size as a function of gas flow rate for fine experiments.

GAS (ℓ/Min)	ε_g (%)	d_b (mm)
0.5	6.00	0.32
1.0	10.83	0.38
1.5	13.60	0.48
2.0	14.24	0.62

Table C.2 Mean bubble size as a function of frother dosage for fine experiments.

FROTHER (ppm)	ε_g (%)	d_b (mm)
14	8.42	0.63
17	12.31	0.43
21	10.69	0.49
28	13.25	0.39

Table C.3 Mean bubble size as a function of gas flow rate for coarse experiments.

GAS (ℓ/Min)	ε_g (%)	d_b (mm)
0.5	13.29	0.07
1.0	14.59	0.28
1.5	16.16	0.40
2.0	16.13	0.55

Table C.4 Mean bubble size as a function of frother dosage for coarse experiments.

FROTHER (ppm)	ε_g (%)	d_b (mm)
14	17.29	0.30
17	13.25	0.40
21	14.66	0.36
28	14.34	0.37

Bubble Size Program

```
program Bub_Size;

uses
  dos, crt, graph,
   Lib, PslLib, MathLib;

var
  GHo,                    { Gas Hold-Up }
  Grate,                  { Gas Flow Rate }
  m,                      { Guess 1 }
  Db       : real;        { Bubble Size (Guess 2) }
  V_gl,                   { Drift-flux Velocity }
  V_inf,                  { Bubble Rise Velocity}
  Reno     : real;        { Renolds # }
  Extended,
  Fini,
  OK       : boolean;
  Ch       : char;

  m2,
  Db2,
  x        : real;
  Fout     : text;
  i,j,k    : integer;

const
  Visc   = 0.010875;      { Viscosity }
  SDen   = 0.995;         { Slurry Density }
  DelDen = 0.994;         { Air/Slurry Density Difference }
  SVel   = 1.58;          { Slurry Velocity }
  Grav   = 981.0;         { Acceleration due to gravity }

begin
  clrscr;
  Put_Centered_String(' Bubble Size Calculations ', 3, 3);
  Gho := 0.0;
  Grate := 0.0;
  m := 0.0;
  Db := 0.0;
  OK := false;
  Fini := false;
```

```
k := 0;
TextColor(White);
TextBox(10,13,70,23);
repeat
  repeat
    Get_Prompted_Real(GHo,1,7,4,  'Gas Hold-Up   : ',5,10,'',25,1);
    Get_Prompted_Real(GRate,1,7,2,'Gas Flow Rate : ',7,10,'',25,1);
    Get_Prompted_Real(m,1,7,2,    'M             : ',9,10,'',25,1);
    Get_Prompted_Real(Db,1,7,4,   'Bubble Size   : ',11,10,'',25,1);
    Put_Centered_String(
          ' Press Y to continue, N to Redo Input, <Esc> to Quit ', 24,3);
    Cursor_Off;
    Get_Key(Extended, Ch);
    case Ch of
      'y','Y': OK := true;
      'n','N': OK := false;
      #27: begin
             Cursor_On;
             clrscr;
             halt
           end;
    end;
  until OK;

  clrln(24, 0);
  window(11,14,69,22);

{ start calculations }
  V_gl := (GRate/Gho)-(SVel/(1-Gho));

  i := 0;
  m2 := m;
  Db2 := db;
  assign(FOut,'Bubbles');
  if not Exist('Bubbles') then
    rewrite(FOut)
  else
    append(Fout);

  writeln(FOut);
  writeln(FOut);
  writeln(FOut);
  writeln(FOut,'Gas Hold-Up   : ' , GHo:7:4);
  writeln(FOut,'Gas Flow Rate : ' , GRate:7:2);
```

```
writeln(FOut,'M              : ' , m:7:2);
writeln(FOut,'Bubble Size    : ' , Db:7:4);
writeln(FOut);

repeat

  i := i +1;
  m := m2;

  x := Power(1-GHo,m);
  V_inf := GRate/(Gho*x) - (GRate+SVel)/x;

  j := 0;
  repeat
    j := j+1;
    Db := Db2;
    Reno := (Db * V_gl * SDen * (1-GHo))/Visc;
    Db2 := sqrt(((18*Visc*V_inf)/(Grav*DelDen))*
(1+0.15*Power(Reno,0.687)));
    writeln(FOut,'i = ', i:3, 'j = ',j:3,'m = ',m:7:2, 'Db = ',Db2:7:4);
    if k < 9 then
      k := k+1
    else
      begin
        gotoxy(1,1);
        delline;
      end;
    gotoXY(1,k);
    write(Tab(5),'i =  ', i:3, 'j = ',j:3,'m = ',m:7:2, 'Db = ',Db2:7:4);
  until abs(1-(Db/Db2)) < 0.01;

  m2 := (4.45+(18*Db)/6.35)*Power(Reno,-0.1);
until abs(m-m2) < 0.1;

if k < 9 then
  k := k+1
else
  begin
    gotoxy(1,1);
    delline;
  end;
gotoXY(1,k);
write(Tab(10),'Final  m  = ',m2:7:2);
if k < 9 then
```

```
      k := k+1
    else
      begin
        gotoxy(1,1);
        delline;
      end;
    gotoXY(1,k);
    write(Tab(10),'Final Db  = ',Db2:8:5);
    writeln(Fout,' Final  m  = ',m2:7:2);
    writeln(Fout,' Final Db  = ',Db2:8:5);
    close(Fout);

    window(1,1,80,25);
    Cursor_Off;
    Put_Centered_String(
          ' Press any key to continue, <Esc> to Quit ', 24,3);
    Get_Key(Extended, Ch);
    case Ch of
      #27: Fini := true;
    end;

    clrln(24, 0);
  until Fini;
  Cursor_On;

end.
```

Sample Results from Bubble Size Program

GAS = 0.5 ℓ/min
Gas Hold-Up : 0.0600
Gas Flow Rate : 0.26
M : 3.00
Bubble Size : 0.1000

i = 1 j = 1 m = 3.00 Db = 0.0371
i = 1 j = 2 m = 3.00 Db = 0.0315
i = 1 j = 3 m = 3.00 Db = 0.0309
i = 1 j = 4 m = 3.00 Db = 0.0308
i = 2 j = 1 m = 3.73 Db = 0.0315
i = 2 j = 2 m = 3.73 Db = 0.0316
Final m = 3.73
Final Db = 0.03158

FROTHER = 14 ppm
Gas Hold-Up : 0.0842
Gas Flow Rate : 0.66
M : 3.00
Bubble Size : 0.1000

i = 1 j = 1 m = 3.00 Db = 0.0689
i = 1 j = 2 m = 3.00 Db = 0.0633
i = 1 j = 3 m = 3.00 Db = 0.0621
i = 1 j = 4 m = 3.00 Db = 0.0619
i = 2 j = 1 m = 3.27 Db = 0.0626
i = 2 j = 2 m = 3.27 Db = 0.0627
Final m = 3.27
Final Db = 0.06271

APPENDIX D

Bias Flow Rate Calculations

Sample Bias Flow Rate Calculations

The bias flow rate is defined as the net flow of water downward through the interface. Sample calculations of the bias flow rate for gas and wash water flow rates are shown below. The calculations for the gas flow rates use the average wash water rate of 0.75 ℓ/min for each gas flow rate. Using the data from table 4.4, the bias flow rate for the gas rate of 0.5 ℓ/min is calculated as follows:

Constants for all calculations:

$\rho_{water} = 0.985\ g/cm^3$
$\rho_{coal} = 1.35\ g/cm^3$
$\mu_{sl} = 0.010875\ g/cm\text{-}s$ (from Appendix C)
$Q_f = 3.0\ \ell/min$

Percent Solids and Yield for Gas = 0.5 ℓ/min:

$F = 4.00\%$
$C = 17.97\%$
$Y_2 = 50.32\%$

Calculate the slurry density ρ_{sl} as follows:

$$\rho_{sl} = \frac{100}{\frac{F}{\rho_{coal}} + \frac{(100-F)}{\rho_{water}}}$$

$$= \frac{100}{\frac{4.00}{1.35} + \frac{(100-4.00)}{0.985}} = 0.9958 g/cm^3$$

Calculate the feed solids rate $Q_{s(f)}$ as follows:

$$Q_{s(f)} = Q_f \times \rho_{sl} \times F$$
$$= 3.0 L/\text{min} \times 0.9958 g/mL \times 0.040$$
$$= 0.1195 kg/\text{min}$$

Calculate the concentrate solids rate $Q_{s(c)}$ as follows:

$$Q_{s(c)} = Y_2 \times Q_{s(f)} = 0.5032 \times 0.1195 kg/\text{min} = 0.0601 kg/\text{min}$$

Calculate the concentrate water rate $Q_{w(c)}$ as follows:

$$Q_{w(c)} = \frac{Q_{s(c)} \times (1 - C)}{\rho_{water} \times C}$$
$$= \frac{0.0601 kg/\text{min} \times (1 - 0.1797)}{0.985 g/mL \times 0.1797} = 0.2745 L/Min$$

The bias rate is the net downward flow of water, and is calculated by taking the difference between the wash water flow rate and the water reporting to the concentrate, as follows:

$BR = Q_{ww} - Q_{w(c)} = 0.75 - 0.2745 = 0.4755$ ℓ/min

Using the data in table 4.5, the bias flow rate for the wash water flow rate of 0.5 ℓ/min is calculated as follows:

Percent Solids and Yield for Wash Water = 0.5 ℓ/min:

F = 4.33%

C = 13.49%

Y_2 = 83.97%

Calculate the slurry density ρ_{sl} as follows:

$$\rho_{sl} = \frac{100}{\frac{4.33}{1.35} + \frac{(100 - 4.33)}{0.985}} = 0.9967 g/cm^3$$

Calculate the feed solids rate $Q_{s(f)}$ as follows:

$$Q_{s(f)} = 3.0 L/\text{min} \times 0.9967\, g/mL \times 0.0433 = 0.1295 kg/\text{min}$$

Calculate the concentrate solids rate $Q_{s(c)}$ as follows:

$$Q_{s(c)} = 0.8397 \times 0.1295\, kg/\text{min} = 0.1087\, kg/\text{min}$$

Calculate the concentrate water rate $Q_{w(c)}$ as follows:

$$Q_{w(c)} = \frac{0.1087\, kg/\text{min} \times 0.8651}{0.985\, g/mL \times 0.1349} = 0.7078 L/Min$$

The bias flow rate is as follows:

$$BR = Q_{ww} - Q_{w(c)} = 0.5 - 0.7078 = -0.2078\ \ell/\text{min}$$

The negative bias flow indicates that the net flow of water is upward, in contrast to the first example.

Table D.1 shows the calculated bias flow rates with respect to the gas flow rates for the fine experiments. Table D.2 shows the calculated bias flow rates with respect to the wash water flow rates for the fine experiments.

Table D.1 Bias flow rate as a function of gas flow rate for fine experiments, with a wash water flow rate of 0.75ℓ/min.

Gas Rate (ℓ/Min)	Bias Rate (ℓ/min)
0.5	0.475
1.0	0.323
1.5	0.129
2.0	-0.188

Table D.2 Bias flow rate as a function of wash water rate for fine experiments.

Wash Water (ℓ/min)	Bias Rate (ℓ/min)
0.0	-0.287
0.5	-0.2078
1.0	0.463
1.5	0.757

The data from tables 4.10 (gas analysis) and 4.11 (wash water analysis) was used to calculate the following bias flow rates for the coarse experiments. Tables D.3 and D.4 show the calculated bias flow rates with respect to gas and wash water flow rates respectively for the coarse experiments.

Table D.3 Bias flow rate as a function of gas flow rate for coarse experiments, with a wash water flow rate of 0.75ℓ/min.

Gas Rate (ℓ/Min)	Bias Rate (ℓ/min)
0.5	0.489
1.0	0.442
1.5	0.444
2.0	0.464

Table D.4 Bias flow rate as a function of wash water rate for coarse experiments.

Wash Water (ℓ/min)	Bias Rate (ℓ/min)
0.0	-0.169
0.5	0.085
1.0	0.631
1.5	1.194

APPENDIX E

Screen Analysis of Concentrate Samples

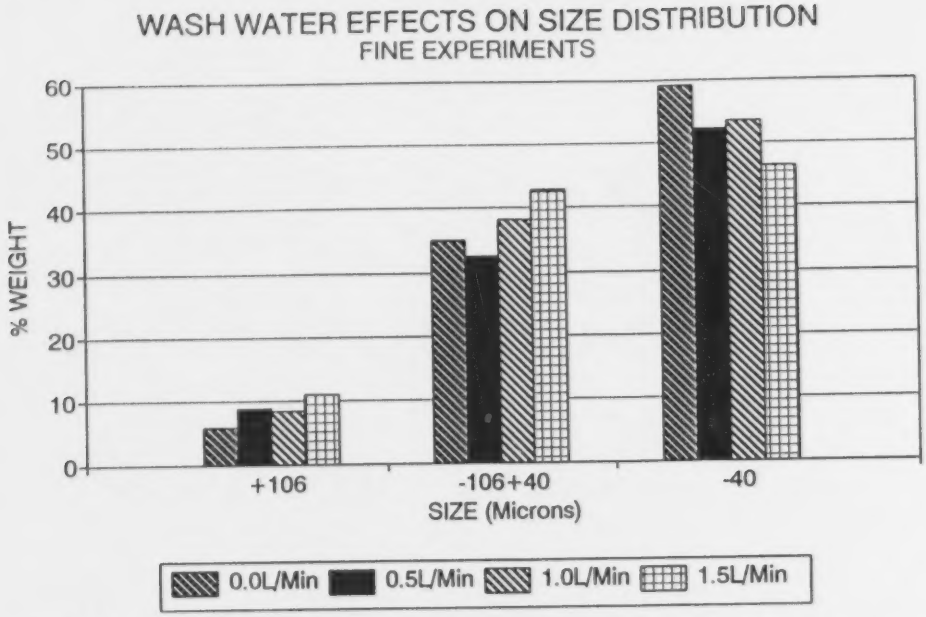

Figure E.1 Effect of wash water flow rate on the weight size fractions in the concentrate for fine experiments.

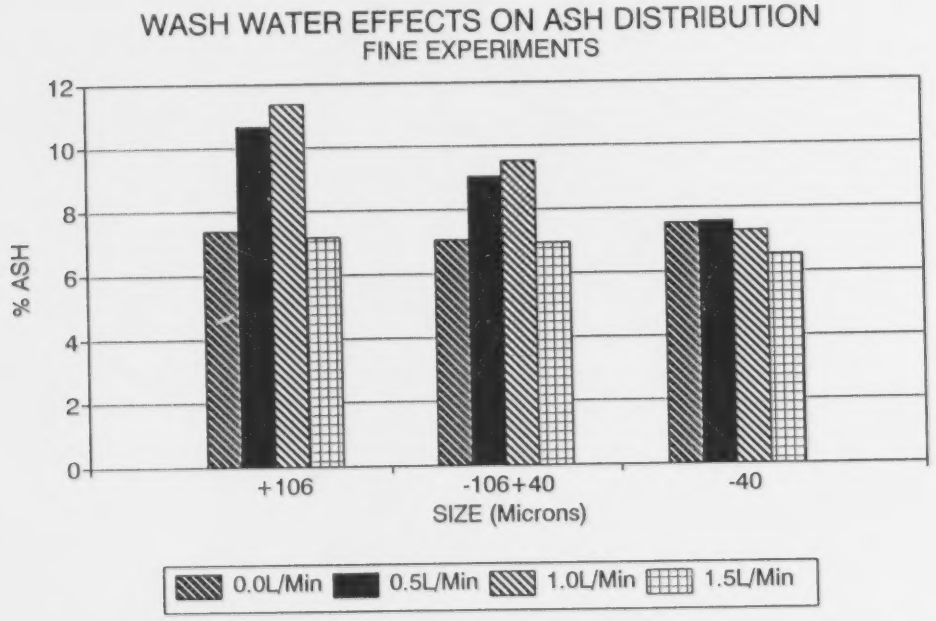

Figure E.2 Effect of wash water on ash content in each size fraction in the concentrate for fine experiments.

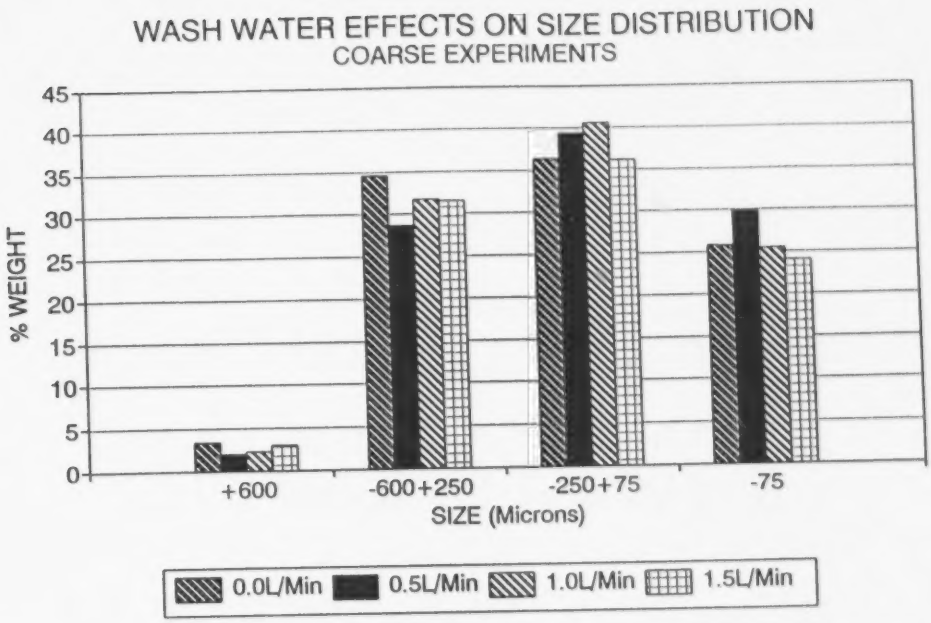

Figure E.3 Effect of wash water flow rate on the weight size fractions in the concentrate for coarse experiments.

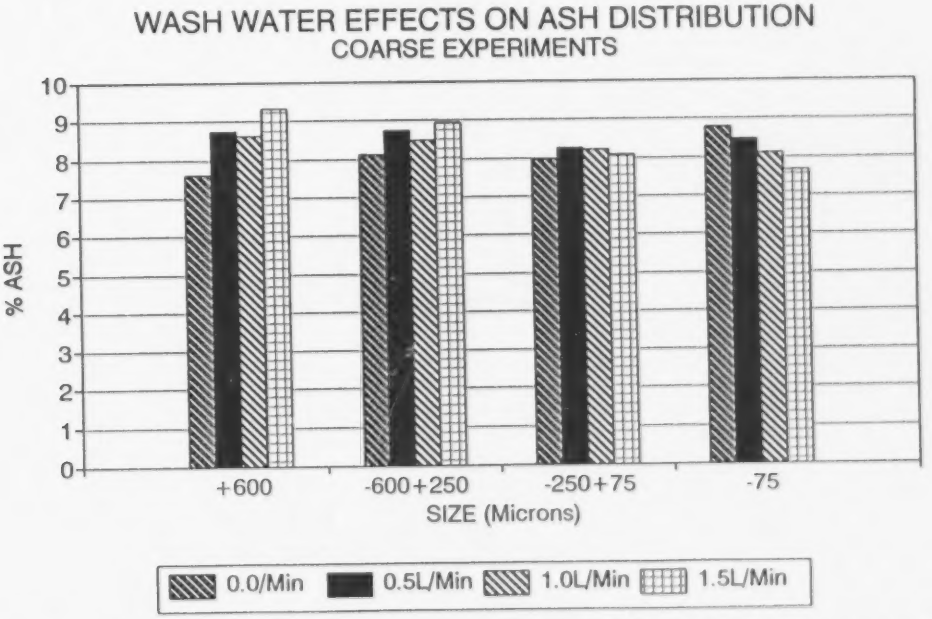

Figure E.4 Effect of wash water on ash content in each size fraction in the concentrate for coarse experiments.